EXPERIMENTAL AND NUMERICAL INVESTIGATION ON WAVE ATTENUATION PERFORMANCE OF A FLOATING PLATFORM

A THESIS SUBMITTED TO
THE GRADUATE SCHOOL OF NATURAL AND APPLIED SCIENCES
OF
MIDDLE EAST TECHNICAL UNIVERSITY

BY

GÜNAY GAZALOĞLU

IN PARTIAL FULFILLMENT OF THE REQUIREMENTS
FOR
THE DEGREE OF MASTER OF SCIENCE
IN
CIVIL ENGINEERING

JANUARY 2023

Approval of the thesis:

EXPERIMENTAL AND NUMERICAL INVESTIGATION ON WAVE ATTENUATION PERFORMANCE OF A FLOATING PLATFORM

submitted by **GÜNAY GAZALOĞLU** in partial fulfillment of the requirements for the degree of **Master of Science** i**n Civil Engineering, Middle East Technical University** by,

Prof. Dr. Halil Kalıpçılar
Dean, Graduate School of **Natural and Applied Sciences** _____

Prof. Dr. Erdem Canbay
Head of the Department, **METU** _____

Prof. Dr. Ahmet Cevdet Yalçıner
Supervisor, **Civil Engineering, METU** _____

Assist. Prof. Dr. Cüneyt Baykal
Co-Supervisor, **Civil Engineering, METU** _____

Examining Committee Members:

Assist. Prof. Dr. Gülizar Özyurt Tarakcıoğlu
Civil Engineering, METU _____

Prof. Dr. Ahmet Cevdet Yalçıner
Civil Engineering, METU _____

Assist. Prof. Dr. Cüneyt Baykal
Civil Engineering, METU _____

Assoc. Prof. Dr. Elif Oğuz
Civil Engineering, METU _____

Assoc. Prof. Dr. Bergüzar Öztunalı Özbahçeci
Civil Engineering, IZTECH _____

Date: 20.01.2023

I hereby declare that all information in this document has been obtained and presented in accordance with academic rules and ethical conduct. I also declare that, as required by these rules and conduct, I have fully cited and referenced all material and results that are not original to this work.

Name Last name : Günay Gazaloğlu

Signature :

ABSTRACT

EXPERIMENTAL AND NUMERICAL INVESTIGATION ON WAVE ATTENUATION PERFORMANCE OF A FLOATING PLATFORM

Gazaloğlu, Günay
Master of Science, Civil Engineering
Supervisor: Prof. Dr. Ahmet Cevdet Yalçıner
Co-Supervisor: Assist. Prof. Dr. Cüneyt Baykal

January 2023, 112 pages

The floating platforms become advantageous in coastal areas for protection as it has flexibility in design, transportability, and low construction cost. However, wave period and wave height are restrictive parameters in the design stages of these platforms. Relatively short-wave periods and low wave heights are required to use floating platforms appropriately. This study aimed to analyze the transmission coefficient of a floating platform under the attack of irregular and regular waves having different wave steepnesses at different water depths. In the physical model experiments, two types of floating structures were tested: rectangular box and horizontal cylinder-type structures. The box was tested at 50 cm of water depth under regular waves and the horizontal pipe platform was tested under irregular and regular waves at 40, 50, and 60 cm water depths for all wave sets. To understand the relation between the single dependent variable and several independent variables, a multiple regression method was applied, and wave transmission formulas were developed for the horizontal cylinder structures, separately for irregular and regular waves. Moreover, computational fluid dynamics (CFD) analyses of wave transmission and energy dissipation for the box and the selected horizontal cylinder-type platform were carried out to validate the

CFD model and to extend the experimental dataset using an open-source CFD library OpenFOAM v1912 together with waves2FOAM wave generation and absorption package.

Keywords: Floating Platforms, Wave Attenuation, Wave Transmission, Energy Dissipation, CFD Modelling

ÖZ

YÜZER BİR PLATFORMUN DALGA SÖNÜMLEME PERFORMANSININ DENEYSEL VE NUMERİK OLARAK İNCELENMESİ

Gazaloğlu, Günay
Yüksek Lisans, İnşaat Mühendisliği
Tez Yöneticisi: Prof. Dr. Ahmet Cevdet Yalçıner
Ortak Tez Yöneticisi: Dr. Öğr. Üyesi Cüneyt Baykal

Ocak 2023, 112 sayfa

Yüzer platform, tasarımda esnekliğe, taşınabilirliğe ve düşük inşaat maliyetine sahip olduğu için kıyı bölgelerinde koruma yapısı olarak kullanılması avantajlı hale gelmektedir ancak dalga periyodu ve dalga yüksekliği bu platformların tasarım aşamalarında kısıtlayıcı parametrelerdir. Uzun dalga periyotları ve yüksek dalga yükseklikleri yüzer dalgakıran kullanımı için uygun özellikler değildir. Bu çalışma, yüzer cismin su çekim yüksekliğini değiştirerek, farklı derinlik ve dalga dikliğine sahip düzensiz ve düzenli dalgalar altında platformun dalga geçirim katsayısını analiz etmeyi amaçlamaktadır. Gerçekleştirilen fiziksel model deneylerinde, iki tür yüzer yapı test edilmiştir: dikdörtgen kutu ve yatay silindir tipi yapılar. Kutu, 50 cm su derinliğinde düzenli dalgalar altında ve yatay silindir tipi platform, tüm dalga setleri için 40, 50 ve 60 cm su derinliklerinde düzensiz ve düzenli dalgalar altında test edilmiştir. Ayrıca, çoklu regresyon yöntemi ile yatay silindir tipi için dalga iletim formülleri geliştirilmiştir. Bunun yanında kutu ve yatay silindir tipi yüzer platfromlar için dalga geçirimi ve enerji sönümlenmesi üzerine HAD analizi gerçekleştirilmiştir. Bu amaçla OpenFOAM hesaplamalı akışkanlar dinamiği yazılımı v-1912 versiyonu *waves2Foam* ile kullanılmıştır.

Anahtar Kelimeler: Yüzer Platformlar, Dalga sönümleme, Dalga iletimi, Enerji Sönümleme, HAD Modelleme

To my family and beloved ones

ACKNOWLEDGMENTS

I am so grateful to my thesis advisors, Prof. Dr. Ahmet Cevdet Yalçıner and Assist. Prof. Dr. Cüneyt Baykal, for their valuable knowledge and experience in guiding me through this thesis study.

I also want to thank Dr. Hasan Gökhan Güler for his guidance, patience, and excellent support, as well as the ideas that motivated me to keep going. Without their mentorship and support, I would not have been able to make progress on my academic path.

I would like to express my appreciation to Prof. Dr. Ayşen Ergin, who taught me the joy of being a coastal engineer and always encouraged us to approach problems from multiple perspectives with her intellectual personality. It was a privilege to work with her.

I am grateful for the education I received from Dr. Işıkhan Güler and Dr. Gülizar Özyurt Tarakcıoğlu.

I want to express my gratitude to Yusuf Korkut, for his limitless technical support during the experimental setup and his effort to overcome the problems, this thesis wouldn't reach its final shape without him.

I would also like to thank Akdeniz İnce, Barış Ufuk Şentürk, Berkay Akyol, Berkay Erler, Bilge Karakütük, Cem Sevindik, Çağatay Uysal, Elif Ayşe Öztürk, Furkan Demir, Gökay Altunbaş, Mert Yaman, Irmak Özdemir, Utku Uzun and Yağız Arda Çiçek for always inspiring me to do my best. I am grateful for the times we shared and for their contributions to my academic knowledge. I also want to extend my special thanks to Diana Poczatek for her support.

I want to express my deep gratitude to my mother, Aysel Gazaloğlu, my father, Behzat Gazaloğlu, and my brother, Mehmet Gazaloğlu, for their endless support. They were always there for me and supported me without hesitation. I appreciate their trust in me and am fortunate to have such wonderful people in my life.

Finally, I want to thank AK-YA DENIZCILIK VE SU ÜRÜNLERI LTD.STI. for producing the models and providing all structure plans and methods. This study was funded by ODTÜ DÖSİM 2021-03-03-1-02-124

TABLE OF CONTENTS

LIST OF TABLES

TABLES

LIST OF FIGURES

FIGURES

LIST OF ABBREVIATIONS

ABBREVIATIONS

CFD	Computational Fluid Dynamics
DHI	Danish Hydraulic Institute
JONSWAP	Joint North Sea Wave Project
OpenFOAM	Open-source Field Operation and Manipulation
RANS	Reynolds Averaged Navier Stokes
SPH	Smoothed-Particle Hydrodynamics
SWL	Still Water Level
VOF	Volume of Fluid

LIST OF SYMBOLS

SYMBOLS

γ_w	Specific gravity of sea water
B_0	Center of buoyancy of a floating body
E_d	Energy dissipation
E_i	Incident wave energy
E_r	Reflected wave energy
E_t	Transmitted wave energy
Fr_m	Model Froude number
Fr_p	Prototype Froude number
H_i	Incident wave height
H_{m0}	Spectral significant wave height
H_r	Reflected wave height
H_R	Radiated wave height
H_s	Incident significant wave height
H_t	Transmitted wave height
I_{yy}	Second moment of inertia in the y-axis,
K_d	Energy dissipation coefficient
K_r	Reflection coefficient
K_t	Transmission coefficient
$P_{wave,i}$	Incident wave induced pressure

$P_{wave,r}$	Reflected wave induced pressure
$P_{wave,t}$	Transmitted wave induced pressure
T_m	Mean wave period
$T_{m-1,0}$	Spectral mean wave period
T_p	Spectral peak wave period
k_i	Wave number
s_m	Wave steepness
u_i	Ensemble-averaged velocity
u_i	Incident horizontal fluid velocity
u_r	Reflected horizontal fluid velocity
u_t	Transmitted horizontal fluid velocity
x_i	Cartesian coordinate
λ_L	Model length scale
λ_T	Model time scale
λ_W	Model weight scale
λ_g	Model gravitational acceleration scale
λ_ρ	Material density
μ_{eff}	Effective dynamic viscosity
ν_{turb}	Turbulent kinematic viscosity
B	Structure width
G	Centre of gravity of a floating body

h	Structure freeboard
H	Structure height
M	Metacentre
N	Number of waves tested
s	Cylinder spacing
V	Submerged volume of the body.
γ	VOF indicator function
D	Structure draft height
Fr	Froude number
L	Wavelength
N	Number of waves
V	Velocity
d	Water depth
g	Gravitational acceleration
p	Pressure
t	Time
η	Free surface elevation
μ	Effective dynamic viscosity
ρ	Water density

CHAPTER 1

INTRODUCTION

From ancient times to the present, civilizations have chosen to live near coastal areas. Even though sheltered bays and gulfs with relatively smooth wave conditions and currents provide a suitable environment for recreational and marine transportation purposes, different solutions are used to ensure safety and service in these regions. Characteristic of wave climate and aspects of the economy, aesthetics play significant roles in the coastal structure design. Depending on these differences, fixed or floating structures can be used among coastal protection structures with different structural features.

In general, fixed types of breakwaters can be listed as conventional (mound), monolithic, and composite types of breakwaters. Furthermore, commonly floating types of structures are box, pontoon, raft/mat and tethered.

Since fixed-type coastal protection structures are highly-costed and long-lasting structures, once they are built, they become a part of the environment where they are located and become almost impossible to move or remove. Apart from these, another factor that limits the use of fixed-type breakwaters is the construction depth. As the water depth reached by fixed structures increases, the dimensions of the structure's cost increase significantly, and the dynamic and static design becomes more challenging.

Conventional breakwaters are mostly applied in relatively shallow water due to economic concerns. However, floating structures can be applied in deep seas. Furthermore, soil conditions are not significantly important, and also floating structures have no impact on sediment movement and water circulation. Lastly, the practicality of floating structures such as modular placement, multiple functioning, and relatively effortless maintainability makes them preferable.

Due to the reasons mentioned above, floating type of breakwaters is one of the oldest and easiest solutions to lessen the effects of waves on coasts. According to Morey (1998), the first known application of a floating breakwater was found in 1811 to protect a fleet in Britain. Moreover, there is an increase in the world today to meet the needs of mooring, berthing, and cargo handling for marine vehicles in a more environment-friendly, economically, and aesthetic way in more sheltered bays, coastal areas in gulfs or very deep sea areas (Biesheuvel, 2013). Floating structures justify this demand with their relatively low cost, portability and reusability, and minimal negative impact on natural life. A lot of experimental and theoretical research have been carried out on the design of various types of floating coastal structures, but the practical use of these types of structures has been limited. The reason for this is that the wave-damping performance of the system changes with the effect of the dynamic response of the system in waves. For this reason, the use of floating structures is possible for bays and gulfs affected by low-period waves.

This study aims to analyze the transmission performance of a horizontal cylinder floating platform under the attack of irregular and regular waves in different water depths and various wave steepness (H/L) by modifying the floating platform's draft height. Also, it is aimed to carry CFD analysis of the floating platform with a particular focus on wave transmission and energy dissipation.

In the physical model experiments, rectangular box, single and dual horizontal cylinder type of floating structures were tested as fixed. Horizontal cylinder floating platforms' transmission performance tests were carried out under irregular and regular waves for all sets at 40, 50, and 60 cm water depths.

The purpose of this study was to obtain answers to the following research questions:

i. What is the effect of change in the geometry and water depth of floating platforms on wave transmission performance in varying wave conditions?

ii. How do horizontal cylinder and box-type floating structures which have the same draft, freeboard, and width, differ in wave attenuation performance?
iii. To what extent applying a double platform feasible on wave attenuation compared to a single horizontal cylinder and box type?

This study is structured as follows:

The literature review in Chapter 2 is divided into four sections. The first section discusses reflective structures such as box, pontoon, frame, and hinge-type structures. The second section discusses dissipative structures, which are divided into three categories: tethered, scrap-tire, and hinge. The third section covers theories on wave transmission for fixed rigid structures. The final section of the literature review covers numerical studies on floating breakwaters.

Chapter 3 covers the methodology for physical model experiments, including dimensional analysis, scaling, wave sets, and experimental cases.

Chapter 4 presents the results of physical experiments under irregular and regular wave conditions for box and different horizontal-cylinder-type floating structures. It also includes the results of multi-regression analysis for irregular and regular waves and discusses the results of the physical experiments.

Chapter 5 discusses the methodology for numerical model studies, including the formulation and description of the CFD model, as well as the meshing and setup of the cases.

Chapter 6 presents the results of the numerical model studies, including the validation of the numerical model for the box and horizontal-cylinder type structures. It also includes the results of three different extended numerical studies.

Chapter 7 summarizes and concludes the study and includes future remarks.

CHAPTER 2

LITERATURE REVIEW

Floating breakwaters can be characterized into two classes that are reflective and dissipative structures in terms of wave attenuation (PIANC, 1994). According to Biesheuvel (2013), reflective-type floating breakwaters reflect the incident wave and do not deform under loads. However dissipative structures show non-elastic deformation, and the key idea is attenuating wave energy by friction and turbulence. When the floating structures are classified according to shape; box, pontoon, frame, mat, tethered and horizontal plate type can be listed (McCartney, 1985).

2.1 Wave Transmission Theories for Fixed Rigid Reflective Structures

Understanding wave-structure interaction is crucial for the design and performance of floating breakwaters. Transmission theories provide a foundation for predicting the transfer of wave energy under the structure. Therefore, in Chapter 2.1, Macagno (1954), Wiegel (1960), Cox (1989), Kriebel and Bollman (1996), and ASCE (2012) wave transmission theories are presented.

The amount of reflected, transmitted, and dissipated energy are the main components while evaluating the floating breakwater performance. The relation of transmission Eq . (2.1), reflection Eq. (2.2), and energy dissipation coefficient are given in Eq.(2.3). Several wave transmission theories have been developed from linear wave theory and they are relevant to wave energy transport.

$$K_t = \frac{H_t}{H_i} \tag{2.1}$$

$$K_r = \frac{H_r}{H_i} \tag{2.2}$$

$$K_t{}^2 + K_r{}^2 + K_d{}^2 = 1 \tag{2.3}$$

In Eq. (2.3), K_t is the transmission coefficient, K_r is the reflection coefficient and K_d is the energy dissipation coefficient.

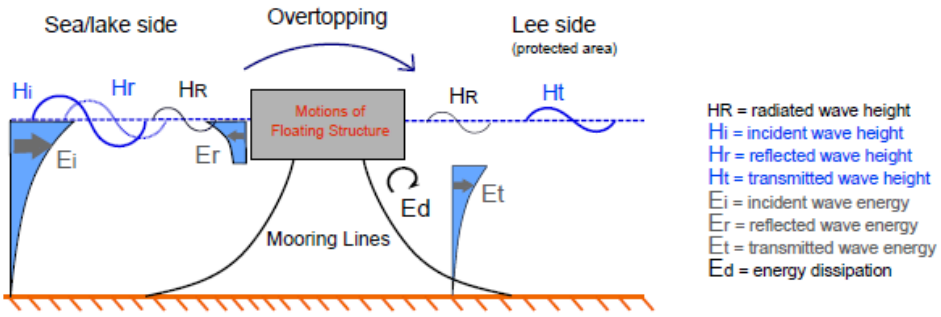

Figure 2.1: The fundamental interactions between waves and floating breakwaters. (adopted from Biesheuvel, 2013)

As shown in Figure 2.1 H_R is radiated wave height which is due to the movement of the floating body, H_i , H_t and H_t, are the wave heights for the incident, reflected, and transmitted waves, respectively. E_r is the reflected wave energy, E_i is incident wave energy, E_t transmitted wave energy and E_d is the dissipated energy. Distribution of incident wave energy can be written as $E_i = E_r + E_t + E_d$. Since for short waves, energy accumulates on the upper part of the water column, it is way easier to block the energy. However, when the waves have a longer period, a larger draft should be applied to block energy. This case brings a drawback to the mooring line system as excessive loads. Therefore, during the design process, these drawbacks and economic relations should be studied in detail.

2.1.1 Macagno (1954)

Macagno (1954) theory is based on the following assumptions: The structure is assumed to be rigid, non-deformable, and fixed (no degree of freedom) Figure 2.2. Moreover, the theory is valid for finite width assumption in deep water according to linear wave theory and it is presumed for non-overtopped waves.

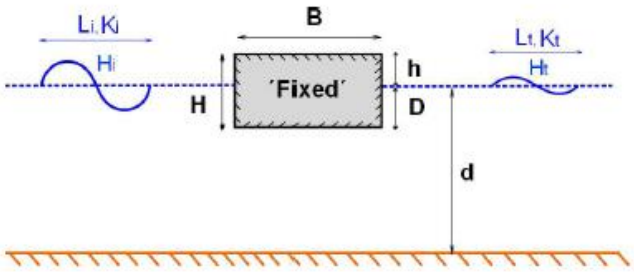

Figure 2.2: Definitions of Macagno's theory (adopted from Biesheuvel, 2013)

Based on the assumptions mentioned above, Macagno developed Eq. (2.4).

$$K_{t,Macagno} = \frac{1}{\sqrt{1 + \left[\frac{k_i B sinh(k_i d)}{2cosh(k_i d - k_i D)}\right]^2}} \tag{2.4}$$

K_t is the function of incident wave number (k_i), structure width (B), structure draft height (D), and water depth (d).

2.1.2 Wiegel (1960)

Wiegel (1960) established a theory that takes wave power into account. Assumptions used by Macagno (1954) such as structure's rigidity, fixed condition, deep water, and no overtopping conditions are also valid for Wiegel (1960). Wave induced pressure P_{wave} and wave-induced horizontal velocity u are the components of time-averaged over one wave period wave power. As can be seen from Eq. (2.5), Wiegel assumed that the power of the wave at the rear side of the structure, which

is transmitted wave, over the complete water depth is equal to incident wave power from the water surface to the bottom of the structure (Figure 2.3).

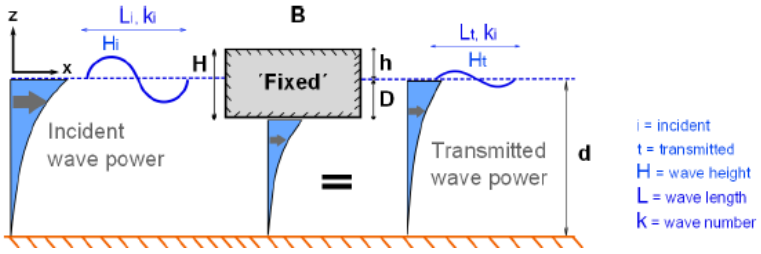

Figure 2.3: Definitions of Weigel's theory (adapted from Biesheuvel, 2013)

After solving the left side of the integral in Eq. (2.5), transmitted wave power $P_{wave,t}$ becomes as in Eq. (2.6.) Right side of the integral solution of Eq. (2.5 also gives the incident wave power $P_{wave,i}$ in Eq. (2.7). Transmission coefficient (K_t) proposed by Wiegel (1960) is the square root of the ratio between the transmitted wave power to incident wave power which shown in Eq. (2.8).

$$\overline{\int_{-d}^{0} P_{wave,t} u_t dz} = \overline{\int_{-d}^{-D} P_{wave,i} u_i \, dz} \tag{2.5}$$

$$P_t = \left(\frac{4\pi(d-D)/L}{\sinh\left(\frac{4\pi d}{L}\right)} + \frac{sinh\left(\frac{4\pi(d-D)}{L}\right)}{\sinh\left(\frac{4\pi d}{L}\right)} \right) \tag{2.6}$$

$$P_i = 1 + \frac{4\pi d/L}{\sinh\left(\frac{4\pi d}{L}\right)} \tag{2.7}$$

$$K_{t,wiegel} = \sqrt{\frac{P_t}{P_i}} = \sqrt{\frac{2k_i(d-D) + \sinh\big(2k_i(d-D)\big)}{\sinh(2k_i d) + 2k_i d}} \tag{2.8}$$

It can be noted that (K_t) is the function of the incident wave number (k_i) structure draft height (D) and water depth (d).

2.1.3 Cox (1989)

Cox (1989) tried to improve the Wiegel (1960) formula by considering the width (B) effect on transmission. He noticed that smaller $\frac{B}{L}$, Macagno (1954) overestimates the transmission while comparing it with Wiegel's theory (Kürüm, 2008). The developed formulation is shown in Eq. (2.9).

$$K_{t,Cox} = K_{t,wiegel} * \left(\frac{2\sqrt{1 + \left(\frac{2\pi B}{L}\right)^2}}{\frac{2 + (2\pi B)^2}{L}} \right) \tag{2.9}$$

2.1.4 Kriebel and Bollman (1996)

Wiegel (1960) theory was examined by several researchers, and it is shown that his formula over-predicts the wave transmission in deep water and under-predicts in shallow water conditions (Biesheuvel, 2013). Moreover, partial wave reflection and energy dissipation were not considered in Wiegel's formula. However, Kriebel and Bollman (1996) improved the Wiegel (1960) theory and suggested a new theory called Modified Power Transmission Theory which includes partial wave reflection and energy dissipation. As can be seen from (2.10), time-averaged over one wave period wave power is the sum of incident wave-induced pressure ($P_{wave,i}$) and reflected wave induced pressure ($P_{wave,r}$) is equal to the transmitted wave-induced wave pressure under the structures' wave column.

$$\overline{\int_{-d}^{-D} (P_{wave,i} + P_{wave,r})(u_{i-}u_r)dz} = \overline{\int_{-d}^{0} P_{wave,t}\, u_t\, dz} \tag{2.10}$$

Furthermore, the net horizontal fluid velocity is considered a subtraction of the incident (u_i) and reflected velocities (u_r). In Eq. (2.10), there are two unknowns, to overcome this problem continuity of the fluid velocities is used as in (2.11).

$$u_t = u_{i\_}u_r \tag{2.11}$$

After substituting dynamic pressure and horizontal velocities in (2.10) by using linear wave theory, (2.12) is obtained.

$$(K_{t,,Kriebel\ and\ Bollman})^2 = (1 - {K_r}^2) * \left(\frac{2k_i(d-D)+\sinh(2k_i(d-D))}{\sinh(2k_id)+2k_id}\right) \tag{2.12}$$

By using the relation of (2.12) and (2.13), (2.14) is represented.

$$K_{t,Kriebel\ and\ Bollman} = (1 - K_r) \tag{2.13}$$

$$K_{t,Kriebel\ and\ Bollman} = \frac{2{K_{t,Wiegel}}^2}{1 + {K_{t,Wiegel}}^2} \tag{2.14}$$

2.1.5 ASCE Manuals and Reports on Engineering Practice (2012)

Firstly, Wiegel (1960) studied the power transmission theory for thin barriers. Then Kriebel and Bollman (1996) extended Wiegel's study and added wave reflection and energy dissipation effect on transmission. Next, Cox (1989) improved the theory of finite width barriers. Task Committee on Marinas 2020 of the Coasts, Oceans, Ports, and Rivers Institute of ASCE, proposed a composite formula ASCE (2012), combining Kriebel and Bollman (1996), Cox (1989), and Wiegel (1960) formulas as shown in Eq. (2.15).

$$K_{t,ASCE} = K_{t,Kriebel\ and\ Bollman} * \left(\frac{K_{t,Cox}}{K_{t,wiegel}}\right) \tag{2.15}$$

2.2 Reflective Floating Structures

Reflective floating structures are mainly divided into four categories.

- Box
- Pontoon
- Frame
- Hinge

2.2.1 Box Type Floating Breakwaters

Box-type floating structures are widely used because of their simple geometry and uniform shape. The dimensional parameters for the box-type structure are as follows: B (structure width), h (freeboard), D (draft), H (height), and d (water depth), as shown in Figure 2.4. Floating modules' connections are flexible or pre-post tensioned to make structures behave as single pieces (McCartney, 1985). According to PIANC (1994), relative depth d/L and relative width B/L are important parameters for energy distribution. However, there are construction and strength limitations for large box structures. Therefore using lighter material inside of the structure's core and splitting the structure into parts can be solutions to overcome these problems. Moreover, the metacenter and radius of gyration of floating breakwaters attached by chains or cables affect their efficiency (Biesheuvel, 2013).

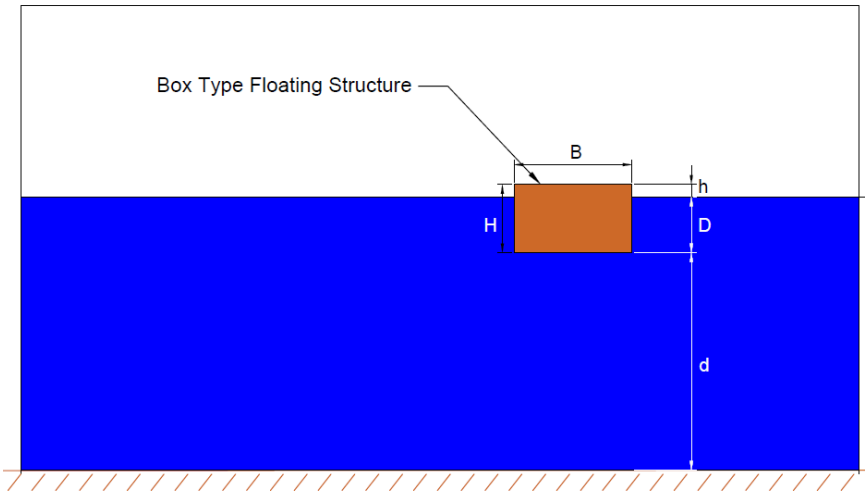

Figure 2.4 Box-type floating breakwater

The efficiency of box-type floating breakwaters was studied by several researchers. The first wave attenuation study was carried out by Lochner et al. (1948) for Bombardon floating breakwater. Then, Carr (1951) and Macagno (1953) conducted experimental studies for rectangular floating boxes and developed theoretical formulas for linear waves. Koutandos et al. (2005) conducted a comprehensive floating box experiment. In the case of a single fixed box under regular waves, after B/L > 0.25 for all D/d = 1/3, 1/4, and 1/5 cases, the transmission coefficient was found less than 0.5. Results showed that floating breakwaters perform better under short periods of waves for d/L > 0.25. Furthermore, for H_i = 0.2 m the shortest wave which is $B/L \approx 0.31$, K_t are 0.25, 0.39, 0.37 for D/d = 1/3, 1/4, 1/5 respectively. However, for the longest wave which is $B/L \approx 0.04$, K_t are 0.82, 0.88, 0.9 for D/d = 1/3, 1/4, 1/5 respectively. When the wave period increases, the wave energy dissipation coefficient decreases due to an increasing trend in the oscillation of air-water vortices at the frontal bottom edge of the structure. Also, the reflection pattern increases while the wave period decreases which proves that floating box breakwater is a reflective structure for a wide range of waves. In another box-type floating breakwater experiment conducted by Martinelli et al. (2008), they studied how the arrangement of floating breakwaters affects wave transmission, the stress on moorings and connections, and the impact of oblique

waves. According to Koraim & Rageh (2014), there are many studies about wave diffraction for box-type floating breakwaters such as Ofuya (1968) and Davidson (1983). Moreover, Gunbak et al. (2014) evaluated the effectiveness of two types of breakwaters for protecting a Marina from waves: 526 meters long floating breakwater and 362 meters long vertical wall breakwater. They conducted 3D hydraulic model experiments to compare the performance of these breakwaters individually and in combination. The results of these experiments indicated that the combination of the vertical wall and floating breakwaters was most effective, with a probability of significant wave height exceeding 0.3m at only 1.08% of the year. In contrast, using only a floating breakwater had a probability of 2.1%.

Williams et al. (2000) examined the two floating boxes placed side by side (Figure 2.5). It is concluded that dual box floating breakwaters are efficient in long waves when the spacing is narrow because of the somehow continuation in width. However, reflecting short waves was achieved by large spacing since two floating boxes behave as independent two structures.

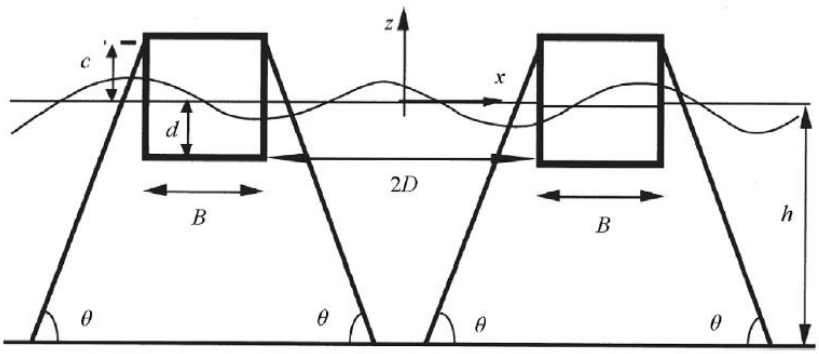

Figure 2.5: Dual Box Floating Breakwater (adapted from Williams et al. 2000)

2.2.2 Pontoon Type Floating Breakwaters

The pontoon type is combining of two floating boxes with a rigid beam that fixed each other (Figure 2.6). Pontoon-type breakwater has higher inertia than box type which provides significant stability (Dai et al., 2018). Moreover, the mass of the

structure can be reduced by satisfying the desired inertia forces, this brings lighter material and less cost.

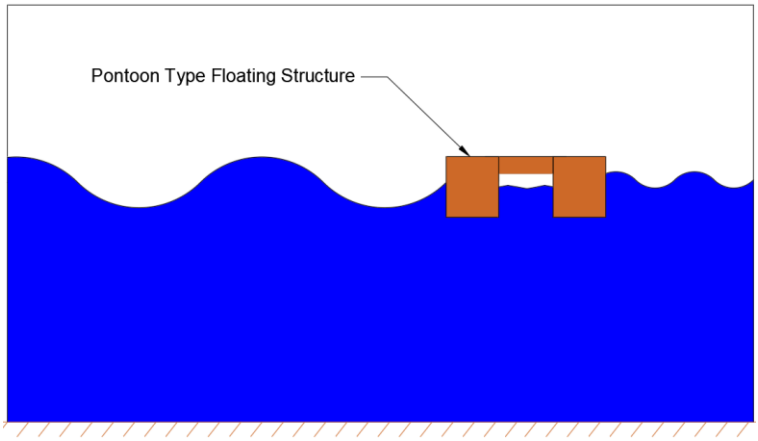

Figure 2.6 Pontoon Type Floating Breakwater

Ofuya (1968) indicated that such pontoon-type structures' draft height has an enormous effect on dissipation. Furthermore, due to the gap between the two boxes, turbulence is generated there, and dissipation of wave energy occurs. Ikeno et al. (1988) studied the pressurized air chamber phenomenon to investigate the change in wave transmission. Simply idea is to have pressurized space between the legs of the floating body to have more dissipation with the help of pressurized air. They found out that a bigger air chamber and pressurized head provide more wave transmission. Koo (2009) enhanced the study of Ikeno et al. (1988) and he placed a nozzle outlet at the top of the pontoon to create a pneumatic chamber. When pontoon and box structures that have the same dimensions are compared, the pontoon is way more efficient in reflecting long and moderate waves (Dai et al., 2018). Also, Loukogeorgaki et al. (2014) investigated the performance of three box-type floating structures that are linked to each other with flexible connectors. Their study focused on wave obliquity and its effect on flexible connectors. In this case, long waves are found critical due to bending mode. These ranges; $B/L < 0.25$ under 60° oblique waves and $B/L < 0.15$ under 40° oblique waves.

2.2.3 Frame Type Floating Breakwater

The frame type is made up of two pontoons and a vertical plate between them (Figure 2.7). Two pontoons have linked each other with frames or truss elements. The attenuation method of the frame type of floating breakwater can be noted as reflective and turbulence. Mostly they are used where there are plenty of timbers (Dai et al., 2018). Timber doesn't have high durability under water. Therefore, modern frame-type floats have been reinforced with concrete and steel.

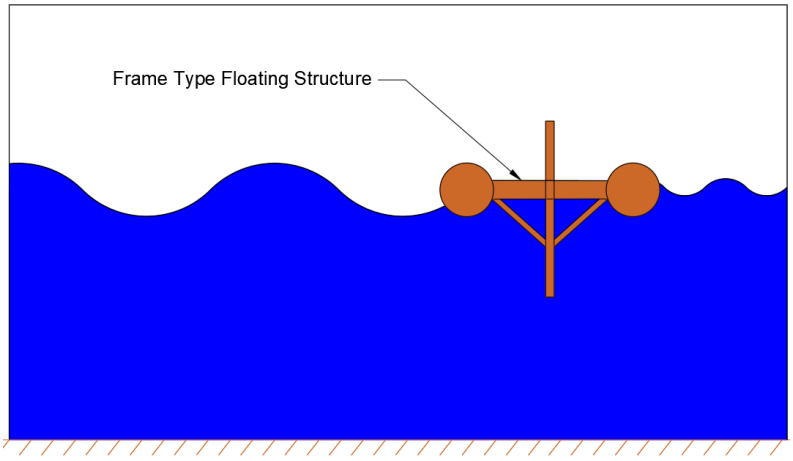

Figure 2.7 Frame Type Floating Breakwater

Nakamura (1999) suggested a developed version of a frame-type floating structure Figure 2.8(a), instead of frames that connect two pontoons, horizontal cylinders were used. However, an experimental study showed that the box structure performed better in terms of wave dissipation than the horizontal cylinder version for $B/L < 0.25$. As can be seen from Figure 2.8(b) and Figure 2.8(c), improved versions of the models are presented. In Figure 2.8(b) two horizontal plates are attached to pontoons to increase efficiency and in Figure 2.8(c) L shape plates are linked to the system to change the natural period of heave movement. Akgul (2016) conducted experiments to examine the impact of the distance between pipes on the transmission performance of a trimaran floating breakwater. He tested various pipe spacing under regular waves and discovered that reducing the distance between

cylinders resulted in a decrease in wave transmission due to the interaction between the cylinders.

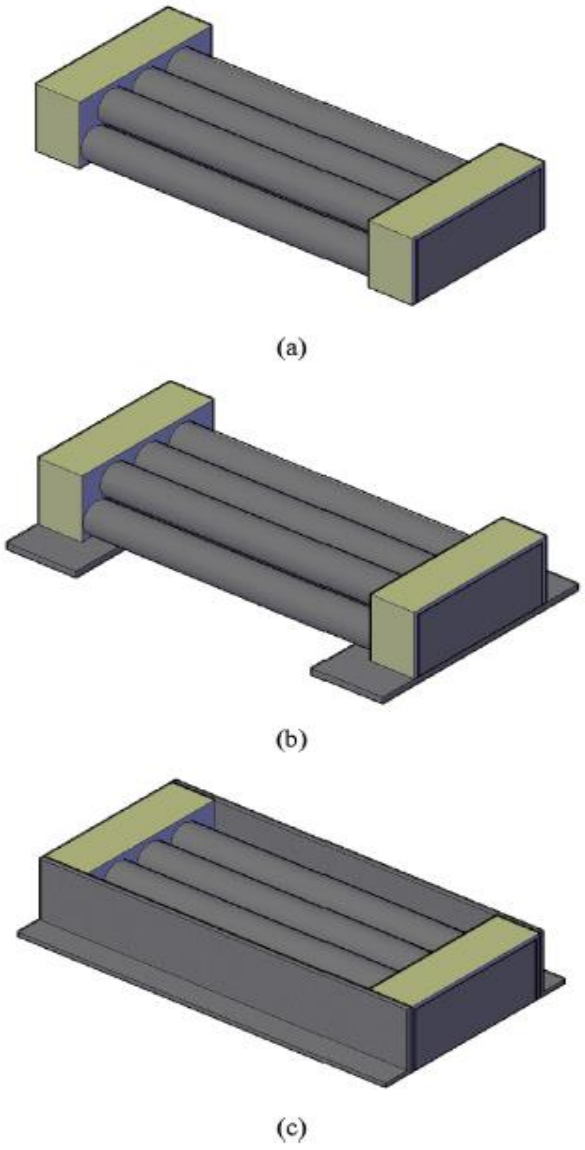

Figure 2.8:Horizontal Cylinders (adopted from Dai et al., 2018)

Chun-Yan et al. (2015) developed a new type of structure called a cylindrical floating breakwater, this system has two components as the classic frame type of floating breakwater (Figure 2.9). However, instead of a vertical plate between floating cylinders, they used a mesh cage made up of many balls which have suspended form in the matrix to dampen wave energy.

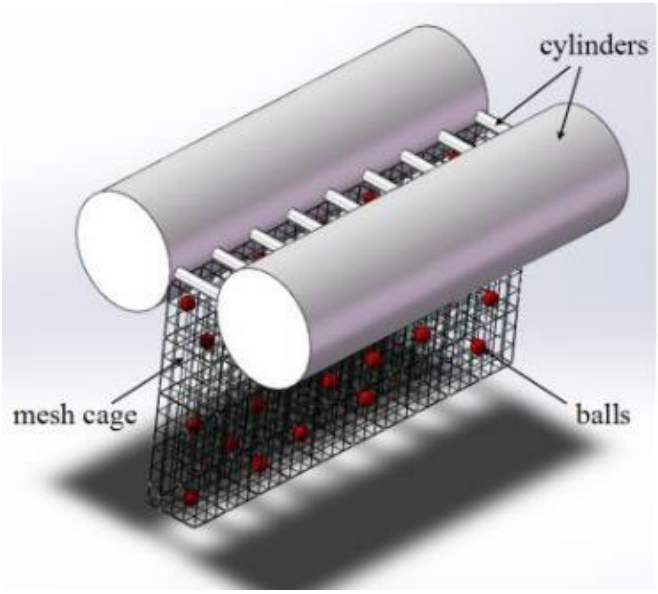

Figure 2.9: Cylindrical Floating Breakwater (adopted from Chun-Yan et al., 2015)

The study by Chun-Yan et al. (2015) found that when the wavelength increases, the transmission coefficient H_t/H_i increases till $L/B < 6.5$. However, after $L/B > 6.5$, *Kt* decreases while wavelength increases. The reason is correlated to pitch, yaw, and heave motions. Once the structure starts to show large oscillations, more energy is dissipated.

2.2.4 Hinge Type Floating Breakwaters

The hinge type of floating breakwater is one of the reflective structures. There is a vertical plate that is placed throughout the water column, vertical plate is connected to the ground by a hinge which provides rotation freedom (Figure 2.10). Moreover, there are cables that are connected to structures from both sides. Biesheuvel (2013) indicates that the buoyancy of the plate and cable itself is responsible for the restoring forces for the system.

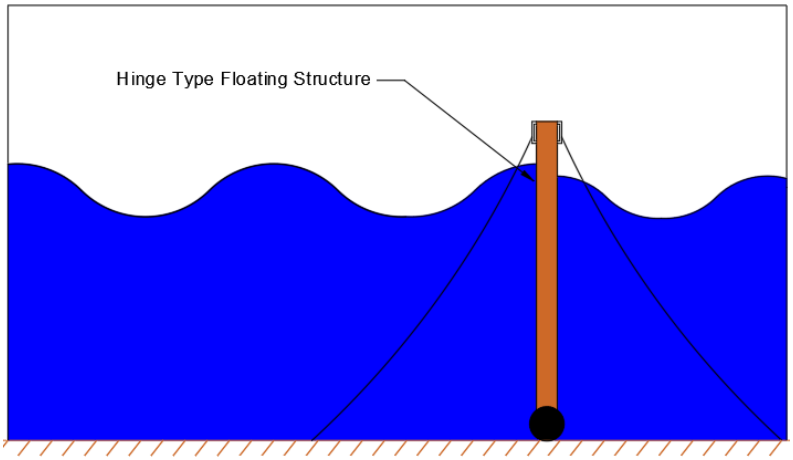

Figure 2.10:Hinge Type of Floating Breakwater

As a summary, in Chapter 2.2 Box, the Pontoon, Frame, and Hinge types of structure's mechanisms are given, and different variations and developments are mentioned. Since floating structure and wave interaction is a complex phenomenon, each type of structure relatively performs better than others under different wave conditions by improving their structure geometry, mooring materials, and anchoring methods with the scope of optimized cost cases.

2.3 Dissipative Structures

Dissipative floating structures are mainly divided into three categories.

- Tethered Type
- Scrap-Tire Type
- Porous Walled

2.3.1 Tethered Type Floating Breakwaters

Tethered type of floating breakwaters consists of many pontoons groups which are attached to the ground with cables (Figure 2.11). Because of buoyancy forces on pontoons, tension forces are subjected to the cables. Pontoons could be either half

submerged or fully submerged. The study conducted by Jones (1978) for container off-loading systems was focused on the efficiency of wave periods between 2-7 seconds for safe ship loading-unloading operations. This study revealed that tethered type of floating structure was able to reduce 50% of the significant wave height with the 7-seconds peak wave period for the Pierson-Moskowitz wave spectrum. The floating breakwaters mentioned in the reflective structures section take advantage of inertia to attenuate the wave by friction and reflection. However, tethered floating type dissipates via drag forces generated by individual floating pontoons on the water surface due to wave pressure gradient (Hales, 1981). According to PIANC (1994), when the natural period of the floating structure is near the wave period, high friction occurs because of large relative flows while the structure starts to fluctuate out of the phase.

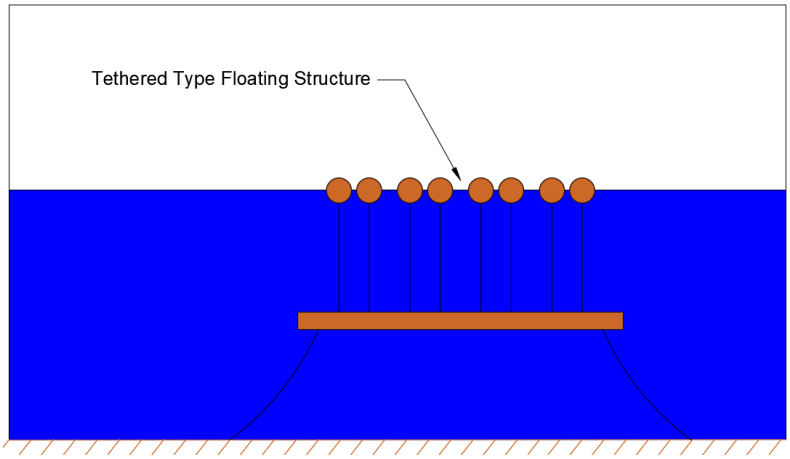

Figure 2.11:Tethered Type of Floating Breakwater

2.3.2 Scrap-Tire Type Floating Breakwaters

Scrap-Tire type of floating structures is made up of scrap or old tires. Hales (1981) indicates that 70% of the rubber industry in the world produces only tires. On the other hand, the recycling of tires is quite insufficient, so there is a huge potential in the tire industry to use this gap as an opportunity for various applications. Moreover, there are lots of advantages of using tires for floating structures; cheap

materials, easiness of mobility, minimal construction equipment, lower anchor loads, and less reflective waves compared to box-type structures (McCartney, 1985). However, there are some drawbacks to using tires in a floating system. For instance, marine growth and accumulation of silt in the tire bottom may cause buoyancy issues. Furthermore, the design life of these structures is not investigated properly. Lastly, wave climate is crucial for the usage of the scrap-tire floating breakwaters. They are only effective in climates where wave height is less than 1 meter and wave period is less than 3 seconds (McCartney, 1985). There are 3 types of tire floating breakwater. First, the wave-maze type was invented by Stitt and Noble (1963), flotation materials are used to fill tires, and also tires are bolted to each other while the triangular pattern is applied Figure 2.12(a). Extensive physical model experiments of maze-type tire floating breakwater were conducted by Kamel and Davidson (1968), they suggested that the width of the shell should not be less than $L/2$ and, structure height should be higher than wave height when the H_i is 1.2 meters (Dai et al., 2018). Another design was developed by Goodyear Tire Company and Candle (1974) carried out the experiments Figure 2.12(b). In this modular design, tires are interlocked to each other with high-strength cables. The last design was a wave-guard, and it is proposed by Harms et al. (1982), there are structure logs and scrap tires inserted through concrete beams Figure 2.12(c). According to McCartney (1985), Goodyear and wave maze have similar transmission results in wavelength to breakwater width ratio L/B. On the other hand, the wave guard shows better efficiency than the other two models.

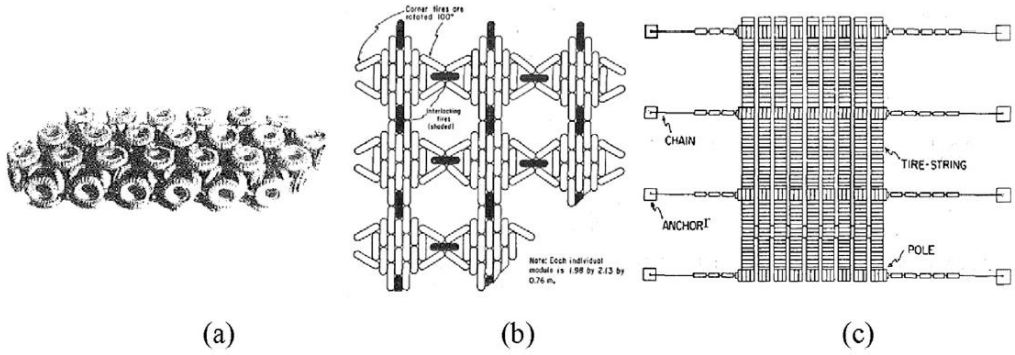

Figure 2.12: Typical mat-type floating breakwaters using scrap tires (adopted from Dai et al., 2018)

2.3.3 Porous Walled Floating Breakwater

When the incident wave hits the porous wall, its energy either will be reflected or dissipated. Richey and Sollitt (1969) studied the porous wall and wave dissipation performance. As can be seen from Figure 2.13, there are two water levels, inner and outer. If η is higher than *"a"*, due to potential wave energy, water flushes into to chamber and is dissipated by turbulence forces. However, if a is higher than η water flushes in the reverse direction till the chamber gets empty. The reverse flow will be the significant attenuator for the next incident wave (Hales, 1981).

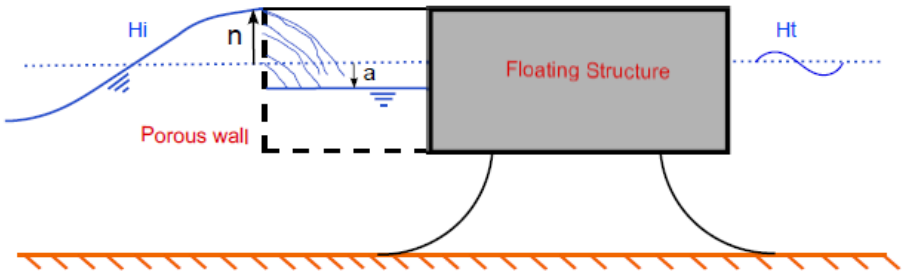

Figure 2.13: Porous Walled Floating Breakwater (adopted from Biesheuvel, 2013)

2.4 Computational Fluid Dynamics (CFD) Modeling Studies Focusing on Floating Breakwaters

There are several CFD modeling studies have been carried out on the transmission and hydrodynamic performance of floating structures. The transmission coefficient is the focus while evaluating the attenuation performance of the structures. Jung et al. (2013) used the volume of fluid (VOF) method to investigate numerically the roll motion of the rectangular shape floating structure under the regular wave. Paci et al. (2016) investigated the hydrodynamic performance of vertical cylinders under regular wave attack, they used OpenFOAM with the boundary conditions of IHFOAM (Higuera et al., 2013). Connell and Cashman (2015) studied the heave motion of the floating body using the ANSYS CFD software which solves the Navier-Stokes equations. Biesheuvel (2013) conducted a study using AQWA which utilizes linear three-dimensional potential flow theory. In this theory, viscous forces are ignored and incompressibility and irrotationality are the assumptions for the fluid motion. Body boundary, linearised free surface, and radiation conditions are satisfied while solving the boundary condition problem. By using the smoothed particle hydrodynamics (SPH) approach, a Lagrangian mesh-free computational methodology, Cheng et al. (2021) evaluated the wave attenuation performance of a double-row floating breakwater. Additionally, Newton's Second law and the Navier-Stokes equations are utilized to model fluid motion and the motion of the floating breakwater, respectively. Zhan et al. (2017) studied T-type floating breakwater under regular and irregular waves. As a CFD package, FLUENT 13.0 was utilized for wave-structure interaction. They applied the zonal hybrid RANS/laminar method, all domain was divided into the stationary zone and some parts were stated as moving zones.

The literature review revealed that there are different types of floating structures, each with its attenuation mechanism. This study aims to examine the attenuation performance of a hybrid structure made up of horizontal cylinders and vertical screens together. After conducting a literature review, it was discovered that there

is no previous study that has examined a structure like the one being tested in this study.

CHAPTER 3

PHYSICAL MODEL EXPERIMENTS

Physical model experiments were carried out to investigate the wave transmission performance of the floating platforms considered in this study. In general, the performance of a floating platform depends on reflected energy, transmitted energy, and dissipated energy. There are many studies on the transmission performance of floating structures. However, each project is unique as each structure has different characteristics dimensions, energy dissipation characteristics, materials, etc.). Therefore, for a better examination of wave attenuation performance and the distinction between different models, dimensional analysis was conducted. Then the scaling procedure was carried out and the model was produced. Next, the experimental setup was completed and experiments were conducted.

3.1 Dimensional Analysis

In Figure 3.1 variables considered in physical model experiments are shown. H_i and T_i are incident wave height and period, H_t, T_t are transmitted wave height and period. *B* is the width, *H* is the height, *h* is the freeboard and *D* is the draft of the floating platform and *d* is the water depth.

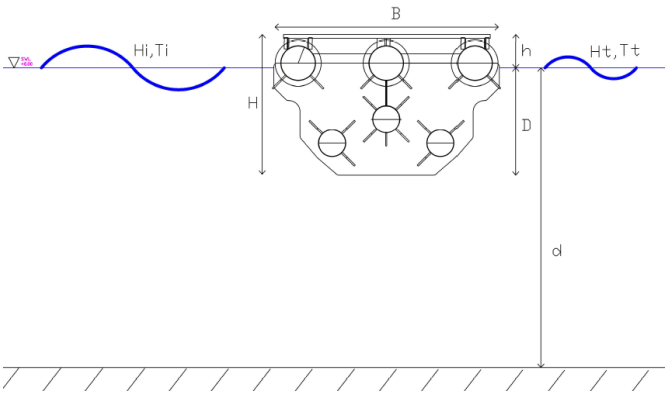

Figure 3.1: Main Variables of Physical Model Experiments.

(The floating platform shown in Figure 3.1 is tested as Case 1 in the present study. Details of the tested platform are described in the forthcoming Section 3.5.2.1.)

Moreover, the density of water ρ_w, gravitational acceleration g, are also governing parameters. Dimensional analysis is carried out by considering all these parameters;

$$H_t = f[H_i, L, B, D, \rho_w, g, d] \tag{3.1}$$

Basic parameters are respectively selected as mass, time, and length-dependent; $\rho_w, g, d,$ and then, Buckingham Pi Theorem is applied. Then K_t function can be written as in 3.2.

$$K_t = f\left[\frac{H_i}{L}, \frac{B}{L}, \frac{d}{L}, \frac{D}{d}\right] \tag{3.2}$$

It is noted that the dimensional analyses have been carried out previously for floating structures in several references (Koutandos et al., 2005, Koraim & Rageh, 2014), confirming the analysis carried out herein.

3.2 Scaling

According to Hughes (1993) gravitational, surface tension, inertial, elastic, and viscous shear forces are the forces that are relevant for floating coastal structures.

Surface tension and elastic compression forces can be neglected because of their relatively small magnitudes. Therefore, the proper law of hydrodynamic scaling depends on dominant forces which could be gravity and viscous. Mostly in coastal engineering problems gravitational forces are considered dominant. Therefore, the model of the floating platform is scaled according to the Froude criterion which is shown in (3.3). The relation of Froude number in the model and prototype is given in (3.4) and (3.5). Variables used in equations are p for fluid density, L for length, V for velocity, F for force, W for structure weight, T for time, and g for gravitational acceleration. Also, the time and length relation are given in (3.6). Force, structure weight, and length relation are given in (3.7).

$$Fr = \sqrt{\frac{inertial\ forces}{gravity\ forces}} = \sqrt{\frac{\rho L^2 V^2}{\rho L^3 g}} = \frac{V}{\sqrt{gL}} \tag{3.3}$$

$$Fr_m = Fr_p \tag{3.4}$$

$$\left(\frac{V}{\sqrt{gL}}\right)_m = \left(\frac{V}{\sqrt{gL}}\right)_p \tag{3.5}$$

$$\frac{\lambda_v}{\sqrt{\lambda_g \lambda_L}} = 1;\ \lambda_g = 1;\ \lambda_v = {\lambda_L}^{0.5};\ \frac{\lambda_L}{\lambda_T} = {\lambda_L}^{0.5};\ \lambda_T = {\lambda_L}^{0.5} \tag{3.6}$$

$$\frac{F_m}{F_p} = \frac{W_m}{W_p} = {\lambda_L}^3 \tag{3.7}$$

If the model is constructed by following proper geometric and dynamic similarity ratios to the prototype, scale effects are negligible (Hughes, 1993). However, when the model structure is tested as non-fixed, mooring lines similitude needs to be examined carefully. Hughes (1993) indicates that scale effects could arise when the mooring line behavior is not exactly linear elastic. Scaling a mooring line that shows nonlinear elongation is difficult. Nevertheless, when the model mooring calibration is carried out, proper scaling could be achieved. Scale effect due to fresh water in the model and salty water in the prototype distinction is considered insignificant.

Model scale selection depends on lots of parameters. These could be laboratory conditions such as wave generator capacity, flume depth, width, and length. Hudson et al. (1979) declared that the floating breakwater model experiments' length scale should be between 1:6 and 1.27. In this study, the model length scale was selected as 1:10 by considering material manufacturability and wave generator capacity. Photos of the prototype and model of the horizontal floating platform can be seen in Figure 3.2.

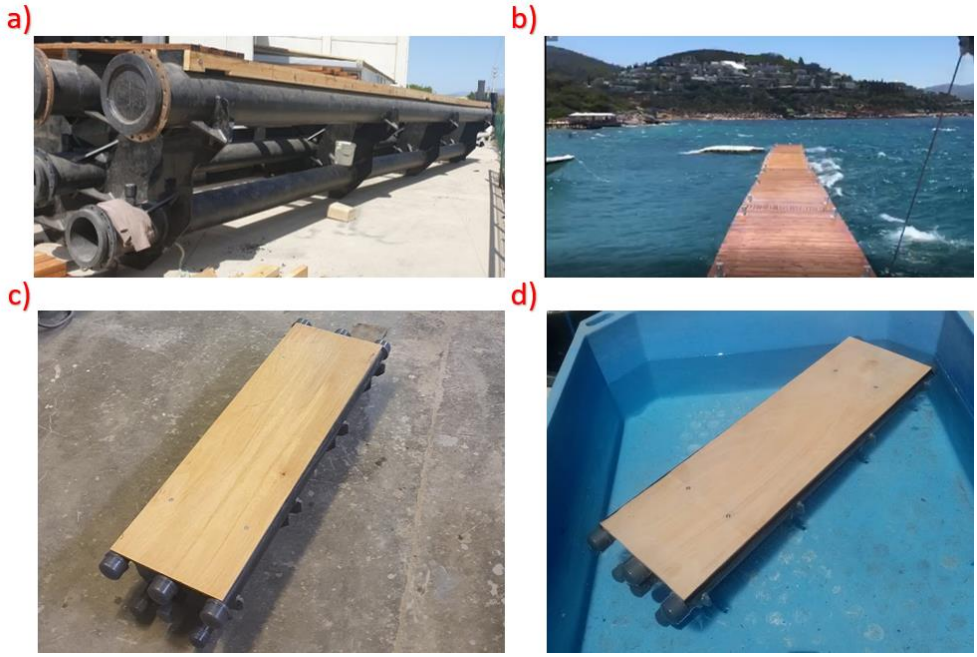

Figure 3.2: a) Prototype photo on the land b) Prototype view in the sea c) Model view on the ground d) Model photo in a flotation tank

3.3 Experimental Setup

Floating platform wave transmission performance experiments were conducted in two different flumes in METU Coastal and Ocean Engineering Laboratory.

3.3.1 Irregular Wave Flume

The first experiment series was carried in a flume which has a piston-type wave generator and can generate user-defined time series such as irregular and regular, solitary wave series (Figure 3.3). In this flume transmission performance of the floating platform was tested under irregular wave series. The flume has 26 meters in length, 6 meters in width, and 1-meter depth with a passive absorption system. There are two inner canals (0.6 and 0.9 m width) inside of the flume and the floating platform was tested in the 0.9-meter width canal. Wave properties were measured by probes (DHI type 202).

Figure 3.3: Irregular Wave Flume

Waves are generated by a single block piston-type wave maker (Figure 3.4). Input data is converted to analog data with the help of Moog SmarTEST ONE for irregular wave series generation. Piston type of wave maker moves only on one axis, back and forward to push the water column.

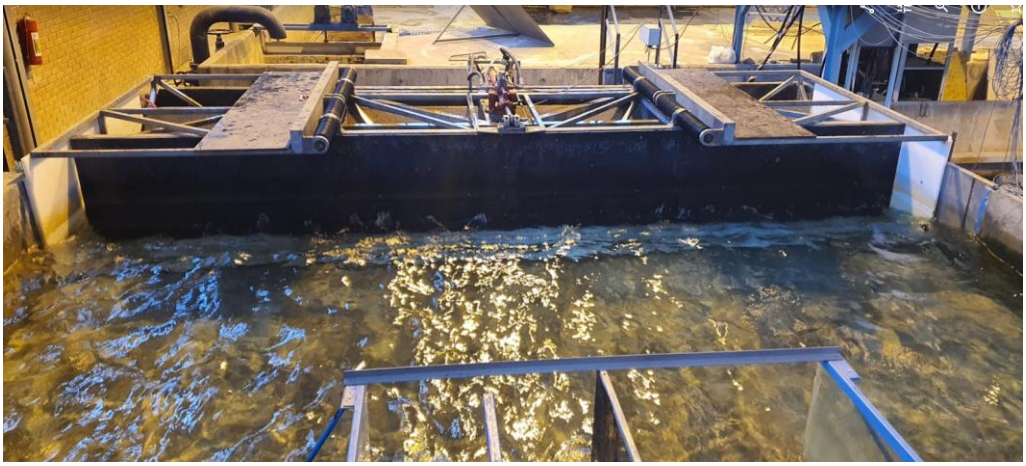

Figure 3.4:Piston Type Wave Generator

The layout of the flume can be seen in Figure 3.5. There were 9 probes in the flume, they were placed in 3 groups and each group has 3 probes. RNJ probes were located in the channel in which there is no structure and aligned to the platform position. IEH group was placed in an offshore direction 230 cm away from the floating platform and the AGB group was located at the rear side, and there is 153 cm to the platform. Moreover, the IEH probe group has a 1200,5 cm distance from the wave generator.

For random wave series, time domain, spectral, and reflection analysis are carried out by the MATLAB tool which was developed in METU, Coastal, and Ocean Engineering Research Centre. The method of reflection analysis is adopted from Mansard and Funke (1980) and 3 probes are placed at a certain distance from each other. After the setup is prepared, the wave calibration process was started and targeted wave parameters were obtained such as significant wave height (H_s), spectral significant wave height (H_{m0}), spectral mean wave period ($T_{m-1,0}$), significant wave period (T_s), and spectral peak wave period (T_p).

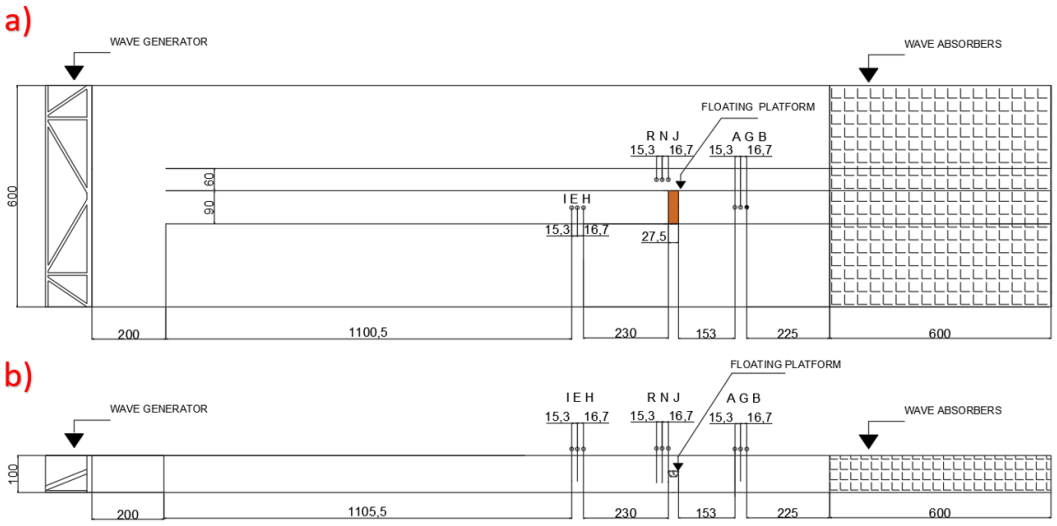

Figure 3.5:Layout of Experimental Setup for Irregular Wave Channel (Dimensions are given in centimeters. a) Top View b) Side View)

The floating platform was fixed to the flume during experiments. Two vertical steel bars were used to hold the structure to resist surge, sway, heave, roll, pitch, and yaw (Figure 3.6). Steel bars reach up to the bottom of the structure to have good clenching. Instead of anchoring the model from the bottom of the flume, it was anchored from the top edge to eliminate any potential turbulence forces caused by the vertical steel legs (Figure 3.7).

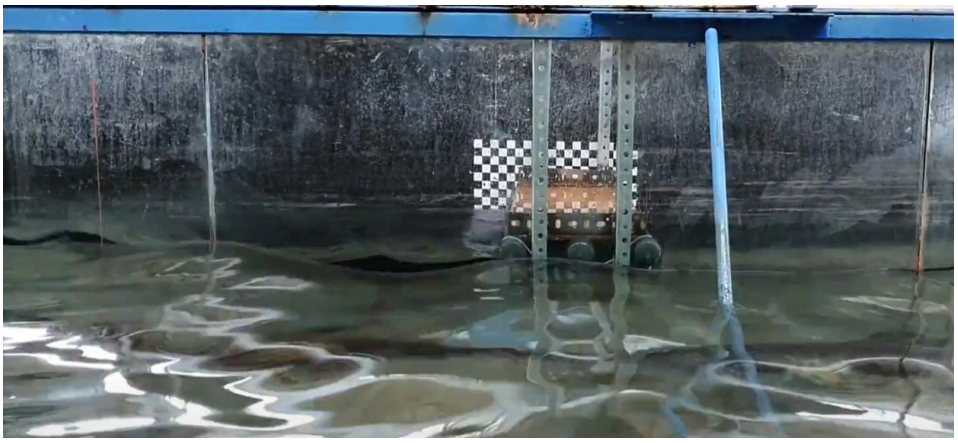

Figure 3.6: Anchored Floating Platform in Irregular Wave Flume (Side View)

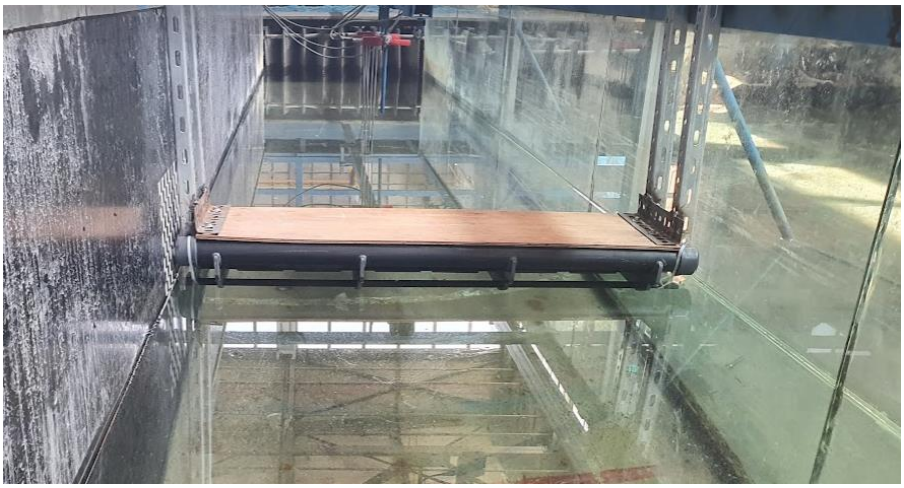

Figure 3.7: Anchored Floating Platform in Irregular Wave Flume (Frontal View)

3.3.2 Regular Wave Flume

The second experiment series was carried out in a flume shown in Figure 3.8, equipped with a paddle-type wave generator (Figure 3.9). In this flume transmission performance of the floating platform was tested under regular wave series. The flume has 26.5 meters in length, 6 meters in width, and 1-meter depth with a passive absorption system. There are two inner canals (0.7 and 1 m width) inside of the flume and the floating platform was tested in a 1-meter width canal. The desired displacement of the paddle was adjusted manually by changing the arm length of the paddle. The speed of the paddle is controlled by a dial box.

Figure 3.8:Regular Wave Flume

Figure 3.9: Paddle Type Wave Maker

The layout of a regular wave flume can be seen in Figure 3.10. There were 9 probes as in irregular wave flume, they were placed in 3 groups and each group has 3 probes. BGR probes were located in the channel in which there is no structure. CAK group was placed in an offshore direction 230 cm away from the floating platform and the DHN group was located at the rear side, and there is 153 cm to the platform. Moreover, the BGR probe group has a 748 cm distance from the wave generator.

For regular wave series, time domain wave characteristic analysis was carried out by MATLAB tool developed in the scope of this study. After the setup is completed, the wave calibration process was started, and targeted mean zero-up and down crossing wave characteristics were obtained.

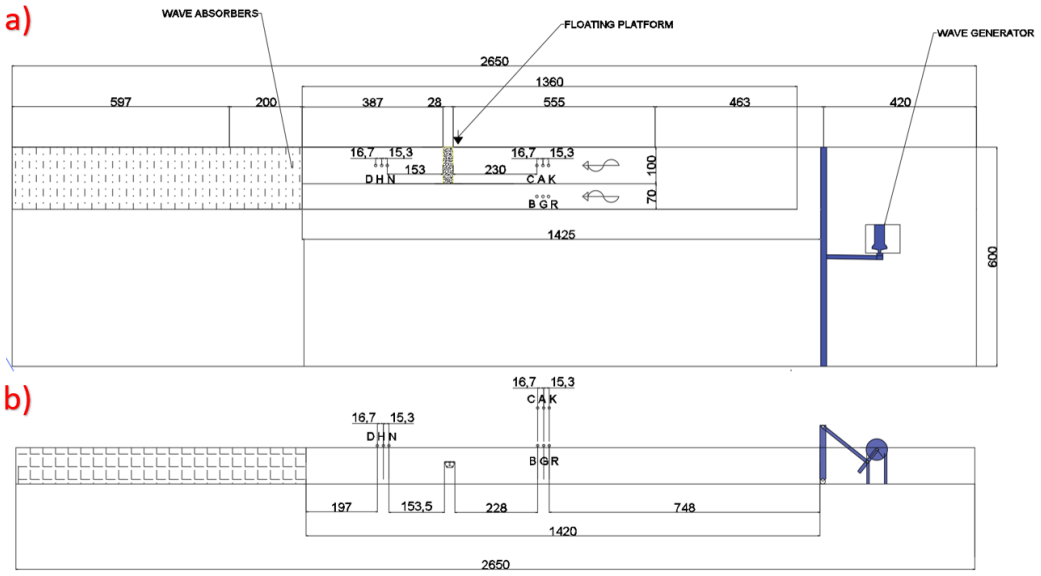

Figure 3.10: Layout of Experimental Setup for Regular Wave Channel (Dimensions are given in centimeters. a) Top View b) Side View)

3.4 Wave Sets

As mentioned in Section 3.3, experiments were carried out in two different wave flumes. The first experiment series aimed to inspect the transmission coefficient (H_t/H_i) of the floating platform under irregular waves. Furthermore, wave number (N) was selected as 1000 waves. Second experiments were conducted under regular wave series and the wave number was determined as 10 waves to minimize the effects of wave reflection inside the flume.

In the irregular wave flume experiments, reflection analysis is conducted. However, in the regular wave flume, there is no reflection analysis so measurements are taken from the channel in which there is no structure. Additionally, in a regular wave flume, the first 10 waves were considered for the

frontal wave gauge as it was observed that reflections from the fixed structure had not yet begun. Also, for the wave gauge located at the rear of the structure, the transmitted waves were not affected by the waves reflecting off the wall at the end of the flume in that period.

A fixed notation for wave sets is used in the forthcoming sections 3.4.1 and 3.4.2. In this notation system, D represents waves with a wave steepness of 0.042, while W represents waves with a wave steepness that varies between 0.01 and 0.05. For regular waves, the mean wave steepness (s_m) is used as a measure, and for irregular waves, the spectral wave steepness ($s_{m-1,0}$) is adopted. Moreover, letters I and R were used to distinguish wave series types as 'I'rregular and 'R'egular waves. Lastly, water depths 40, 50, and 60 cm also were included in wave name notation. Overall in the irregular wave flume, 18 experiments were conducted while in the regular wave flume, 110 experiments were carried out.

3.4.1 Irregular Wave Sets

To have a comprehensive wave transmission analysis, wave sets were organized to consider a variety of wave steepness (s_m) in different water depths. As shown in Table 3.1, the floating platform was tested under three waves (D1, D2, and D3) which have different periods (model values are 0.79, 1.11, 1.42 s) and constant wave steepness ($s_{m-1,0}$) $= 0.042$ in 40, 50 and 60 cm water depths. In these wave sets, overtopping was aimed just for D2 and D3 waves and the JONSWAP spectrum with a peak enhancement factor of $\gamma = 3.3$ was applied to generate random wave series.

Table 3.1: Wave sets under irregular waves in 40, 50, and 60 cm water depth with a constant wave steepness (sm = 0.042)

		Prototype		Model	
Wave Name	**Wave Steepness** ($s_{m-1,0}$)	H_{m0} *(m)*	$T_s(s)$	H_{m0} *(cm)*	$T_s(s)$
I40-D1	0.042	0.41	2.5	4.05	0.79
I40-D2	0.042	0.72	3.5	7.22	1.11
I40-D3	0.042	1.03	4.5	10.28	1.42
I50-D1	0.042	0.41	2.5	4.08	0.79
I50-D2	0.042	0.76	3.5	7.55	1.11
I50-D3	0.042	1.1	4.5	11.04	1.42
I60-D1	0.042	0.41	2.5	4.09	0.79
I60-D2	0.042	0.78	3.5	7.76	1.11
I60-D3	0.042	1.17	4.5	11.65	1.42

In the second part of the experiments, the wave sets were prepared considering wave steepness ($s_{m-1,0}$) change in 50 cm water depth (Table 3.2). Unlike Table 3.1, wave heights were kept constant at 6 cm and wave periods had a range between 0.89 to 2.85 seconds. In these wave sets, overtopping was not aimed, but there is run-up behavior due to reflected wave according to wave period (higher reflection for shorter waves).

Table 3.2:Wave sets under irregular waves in 50 cm water depth with varying wave steepness between 0.01-0.05.

		Prototype		**Model**	
Wave Name	**Wave Steepness**	**Water Depth= 5 m**		**Water Depth= 50 cm**	
		H_{m0} *(m)*	$T_s(s)$	H_{m0} *(cm)*	$T_s(s)$
I50-W1	0.01	0.60	9	6	2.85
I50-W2	0.015	0.60	6.3	6	1.99
I50-W3	0.02	0.60	5	6	1.58
I50-W4	0.025	0.60	4.25	6	1.34
I50-W5	0.03	0.60	3.75	6	1.19
I50-W6	0.035	0.60	3.4	6	1.08
I50-W7	0.04	0.60	3.15	6	1.00
I50-W8	0.045	0.60	2.95	6	0.93
I50-W9	0.05	0.60	2.8	6	0.89

3.4.2 Regular Wave Sets

Wave sets were divided into two groups following the same ideas in Section 3.4.1. Three waves were tested (D1, D2, and D3) which have different periods (0.79, 1.11, 1.42 s) and constant mean wave steepness ($sm = \frac{H}{L} = 0.042$) at 40, 50, and 60 cm water depths (Table 3.3).

Table 3.3:Wave sets under regular waves in 40, 50, and 60 cm water depth with a constant wave steepness (0.042 sm)

		Prototype		Model	
Wave Name	**Wave Steepness (s_m)**	**H_m (m)**	**$T_m(s)$**	**H_m (cm)**	**$T_m(s)$**
R40-D1	0.042	0.41	2.5	4.05	0.79
R40-D2	0.042	0.72	3.5	7.22	1.11
R40-D3	0.042	1.03	4.5	10.28	1.42
R50-D1	0.042	0.41	2.5	4.08	0.79
R50-D2	0.042	0.76	3.5	7.55	1.11
R50-D3	0.042	1.1	4.5	11.04	1.42
R60-D1	0.042	0.41	2.5	4.09	0.79
R60-D2	0.042	0.78	3.5	7.76	1.11
R60-D3	0.042	1.17	4.5	11.65	1.42

In the second part of regular wave experiments, wave sets were formed regarding the variety of wave steepness (s_m) in 40, 50, and 60 cm water depths (Table 3.4).

Table 3.4: Wave sets under regular waves in 40, 50, and 60 cm water depth with varying wave steepness between 0.01-0.05.

		Prototype		Model	
Wave Name	**Wave Steepness (s_m)**	**H_m (m)**	**$T_m(s)$**	**H_m (cm)**	**$T_m(s)$**
R40-W3	0.02	0.6	5.3	6	1.68
R40-W4	0.025	0.6	4.43	6	1.4
R40-W5	0.03	0.6	3.88	6	1.23
R40-W6	0.035	0.6	3.49	6	1.1
R40-W7	0.04	0.6	3.21	6	1.02

Table 3.4(continued)

R40-W8	0.045	0.6	2.99	6	0.95
R40-W9	0.05	0.6	2.82	6	0.89
R50-W3	0.02	0.6	5	6	1.58
R50-W4	0.025	0.6	4.25	6	1.34
R50-W5	0.03	0.6	3.75	6	1.19
R50-W6	0.035	0.6	3.4	6	1.08
R50-W7	0.04	0.6	3.15	6	1
R50-W8	0.045	0.6	2.95	6	0.93
R50-W9	0.05	0.6	2.8	6	0.89
R60-W3	0.02	0.6	4.75	6	1.5
R60-W4	0.025	0.6	4.09	6	1.29
R60-W5	0.03	0.6	3.66	6	1.16
R60-W6	0.035	0.6	3.36	6	1.06
R60-W7	0.04	0.6	3.12	6	0.99
R60-W8	0.045	0.6	2.93	6	0.93
R60-W9	0.05	0.6	2.78	6	0.88

3.5 Experimental Cases

During physical model experiments, the performance of three types of floating structures was tested: a rectangular box, a single horizontal cylinder (Case 1, 2, and 3), and a dual horizontal cylinder (Table 3.5). The rectangular box and dual horizontal cylinder were only tested at a water depth of 50 cm with all types of regular waves and without any changes made to the structures. The transmission performance of the horizontal cylinder floating platforms was evaluated under both regular and irregular waves at water depths of 40, 50, and 60 cm.

Table 3.5 Summary of experimental cases

Structure Type	Wave Condition	Water Depth
Box	Regular	50 cm
Case 1	Irregular and Regular	40, 50, and 60 cm
Case 2	Regular	40, 50, and 60 cm
Case 3	Regular	40, 50, and 60 cm
Dual Case 2	Regular	50 cm

3.5.1 Box Type Floating Breakwater

The box-type floating breakwater was considered as a simple case for comparison purposes with the horizontal cylinders floating platform. Moreover, this case was used for CFD validation purposes. As shown in Figure 3.11 all structural dimension of the box was adopted from the floating platform such as structure height, draft, freeboard, and width. The fixed system is the same as the previous model as can be seen in Figure 3.12. Additionally, box-type of floating breakwater experiments were conducted at 50 cm water depth.

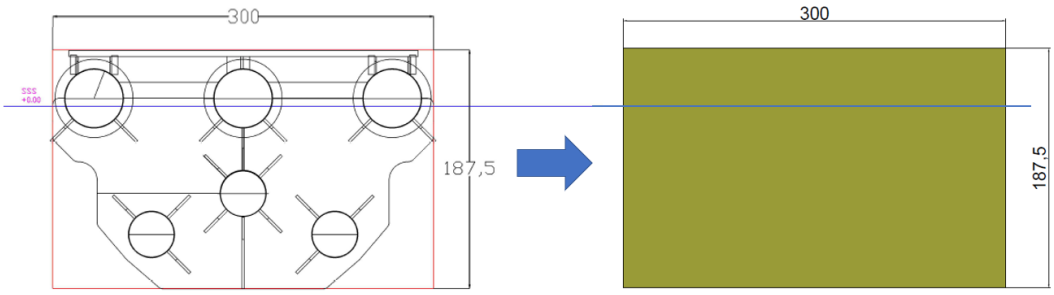

Figure 3.11: Box Type Floating Platform Model Cross-Section Dimensions. (All dimensions given in the figure are in millimeters.)

Figure 3.12: Box Floating Platform Model Front View

3.5.2 Horizontal Cylinder Type of Floating Platform

A horizontal floating platform consisting of 6 horizontally placed pipes along the axis of the floating structure. These three cylinders are located on the water's surface and three are under the water.

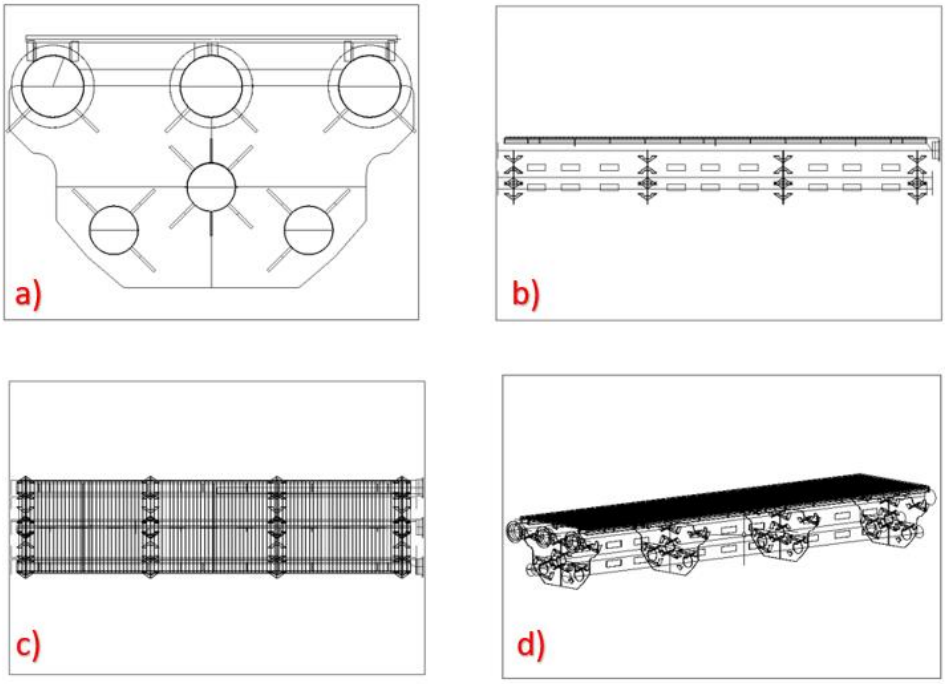

Figure 3.13: a) Side view of the model b) Front c) Plan d) 3D view

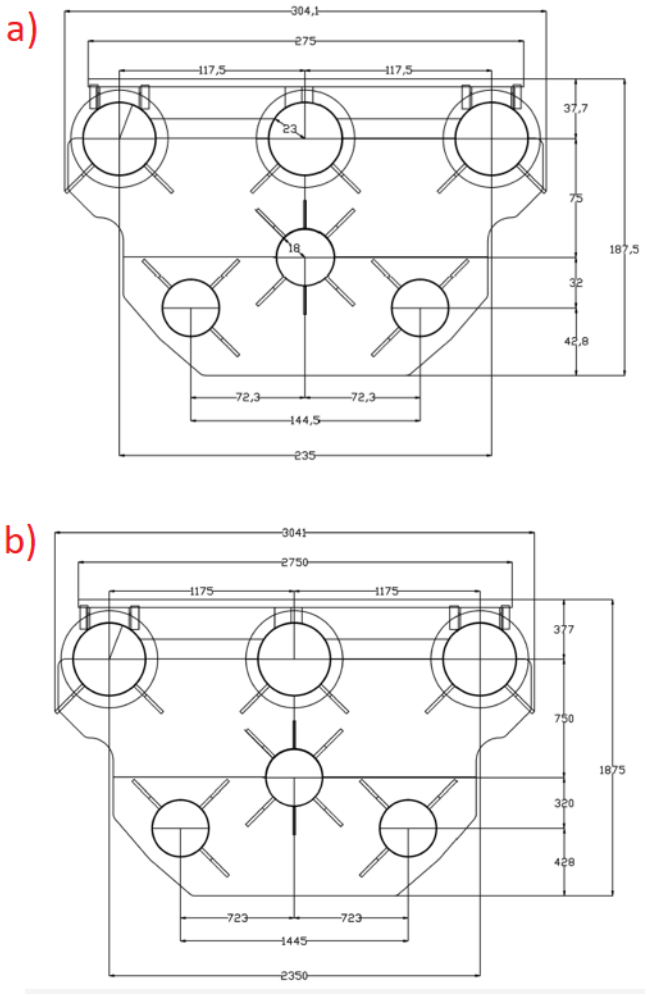

Figure 3.14: a) Floating platform model dimensions b) Floating platform prototype dimensions. (All dimensions given in the figure are in millimeters.)

The model dimensions of the floating platform are shown in Figure 3.14-a and the prototype dimensions are shown in Figure 3.14-b. In a platform consisting of 6 pipes in total, three large pipes have a radius of 23 mm in the model scale, while the other three have a radius of 18 mm. The horizontal distance between the large radius pipes is 117.5 mm, while the small radius pipes are placed at 72.3 mm intervals. Large radius pipes are all in the same horizontal axis, two of the small radius pipes are positioned in the same horizontal axis and the other one is 32 mm above them and its center is in the middle of the two.

3 cases are considered for the draft arrangements.

i) No screen (Case 1)

ii) Short screen (Case 2)

iii) Long screen (Case 3)

3.5.2.1 Floating Platform with No Screen (Case 1)

In Case 1, the floating platform was tested without a screen as can be seen in Figure 3.15 and Figure 3.16. The freeboard which is a vertical distance between the still water level (SWL +0.00) to the top of the structure was kept at 4.4 cm in all model scale experiments. Furthermore, tests were conducted at 40, 50, and 60 cm water depths under all wave sets (both regular and irregular). In the vertical direction, a plate was fixed between the middle large pipe and the middle small pipe to block the gap. The blocking plate reached up to 50.7 mm under SWL.

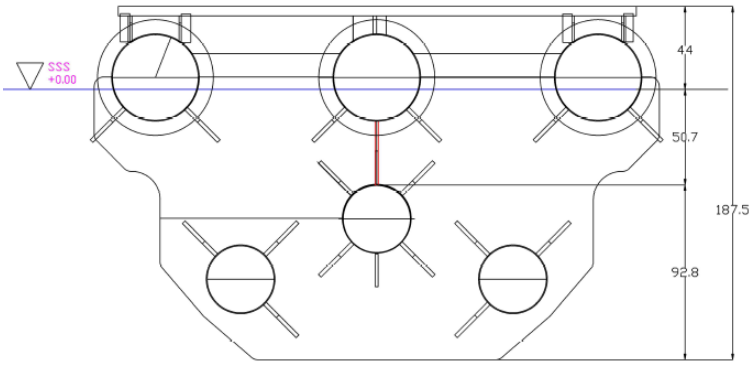

Figure 3.15: Floating Platform Case1 Model Cross-Section Dimensions. (All dimensions given in the figure are in millimeters.)

Figure 3.16: Floating Platform Case1 Model Front View

3.5.2.2 Floating Platform with Short Screen (Case 2)

Case 2 experiments were performed with a short screen as can be seen in Figure 3.17 and Figure 3.18. The freeboard was adjusted to 4.4 cm in model scale and experiments were conducted in 40, 50, and 60 cm water depth under all wave sets. The blocking plate reached up to 143.5 mm under SWL and the structure height is 187.5 mm.

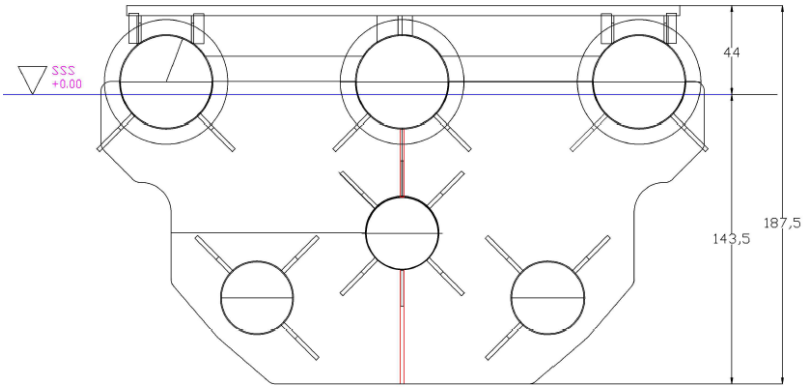

Figure 3.17: Floating Platform Case2 Model Cross-Section Dimensions. (All dimensions given in the figure are in millimeters.)

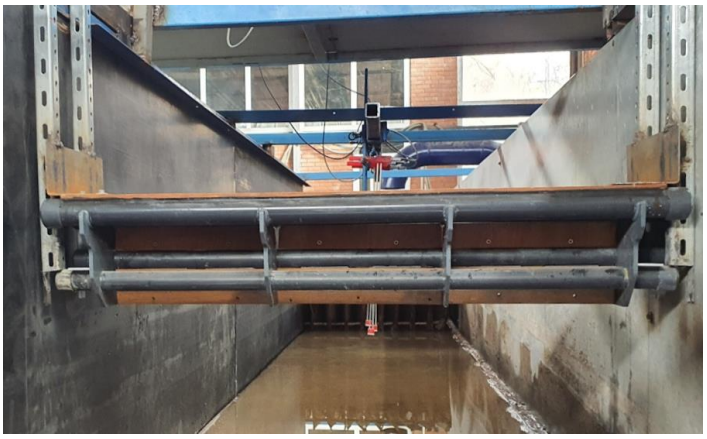

Figure 3.18: Floating Platform Case 2 Model Front View

3.5.2.3 Floating Platform with Long Screen (Case 3)

In this Case 3 experiments large screen was used as can be seen from Figure 3.19 and Figure 3.20. The freeboard was adjusted to 4.4 cm in model scale and experiments were conducted in 40, 50, and 60 cm water depth under all wave sets. The blocking plate reached up to 233.5 mm and the structure height is 277.5 mm.

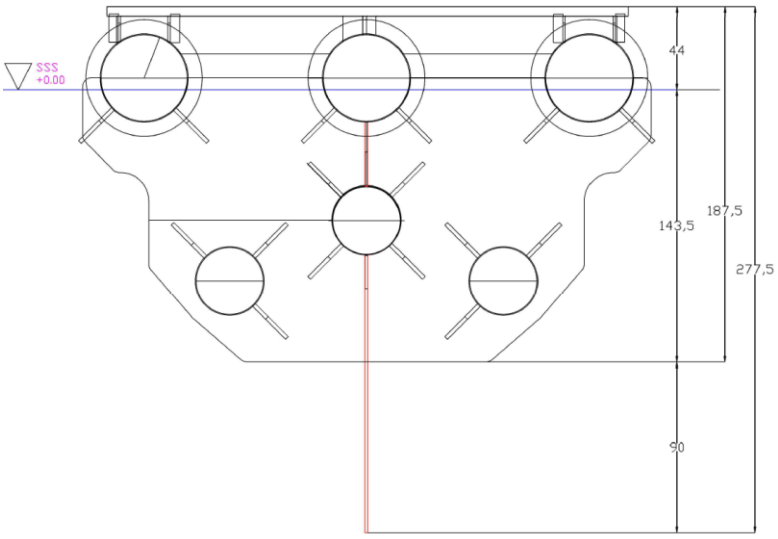

Figure 3.19: Floating Platform Case3 Model Cross-Section Dimensions. (All dimensions given in the figure are in millimeters.)

Figure 3.20: Floating Platform Case 3 Model Front View

3.5.2.4 Dual Floating Platform with Short Screen (Dual Case 2)

Dual floating platform experiments were also carried out by placing two Case 2 types of structures side by side (Figure 3.21 and Figure 3.22). Both structures were fixed to the flume wall and each other to compensate for the wave action on the structure. The distance between the two structures was determined by considering the prototype scale applicability. Therefore, according to the suggestion of the manufacturer company 200 millimeters in model scale and 2 meters in prototype, a gap was applied to prevent any collision. Dual Case 2 experiments were carried out at 50 cm water depth.

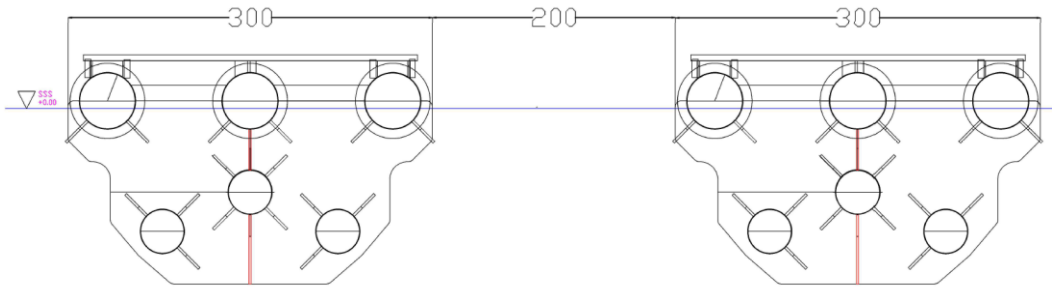

Figure 3.21: Dual Floating Platform with Short Screen Model Cross-Section Dimensions. (All dimensions given in the figure are in millimeters.)

Figure 3.22: Dual Floating Platform Model Front View

CHAPTER 4

RESULTS OF EXPERIMENTS

The floating platforms were tested under irregular and regular waves. Therefore, transmission results are divided into two sections. Before starting the experiments wave calibration process is conducted. Then, targetted wave characteristics are calibrated and after each experiment is completed, results are analyzed. Moreover, In this chapter multi regression studies are carried out for different cases.

4.1 Wave Measurements

As a representative example, regular wave measurement results for Case 1 are presented in Table 4.1. While carrying out wave measurement, the mean value approach is used for wave height and period.

Table 4.1:Measured and targeted wave characteristics for Case1 wave conditions (given in model scale).

	Target		Measured	
Wave Name	H_m (cm)	$T_m(s)$	H_m (cm)	$T_m(s)$
R40-D1	4.05	0.79	4.1	0.8
R40-D2	7.22	1.11	7.2	1.11
R40-D3	10.28	1.42	10.2	1.41
R50-D1	4.08	0.79	4.12	0.79
R50-D2	7.55	1.11	7.45	1.11
R50-D3	11.04	1.42	11.13	1.41
R60-D1	4.09	0.79	4.02	0.8
R60-D2	7.76	1.11	7.53	1.11
R60-D3	11.65	1.42	11.4	1.42

Table 4.1 (continued)

R40-W3	6	1.68	5.8	1.62
R40-W4	6	1.4	5.8	1.36
R40-W5	6	1.23	6.2	1.20
R40-W6	6	1.1	6.1	1.12
R40-W7	6	1.02	6	1.02
R40-W8	6	0.95	6.3	0.94
R40-W9	6	0.89	6.2	0.89
R50-W3	6	1.58	5.7	1.55
R50-W4	6	1.34	6	1.32
R50-W5	6	1.19	6.2	1.2
R50-W6	6	1.08	6.1	1.1
R50-W7	6	1	6.1	1
R50-W8	6	0.93	5.9	0.95
R50-W9	6	0.89	5.9	0.9
R60-W3	6	1.5	6.3	1.47
R60-W4	6	1.29	6.1	1.3
R60-W5	6	1.16	6	1.17
R60-W6	6	1.06	6	1.1
R60-W7	6	0.99	5.8	1
R60-W8	6	0.93	5.7	0.92
R60-W9	6	0.88	6	0.88

4.2 Multiple Regression Analysis

Multiple regression is a technique employed to understand the association between a dependent variable and one or more independent variables. The objective of multiple regression is to discover the optimal linear combination of the independent variables that can predict the dependent variable. This approach assumes a linear association between the independent variables and the dependent variable and can be utilized to examine the relative significance of each independent variable in describing the variation in the dependent variable. In this study, the multiple regression method was applied to analyze the strength of the relationship between a transmission coefficient (Kt) and dimensionless parameters which are stated in

Section 3.1. The relation between the single dependent variable and several independent variables was investigated by the MATLAB multiple regression tool.

In this study, the dependent variable is stated as the transmission coefficient (Kt) and the independent variables are considered as $\frac{B}{L}, \frac{d}{L}, \frac{H}{L}, \frac{D}{d}$. According to these variables Eq. (4.1) can be given.

$$Kt = a\left(\frac{B}{L}\right)^{x}\left(\frac{d}{L}\right)^{y}\left(\frac{H}{L}\right)^{z}\left(\frac{D}{d}\right)^{w} \tag{4.1}$$

In Eq. (4.1) *a, x, y,* and *z* are the weights that are the output of multiple regression analysis. Alternative representations of (4.1) can be seen in (4.2) and (4.3).

$$\ln(Kt) = ln\left[a\left(\frac{B}{L}\right)^{x}\left(\frac{d}{L}\right)^{y}\left(\frac{H}{L}\right)^{z}\left(\frac{D}{d}\right)^{w}\right] \tag{4.2}$$

$$\ln(Kt) = \ln(a) + x * ln\left(\frac{B}{L}\right) + y * ln\left(\frac{d}{L}\right) + z * ln\left(\frac{H}{L}\right) + w * ln\left(\frac{D}{d}\right) \tag{4.3}$$

4.3 Regression Model Evaluation Metrics

In this study evaluation metrics are used to evaluate how developed formulas by multiple regression method or numerical model results correlate with experimental results.

As regression model evaluation metrics MAE, RMSE, and Adjusted R squared are used (4.4), (4.5), and (4.6) respectively.

The mean absolute error is a regression model which measures the mean absolute difference between the actual values and the predicted values.

$$\text{MAE} = \frac{\sum_{i=1}^{N} |prediction - true\ value|}{N} \tag{4.4}$$

Root Mean Square Error (RMSE) is the residuals' standard deviation (prediction errors). The distance between the data points and the regression line is measured by residuals, and the spread of these residuals is measured by RMSE.

$$\text{RMSE} = \sqrt{\frac{\sum_{i=1}^{N}(prediction_i - true\ value_i)^2}{N}}, \tag{4.5}$$

R-squared values always rise as more independent variables are included. The R^2 scores of the model are affected when the redundant variables are included. This issue is resolved by the corrected R-squared. When significant factors are added, the values of the adjusted R squared rise; when insignificant variables are added, they fall.

$$\text{Adjusted R squared} = 1 - \frac{(1 - R^2)(N - 1)}{N - p - 1} \tag{4.6}$$

In these equations, *N* represents the total sample size and p is the number of the independent variable.

4.4 Wave Transmission Results Under Irregular Waves

Irregular wave cases are separated into two categories regarding the constant and varying wave steepness for Case 1. Multiple regression analysis is conducted and the representative formula is developed for Case 1 under the irregular wave conditions.

4.4.1 Wave Transmission Results for No Screen (Case 1)

Irregular wave transmission results in which the waves have constant steepness (0.042) at 40, 50, and 60 cm water depths for three different wave characteristics (D1, D2, and D3) can be seen in Table 4.2. The highest *Kt* value was measured in I60-D3 (0.82) and the lowest in I40-D1 (0.53). In general, as the water depth increases, the *Kt* value also increases.

Table 4.2: Irregular waves transmission result for Case 1 in 40, 50, and 60 cm water depth with a constant wave steepness (*sm* = 0.042)

		Prototype		Model		
Wave Name	**Wave Steepness (s_m)**	**H_{m0} (m)**	**$T_s(s)$**	**H_{m0} (cm)**	**$T_s(s)$**	***Kt***
I40-D1	0.042	0.41	2.5	4.05	0.79	**0.53**
I40-D2	0.042	0.72	3.5	7.22	1.11	**0.71**
I40-D3	0.042	1.03	4.5	10.28	1.42	**0.79**
I50-D1	0.042	0.41	2.5	4.08	0.79	**0.55**
I50-D2	0.042	0.76	3.5	7.55	1.11	**0.73**
I50-D3	0.042	1.1	4.5	11.04	1.42	**0.81**
I60-D1	0.042	0.41	2.5	4.09	0.79	**0.55**
I60-D2	0.042	0.78	3.5	7.76	1.11	**0.75**
I60-D3	0.042	1.17	4.5	11.65	1.42	**0.82**

The results of transmission of the waves have varying steepness cases at 50 cm water depth for nine wave characteristics given in Table 4.3 which demonstrates the significant impact of wave period on *Kt* values. As the wave period increases, the *Kt* value increases. The lowest *Kt* value (0.57) was found at a wave period of 0.89, while the highest value (0.94) was observed at a wave period of 2.85 in the model scale.

Table 4.3: Irregular waves transmission result for Case 1 in 50 cm water depth with varying wave steepness between 0.01-0.05.

		Prototype		**Model**		
Wave Name	**Wave Steepness (s_m)**	**Water Depth= 5 m**		**Water Depth= 50 cm**		
		H_{m0} (m)	**$T_s(s)$**	**H_{m0} (cm)**	**$T_s(s)$**	***Kt***
I50-W1	0.01	0.60	9	6	2.85	**0.94**
I50-W2	0.015	0.60	6.3	6	1.99	**0.92**
I50-W3	0.02	0.60	5	6	1.58	**0.89**
I50-W4	0.025	0.60	4.25	6	1.34	**0.86**

Table 4.3 (continued)

I50-W5	0.03	0.60	3.75	6	1.19	**0.78**
I50-W6	0.035	0.60	3.4	6	1.08	**0.74**
I50-W7	0.04	0.60	3.15	6	1.00	**0.69**
I50-W8	0.045	0.60	2.95	6	0.93	**0.62**
I50-W9	0.05	0.60	2.8	6	0.89	**0.57**

The structure's draft is kept the same and the platform is tested in three different depths for all wave conditions. Relative structure width and transmission coefficient relation are given in Figure 4.1 for $\frac{D}{d} = 0.2, 0.24, 0.3$. Highest Kt is measured as 0.94 for B/L = 0.05 and D/d =0.24 whereas the lowest Kt is 0.53 for B/L = 0.31, and D/d=0.3.

Throughout the thesis study, the cross-sectional view of the structures is provided in the figures showing the results of transmission coefficient with respect to relative width (B/L), relative depth (d/L), and wave steepness (H/L).

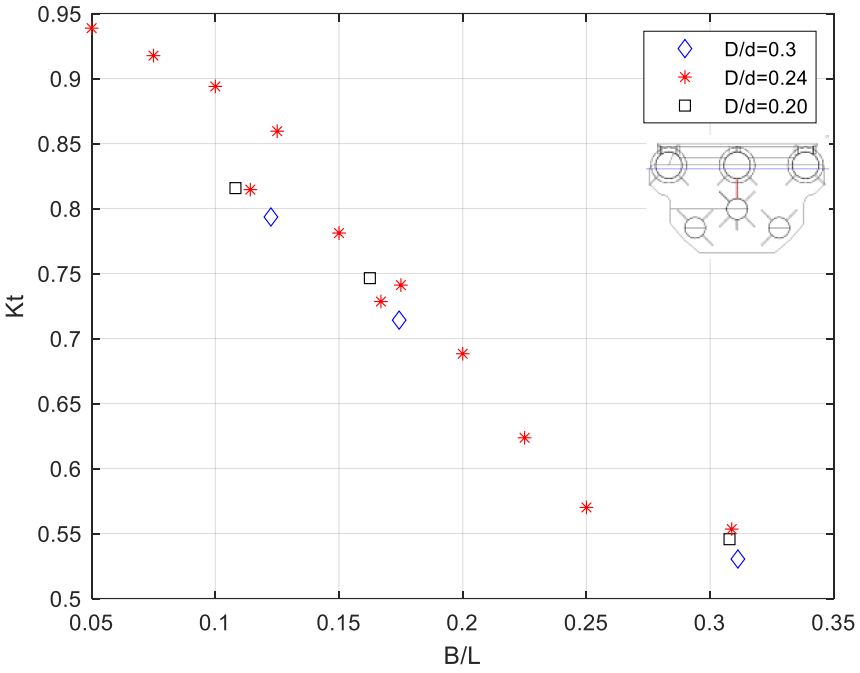

Figure 4.1: Change in the Transmission Coefficient of Case 1 with respect to Relative Structure Width *(B/L)*.

Relative depth and transmission coefficient relation are given in Figure 4.2 for $\frac{D}{d} = 0.2, 0.24, 0.3$. When d/L = 0.083 and D/d = 0.24, *Kt* gets the highest value of 0.94 and the lowest *Kt* is measured as 0.53 for d/L=0.41 and D/d = 0.3. However, for the highest d/L = 0.62, *Kt* gets a value of 0.55.

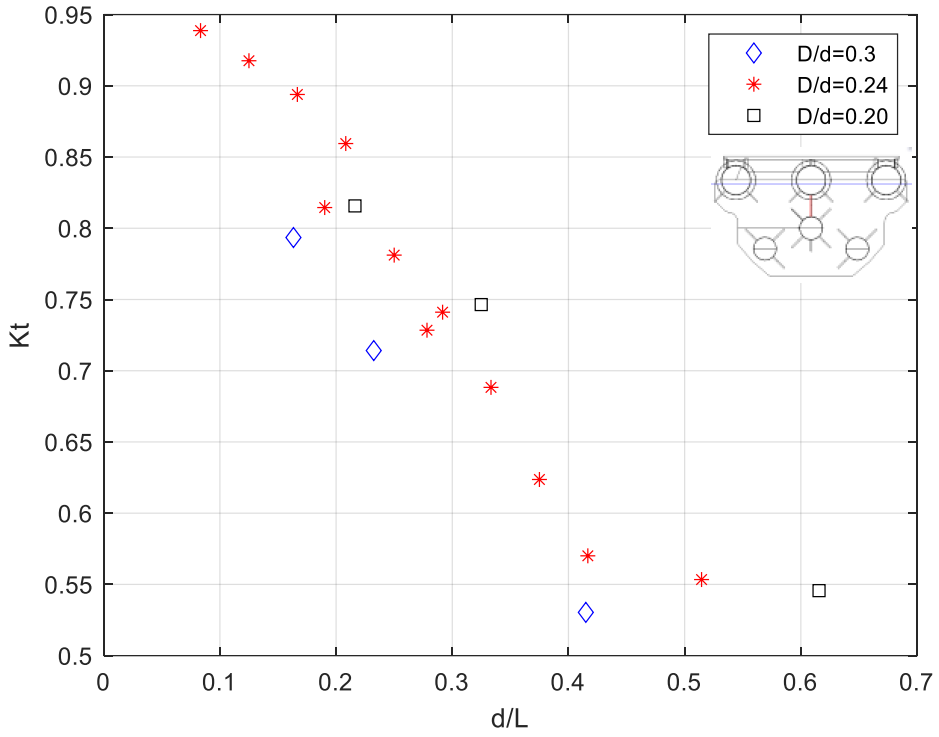

Figure 4.2: Change in the Transmission Coefficient of Case 1 with respect to Relative Depth (d/L).

Wave steepness and transmission coefficient relation are given in Figure 4.3 for $\frac{D}{d} =$ 0.24. When H/L = 0.01, *Kt* got the highest value of 0.94 and the lowest *Kt* is measured as 0.57 for H/L = 0.05.

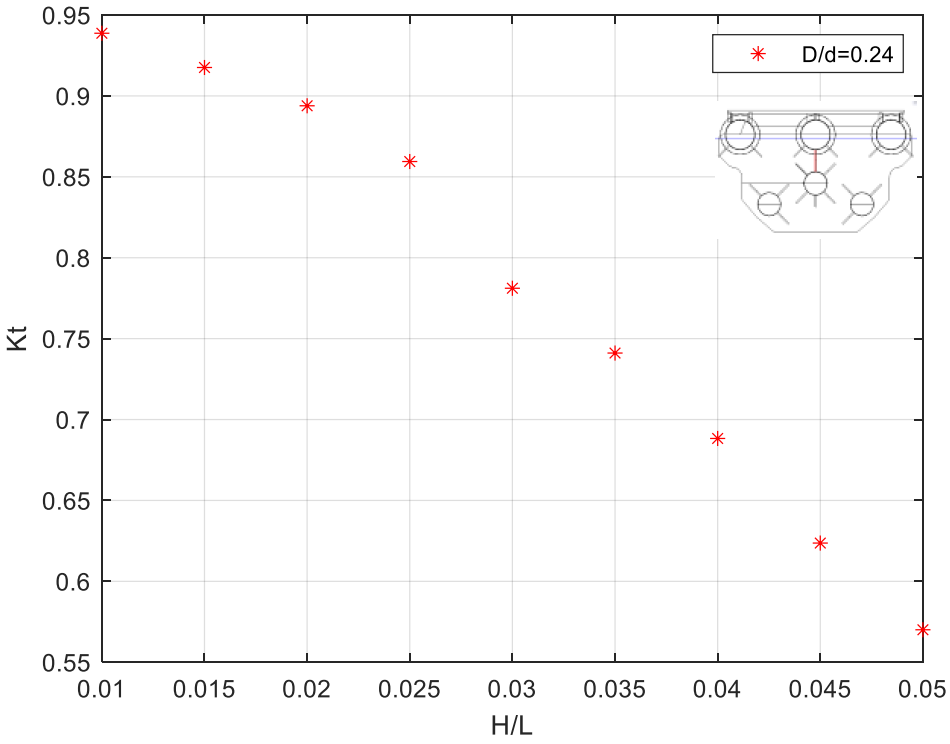

Figure 4.3: Change in the Transmission Coefficient of Case 1 with Wave Steepness (H/L).

4.4.1.1 Multiple Regression Analysis for Case 1

According to the method shown in Section 4.2, wave transmission formula for Case 1 under irregular waves is given in Eq. (4.7).

$$Kt = 0.53\left(\frac{B}{L}\right)^{-0.67}\left(\frac{d}{L}\right)^{0.27}\left(\frac{H}{L}\right)^{0.07}\left(\frac{D}{d}\right)^{0.23} \tag{4.7}$$

Measured and predicted *Kt* values are plotted as shown in Figure 4.4. Mean absolute error, root mean square error, and adjusted R-squared are calculated as 3.4%, 6.3%, and 0.88 respectively.

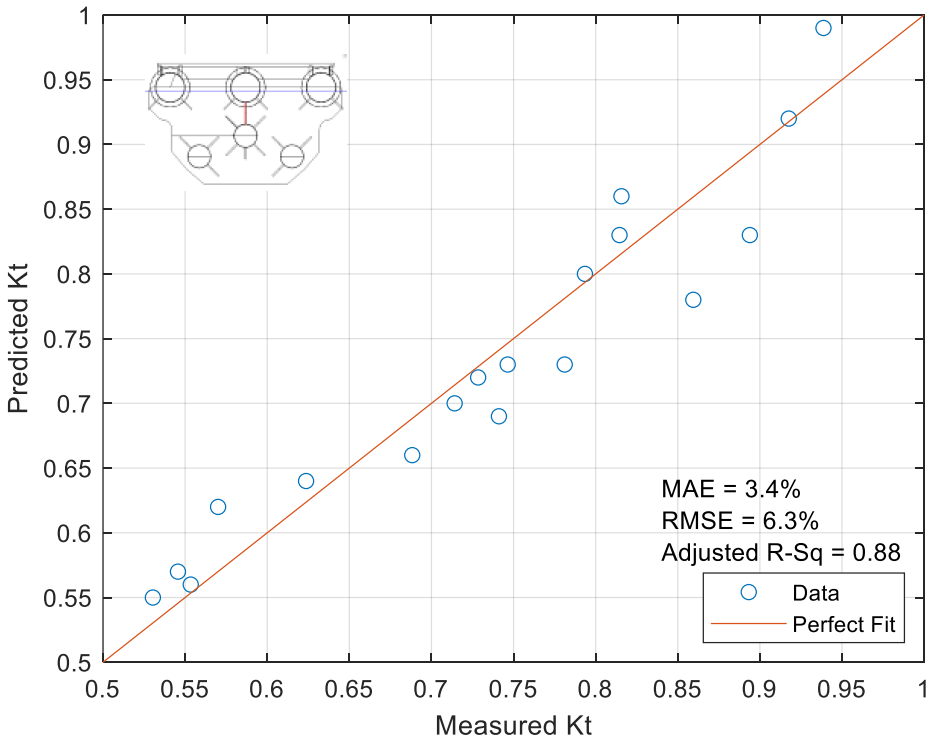

Figure 4.4:Measured and Predicted Kt Values Comparison.

4.5 Wave Transmission Results Under Regular Waves

In this section, three different structural cases were tested. As the irregular waves, regular wave cases also are separated into two categories regarding wave steepness. Multiple regression analysis is conducted and the representative formula is developed for Cases 1, 2, and 3 under regular wave conditions.

4.5.1 Wave Transmission Results for No Screen (Case 1)

Regular wave transmission results in which the waves have constant steepness (0.042) in 40, 50, and 60 cm water depth for three different wave characteristics (D1, D2, and D3) can be seen in Table 4.4. The *Kt* values for R40-D1, 2 and 3 and R50-D1, 2 and 3 are similar, while the *Kt* values for R60-D1, 2, and 3 are relatively

larger. The highest *Kt* value measured is in R60-D3 (0.81) and the lowest in R40-D1 (0.45).

Table 4.4: Regular waves transmission results for Case 1 in 40, 50, and 60 cm water depth with a constant wave steepness (*sm* = 0.042)

		Prototype		Model		
Wave Name	Wave Steepness (s_m)	H_m (m)	$T_m(s)$	H_m (cm)	$T_m(s)$	Kt
R40-D1	0.042	0.41	2.5	4.05	0.79	**0.45**
R40-D2	0.042	0.72	3.5	7.22	1.11	**0.67**
R40-D3	0.042	1.03	4.5	10.28	1.42	**0.77**
R50-D1	0.042	0.41	2.5	4.08	0.79	**0.48**
R50-D2	0.042	0.76	3.5	7.55	1.11	**0.66**
R50-D3	0.042	1.1	4.5	11.04	1.42	**0.76**
R60-D1	0.042	0.41	2.5	4.09	0.79	**0.52**
R60-D2	0.042	0.78	3.5	7.76	1.11	**0.73**
R60-D3	0.042	1.17	4.5	11.65	1.42	**0.81**

The results of transmission of the waves have varying steepness cases in 40, 50, and 60 cm water depth for seven wave characteristics (W3-W9) are given in Table 4.5 which shows the significant impact of wave period on *Kt* values for 3 different depths. As the wave period increases, the *Kt* value increases. The table shows that the lowest *Kt* value (0.57) was measured at a wave period of 0.89 for both R40-W9 and R60-W9, and the highest *Kt* value (0.93) was found at a wave period of 2.85 s in R60-W3 in the model scale.

Table 4.5: Regular waves transmission results for Case 1 in 40, 50, and 60 cm water depth with varying wave steepness between 0.02-0.05.

		Prototype		Model		
Wave Name	Wave Steepness (s_m)	H_m (m)	$T_m(s)$	H_m (cm)	$T_m(s)$	Kt
R40-W3	0.02	0.6	5.3	6	1.68	**0.90**
R40-W4	0.025	0.6	4.43	6	1.4	**0.80**
R40-W5	0.03	0.6	3.88	6	1.23	**0.72**
R40-W6	0.035	0.6	3.49	6	1.1	**0.69**

Table 4.5 (continued)

R40-W7	0.04	0.6	3.21	6	1.02	**0.67**
R40-W8	0.045	0.6	2.99	6	0.95	**0.61**
R40-W9	0.05	0.6	2.82	6	0.89	**0.57**
R50-W3	0.02	0.6	5	6	1.58	**0.88**
R50-W4	0.025	0.6	4.25	6	1.34	**0.82**
R50-W5	0.03	0.6	3.75	6	1.19	**0.77**
R50-W6	0.035	0.6	3.4	6	1.08	**0.71**
R50-W7	0.04	0.6	3.15	6	1	**0.65**
R50-W8	0.045	0.6	2.95	6	0.93	**0.60**
R50-W9	0.05	0.6	2.8	6	0.89	**0.58**
R60-W3	0.02	0.6	4.75	6	1.5	**0.93**
R60-W4	0.025	0.6	4.09	6	1.29	**0.80**
R60-W5	0.03	0.6	3.66	6	1.16	**0.78**
R60-W6	0.035	0.6	3.36	6	1.06	**0.74**
R60-W7	0.04	0.6	3.12	6	0.99	**0.70**
R60-W8	0.045	0.6	2.93	6	0.93	**0.66**
R60-W9	0.05	0.6	2.78	6	0.88	**0.57**

Relative structure width and transmission coefficient relation are given in Figure 4.5 for $\frac{D}{d} = 0.2, 0.24, 0.3$. Highest *Kt* is measured at 0.93 for B/L = 0.1 and D/d = 0.20, and the lowest *Kt* is measured at 0.45 for B/L = 0.31 and D/d = 0.3.

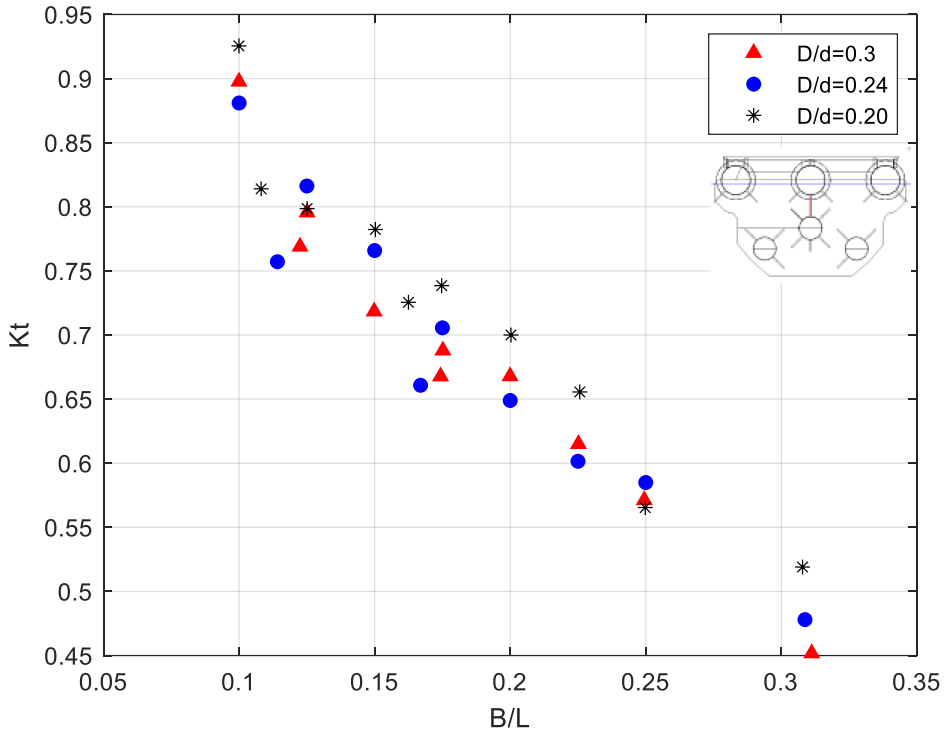

Figure 4.5: Change in the Transmission Coefficient of Case 1 with respect to Relative Structure Width (B/L).

Relative depth and transmission coefficient relation are given in Figure 4.6 for D/d = 0.2, 0.24, 0.3. When d/L = 0.20 and D/d = 0.20, Kt gets the highest value of 0.93 and the lowest Kt is measured as 0.45 for d/L = 0.41 and D/d = 0.3. However, for the highest d/L = 0.62, Kt gets 0.52.

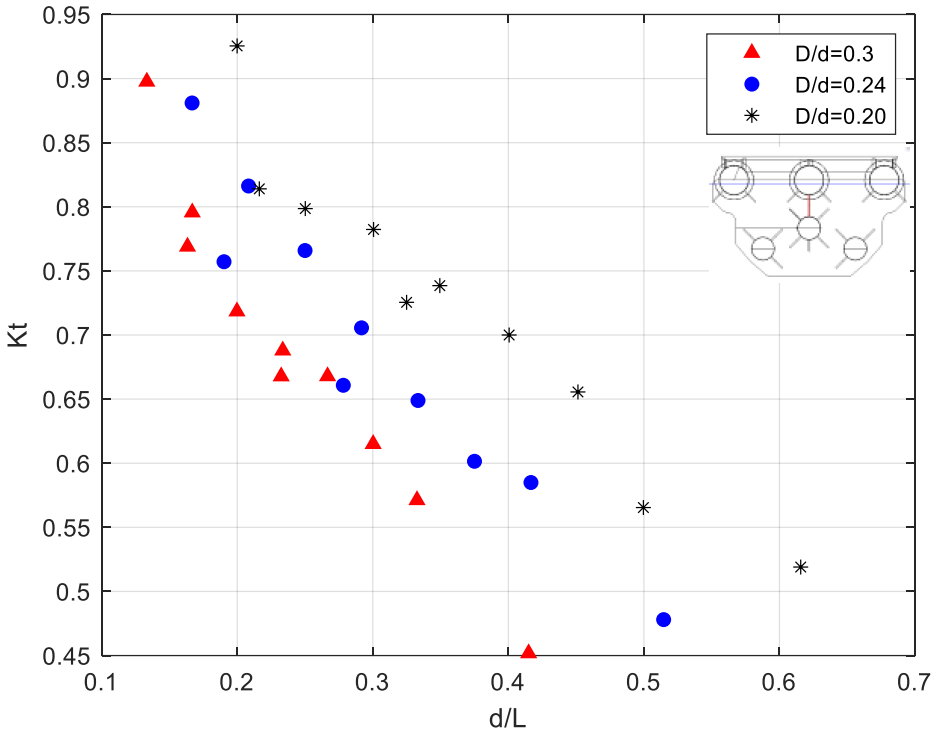

Figure 4.6: Change in the Wave Transmission Coefficient of Case 1 with respect to Relative Depth (d/L).

Wave steepness and transmission coefficient relation are given in

Figure 4.7 for D/d = 0.2, 0.24, 0.3. When H/L = 0.02 and D/d = 0.20, Kt gets the highest value of 0.93 and the lowest Kt is measured as 0.57 for H/L = 0.05 and D/d = 0.20.

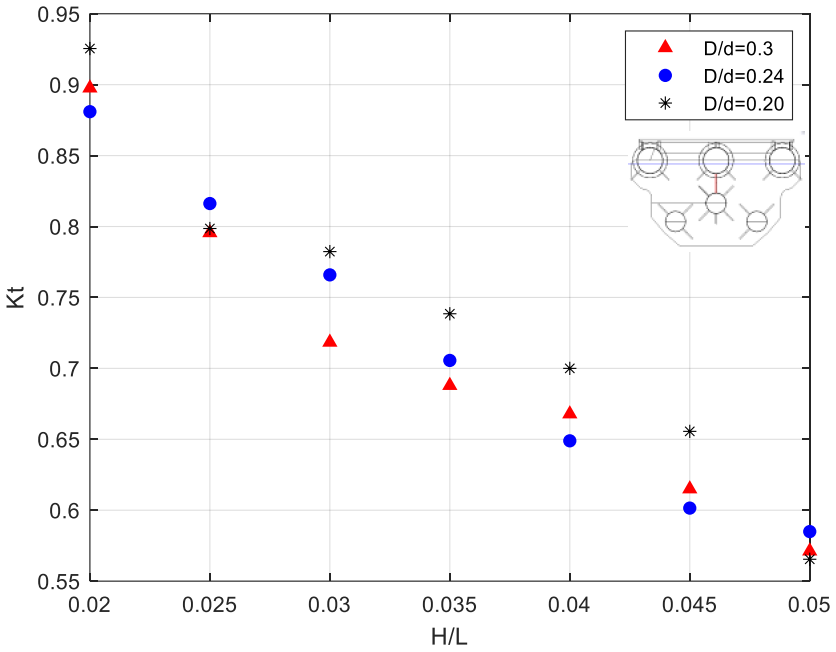

Figure 4.7: Change in the Wave Transmission Coefficient of Case 1 with Wave Steepness (H/L).

4.5.2 Wave Transmission Results for Short Screen (Case 2)

Regular wave transmission results in which the waves have constant steepness (0.042) in 40, 50, and 60 cm water depth for three different wave characteristics (D1, D2, and D3) can be seen in Table 4.6. *Kt* values are similar to each other for different depths, the highest *Kt* value measured at 0.77 in I60-D3 and the lowest at 0.34 in I60-D1.

Table 4.6: Regular waves transmission result for Case 2 in 40, 50, and 60 cm water depth with a constant wave steepness (*sm* = 0.042)

		Prototype		Model		
Wave Name	**Wave Steepness (s_m)**	**H_m (m)**	**$T_m(s)$**	**H_m (cm)**	**$T_m(s)$**	***Kt***
R40-D1	0.042	0.41	2.5	4.05	0.79	**0.37**
R40-D2	0.042	0.72	3.5	7.22	1.11	**0.56**

Table 4.6 (continued)

R40-D3	0.042	1.03	4.5	10.28	1.42	**0.75**
R50-D1	0.042	0.41	2.5	4.08	0.79	**0.37**
R50-D2	0.042	0.76	3.5	7.55	1.11	**0.63**
R50-D3	0.042	1.1	4.5	11.04	1.42	**0.74**
R60-D1	0.042	0.41	2.5	4.09	0.79	**0.34**
R60-D2	0.042	0.78	3.5	7.76	1.11	**0.61**
R60-D3	0.042	1.17	4.5	11.65	1.42	**0.77**

The results of transmission of the waves have varying steepness cases in 40, 50, and 60 cm water depth for seven waves characteristic (W3-W9) are given in Table 4.7. This table demonstrates the significant impact of wave period on *Kt* values. As the wave period increases, the *Kt* value increases. The *Kt* values in the model scale indicate that the lowest value (0.43) was observed at a wave period of 0.89 in R50-W9, while the highest value (0.94) was found at T_m = 2.85 (s) in R60-W3.

Table 4.7: Regular waves transmission result for Case 2 in 40, 50, and 60 cm water depth with varying wave steepness between 0.02-0.05.

		Prototype		Model		
Wave Name	**Wave Steepness (s_m)**	H_m (m)	$T_m(s)$	H_m (cm)	$T_m(s)$	Kt
R40-W3	0.02	0.6	5.3	6	1.68	**0.89**
R40-W4	0.025	0.6	4.43	6	1.4	**0.78**
R40-W5	0.03	0.6	3.88	6	1.23	**0.71**
R40-W6	0.035	0.6	3.49	6	1.1	**0.64**
R40-W7	0.04	0.6	3.21	6	1.02	**0.58**
R40-W8	0.045	0.6	2.99	6	0.95	**0.50**
R40-W9	0.05	0.6	2.82	6	0.89	**0.45**
R50-W3	0.02	0.6	5	6	1.58	**0.88**
R50-W4	0.025	0.6	4.25	6	1.34	**0.73**
R50-W5	0.03	0.6	3.75	6	1.19	**0.68**
R50-W6	0.035	0.6	3.4	6	1.08	**0.62**
R50-W7	0.04	0.6	3.15	6	1	**0.61**
R50-W8	0.045	0.6	2.95	6	0.93	**0.51**
R50-W9	0.05	0.6	2.8	6	0.89	**0.43**

Table 4.7 (continued)

R60-W3	0.02	0.6	4.75	6	1.5	**0.94**
R60-W4	0.025	0.6	4.09	6	1.29	**0.84**
R60-W5	0.03	0.6	3.66	6	1.16	**0.71**
R60-W6	0.035	0.6	3.36	6	1.06	**0.69**
R60-W7	0.04	0.6	3.12	6	0.99	**0.68**
R60-W8	0.045	0.6	2.93	6	0.93	**0.57**
R60-W9	0.05	0.6	2.78	6	0.88	**0.48**

Relative structure width and transmission coefficient relation are given in Figure 4.8 for $\frac{D}{d} = 0.24, 0.29, 0.36$. Highest *Kt* is measured at 0.94 for B/L = 0.1 and D/d = 0.24, and the lowest *Kt* is measured 0.34 for B/L = 0.31 and D/d =0.24.

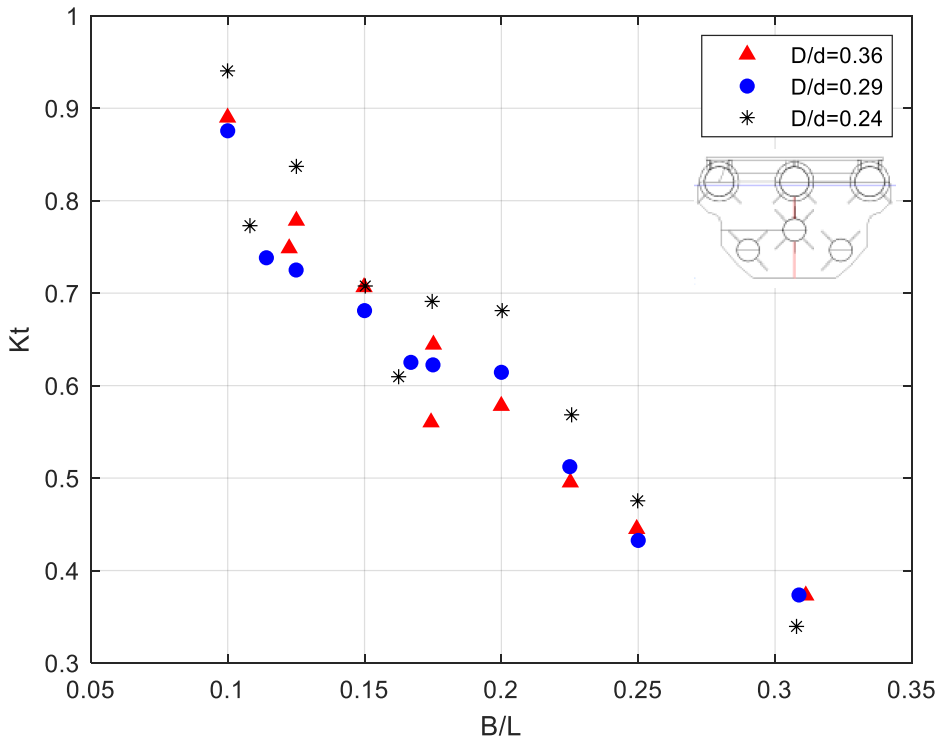

Figure 4.8: Change in the Wave Transmission Coefficient of Case 2 with respect to Relative Structure Width (B/L).

Relative depth and transmission coefficient relation is given in Figure 4.9 for D/d is equal to 0.24, 0.29, 0.36. When d/L = 0.20 and D/d = 0.24, Kt gets the highest value of 0.94 and the lowest Kt is measured as 0.34 for d/L = 0.62 and D/d = 0.24.

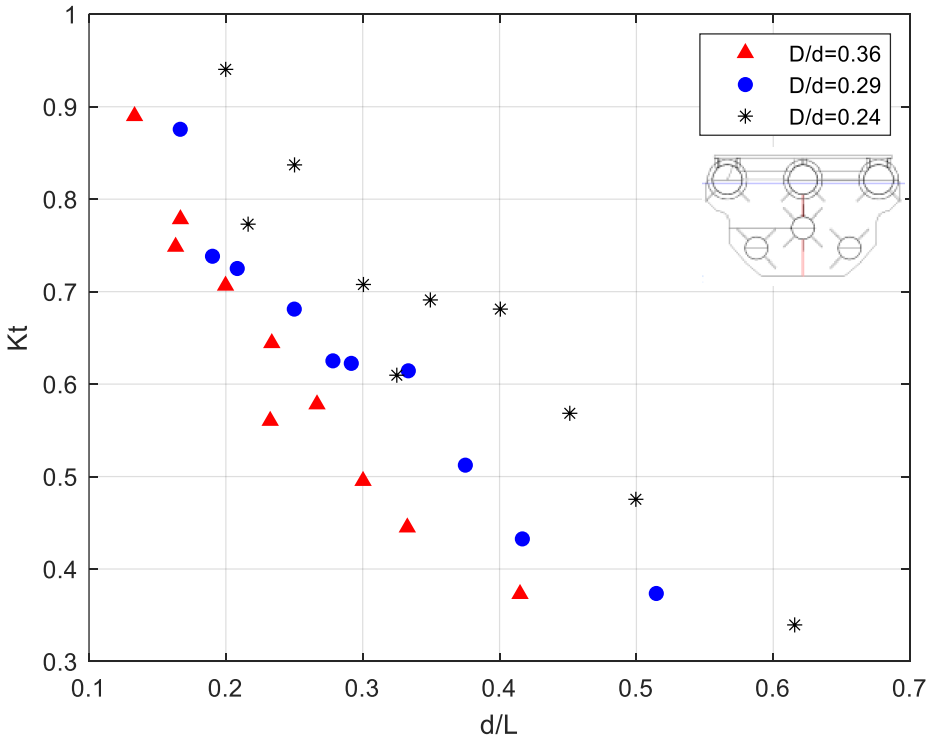

Figure 4.9: Change in the Wave Transmission Coefficient of Case 2 with respect to Relative Depth (d/L).

Wave steepness and transmission coefficient relation are given in Figure 4.10 for D/d = 0.24, 0.29, 0.36. When H/L = 0.02 and D/d = 0.24, Kt gets the highest value of 0.94 and the lowest Kt is measured as 0.43 for H/L = 0.05 and D/d = 0.29.

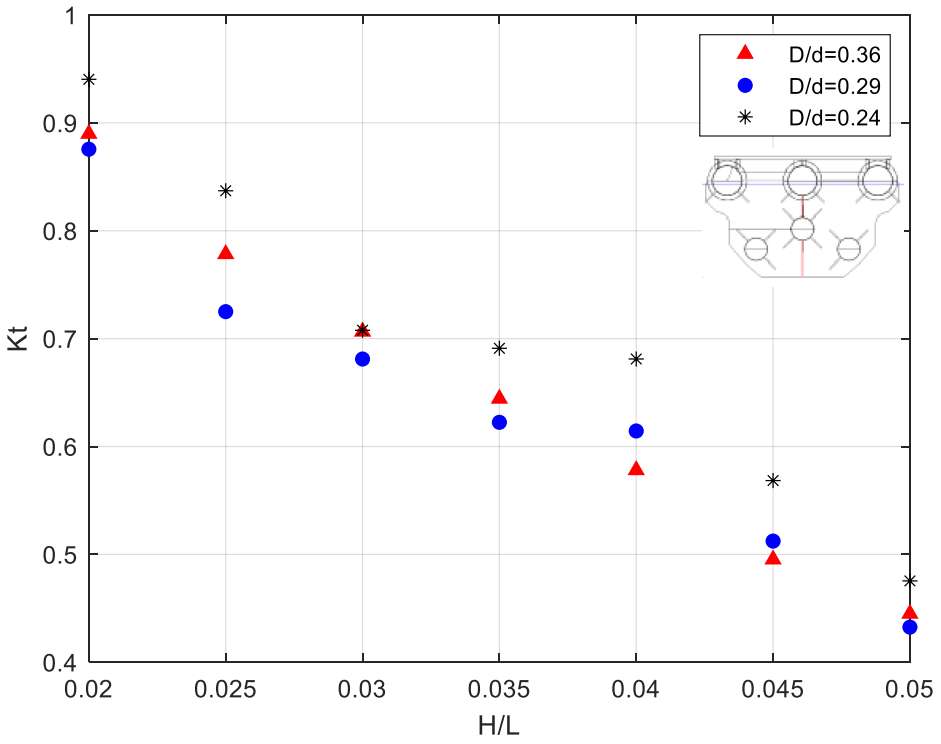

Figure 4.10: Change in the Wave Transmission Coefficient of Case 2 with Wave Steepness (H/L).

4.5.3 Wave Transmission Results for the Long Screen (Case 3)

Regular wave transmission results in which the waves have constant steepness (0.042) in 40, 50, and 60 cm water depth for three different wave characteristics (D1, D2, and D3) can be seen in Table 4.8. The *Kt* values are generally consistent among the different depths, with the exception of R40-D2 when compared to R50-D2 and R60-D2. The highest *Kt* value was measured at (0.63) for the three different depths R40, R50, and R60, while the lowest *Kt* was found (0.22) in R50-D1.

Table 4.8: Regular waves transmission result for Case 3 in 40, 50, and 60 cm water depth with a constant wave steepness (*sm* = 0.042)

		Prototype		Model		
Wave Name	**Wave Steepness (s_m)**	**H_m (m)**	**$T_m(s)$**	**H_m (cm)**	**$T_m(s)$**	***Kt***
R40-D1	0.042	0.41	2.5	4.05	0.79	**0.24**
R40-D2	0.042	0.72	3.5	7.22	1.11	**0.39**
R40-D3	0.042	1.03	4.5	10.28	1.42	**0.63**
R50-D1	0.042	0.41	2.5	4.08	0.79	**0.22**
R50-D2	0.042	0.76	3.5	7.55	1.11	**0.46**
R50-D3	0.042	1.1	4.5	11.04	1.42	**0.63**
R60-D1	0.042	0.41	2.5	4.09	0.79	**0.25**
R60-D2	0.042	0.78	3.5	7.76	1.11	**0.47**
R60-D3	0.042	1.17	4.5	11.65	1.42	**0.63**

The results of transmission of the waves have varying steepness cases in 40, 50, and 60 cm water depth for seven wave characteristics (W3-W9) are given in Table 4.9. The table illustrates the strong correlation between wave period and *Kt* values. An increase in wave period leads to an increase in *Kt* value. The *Kt* values in the model scale reveal that the minimum value (0.25) was recorded at a wave period of 0.89 in R50-W9, whereas the maximum value (0.70) was found at a wave period of 2.85 in R40-W3 and R50-W3.

Table 4.9: Regular waves transmission result for Case 3 in 40, 50, and 60 cm water depth with varying wave steepness between 0.02-0.05.

		Prototype		Model		
Wave Name	**Wave Steepness (s_m)**	**H_m (m)**	**$T_m(s)$**	**H_m (cm)**	**$T_m(s)$**	***Kt***
R40-W3	0.02	0.6	5.3	6	1.68	**0.70**
R40-W4	0.025	0.6	4.43	6	1.4	**0.66**
R40-W5	0.03	0.6	3.88	6	1.23	**0.63**
R40-W6	0.035	0.6	3.49	6	1.1	**0.49**
R40-W7	0.04	0.6	3.21	6	1.02	**0.41**
R40-W8	0.045	0.6	2.99	6	0.95	**0.32**
R40-W9	0.05	0.6	2.82	6	0.89	**0.31**

Table 4.9 (continued)

R50-W3	0.02	0.6	5	6	1.58	**0.70**
R50-W4	0.025	0.6	4.25	6	1.34	**0.65**
R50-W5	0.03	0.6	3.75	6	1.19	**0.58**
R50-W6	0.035	0.6	3.4	6	1.08	**0.46**
R50-W7	0.04	0.6	3.15	6	1	**0.38**
R50-W8	0.045	0.6	2.95	6	0.93	**0.28**
R50-W9	0.05	0.6	2.8	6	0.89	**0.25**
R60-W3	0.02	0.6	4.75	6	1.5	**0.69**
R60-W4	0.025	0.6	4.09	6	1.29	**0.62**
R60-W5	0.03	0.6	3.66	6	1.16	**0.57**
R60-W6	0.035	0.6	3.36	6	1.06	**0.51**
R60-W7	0.04	0.6	3.12	6	0.99	**0.42**
R60-W8	0.045	0.6	2.93	6	0.93	**0.34**
R60-W9	0.05	0.6	2.78	6	0.88	**0.27**

Relative structure width and transmission coefficient relation are given in Figure 4.11 for $\frac{D}{d} = 0.39, 0.47\ and\ 0.58$. Highest *Kt* is measured 0.70 for B/L = 0.1 and D/d = 0.47, and the lowest *Kt* is measured at 0.22 for B/L = 0.31 and D/d = 0.47.

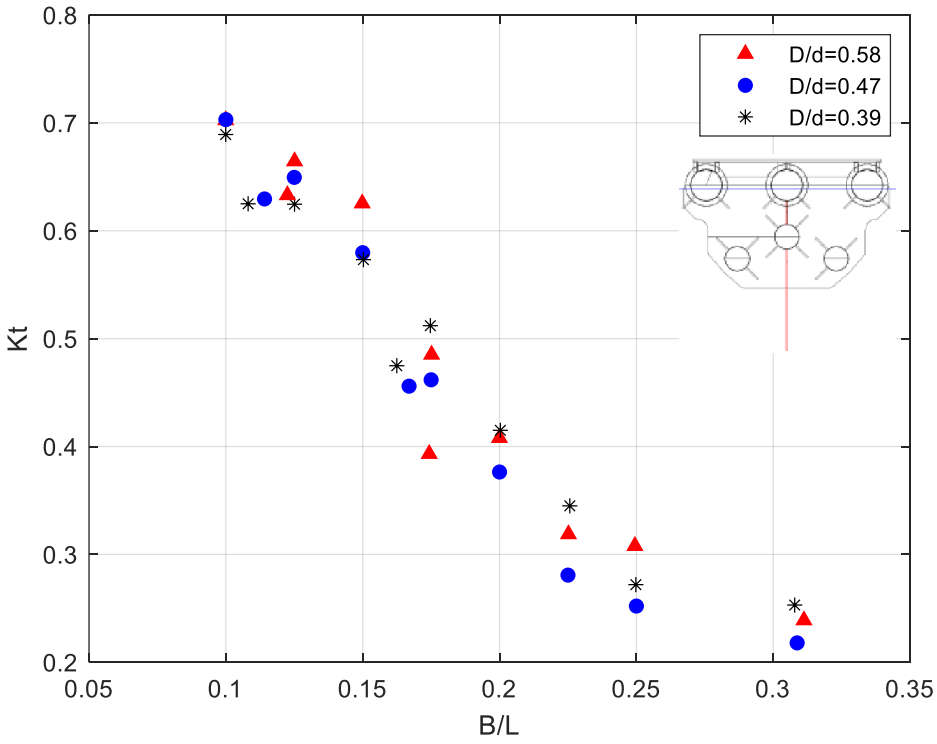

Figure 4.11: Change in the Wave Transmission Coefficient of Case 3 with respect to Relative Structure Width (B/L).

Relative depth and transmission coefficient relation are given in Figure 4.12 for D/d = 0.39, 0.47, 0.58. When d/L = 0.13 and D/d = 0.58, Kt gets the highest value of 0.70 and the lowest Kt is measured as 0.22 for d/L = 0.51 and D/d = 0.47. However, for the highest d/L = 0.62, Kt gets 0.25.

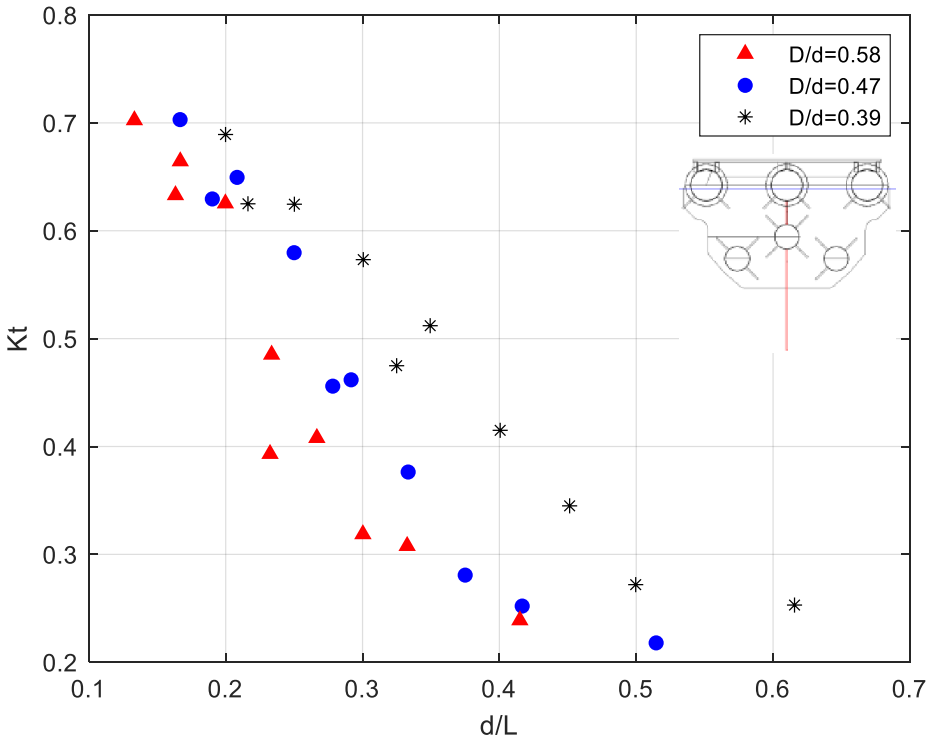

Figure 4.12: Change in the wave transmission coefficient of Case 3 with respect to relative depth (d/L).

Wave steepness and transmission coefficient relation are given in Figure 4.13 for D/d = 0.39, 0.47, 0.58. When H/L = 0.02 and D/d = 0.47, *Kt* gets the highest value of 0.7 and the lowest *Kt* is measured as 0.25 for H/L = 0.05 and D/d = 0.47.

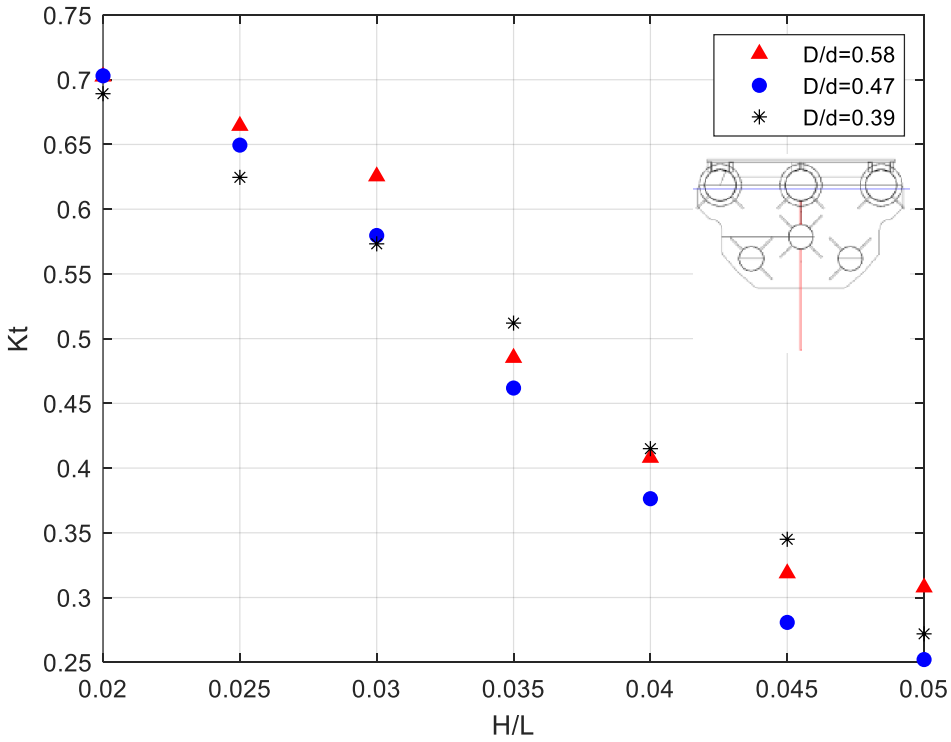

Figure 4.13: Change in the Wave Transmission Coefficient of Case 3 with Wave Steepness (H/L).

4.5.3.1 Multi-Regression Analysis

The wave transmission formula for single horizontal cylinder structures (Case 1, 2, and 3) under regular waves is given in (4.8).

$$Kt = 0.08\left(\frac{B}{L}\right)^{-0.16}\left(\frac{d}{L}\right)^{-0.54}\left(\frac{H}{L}\right)^{-0.09}\left(\frac{D}{d}\right)^{-0.60} \tag{4.8}$$

Measured and predicted *Kt* values are plotted as shown in Figure 4.14. Mean absolute error, root mean squared error, and adjusted R-squared are calculated as 4.8%, 11.3%, and 0.89 respectively.

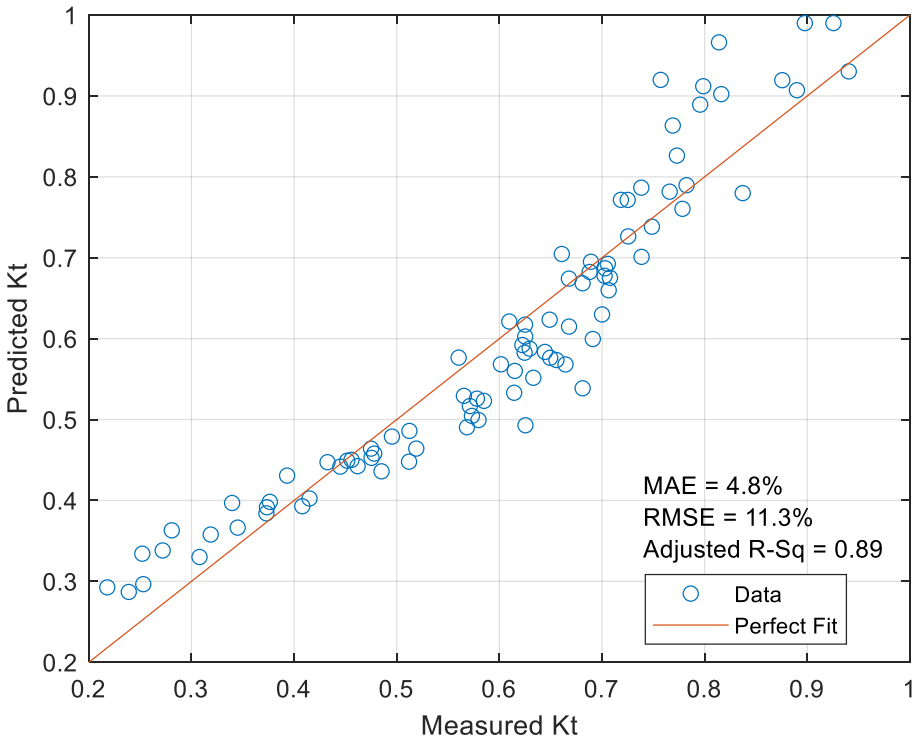

Figure 4.14: Measured and Predicted *Kt* Values Comparison.

4.5.4 Wave Transmission Results for Dual Platform Short Screen (Dual Case 2) and Box Platform

Case 2 and box structure have the same structural features such as height, draft, freeboard, and width. Additionally, the dual Case 2 consists of two Case 2 type platforms placed next to each other at a specific distance. Regular wave transmission results in which the waves have constant steepness (sm = 0.042) in 40, 50, and 60 cm water depth for three different wave characteristics (D1, D2, and D3) can be seen in Table 4.10. When comparing the *Kt* results for three different structures, it can be seen that the highest value belongs to Case 2. Additionally, the results for the Box and Dual Case 2 are similar to each other.

Table 4.10: Regular waves transmission results for Case 2, Dual Case 2, and Box in 50 cm water depth with a constant wave steepness (*sm* = 0.042)

		Prototype		Model				
Wave Name	Wave Steepness (s_m)	H_m (m)	$T_m(s)$	H_m (cm)	$T_m(s)$	*Kt-Case 2*	*Kt-Dual Case2*	*Kt-Box*
R50-D1	0.042	0.41	2.5	4.08	0.79	**0.37**	**0.15**	**0.12**
R50-D2	0.042	0.76	3.5	7.55	1.11	**0.63**	**0.46**	**0.41**
R50-D3	0.042	1.1	4.5	11.04	1.42	**0.74**	**0.57**	**0.66**

The results of transmission of the waves have varying steepness cases in 40, 50, and 60 cm water depth for seven wave characteristics (W3-W9) are given in Table 4.11. The table shows a similar distribution pattern for *Kt* values among the three different structures. The highest *Kt* value is found in Case 2, and the Box and Dual platforms have a similar distribution pattern.

Table 4.11: Regular waves transmission result for Case 2, Dual Case 2, and Box in 50 cm water depth with varying wave steepness between 0.02-0.05.

		Prototype		**Model**				
Wave Name	**Wave Steepness (s_m)**	**Water Depth= 5 m**		**Water Depth= 50 cm**				
		H_m (m)	$T_m(s)$	H_m (cm)	$T_m(s)$	*Kt – Case 2*	*Kt-Dual Case2*	*Kt-Box*
R50-W3	0.02	0.60	5	6	1.58	**0.88**	**0.73**	**0.76**
R50-W4	0.025	0.60	4.25	6	1.34	**0.73**	**0.68**	**0.59**
R50-W5	0.03	0.60	3.75	6	1.19	**0.68**	**0.64**	**0.51**
R50-W6	0.035	0.60	3.4	6	1.08	**0.62**	**0.50**	**0.39**
R50-W7	0.04	0.60	3.15	6	1.00	**0.61**	**0.32**	**0.27**
R50-W8	0.045	0.60	2.95	6	0.93	**0.51**	**0.30**	**0.21**
R50-W9	0.05	0.60	2.8	6	0.89	**0.43**	**0.23**	**0.18**

Relative structure width and transmission coefficient relation are given in Figure 4.15 for Case 2, Dual Case 2, and Box. The highest *Kt* is measured at 0.87 for B/L=0.1 for Case 2, and the lowest *Kt* is measured at 0.12 for B/L = 0.31 for Box.

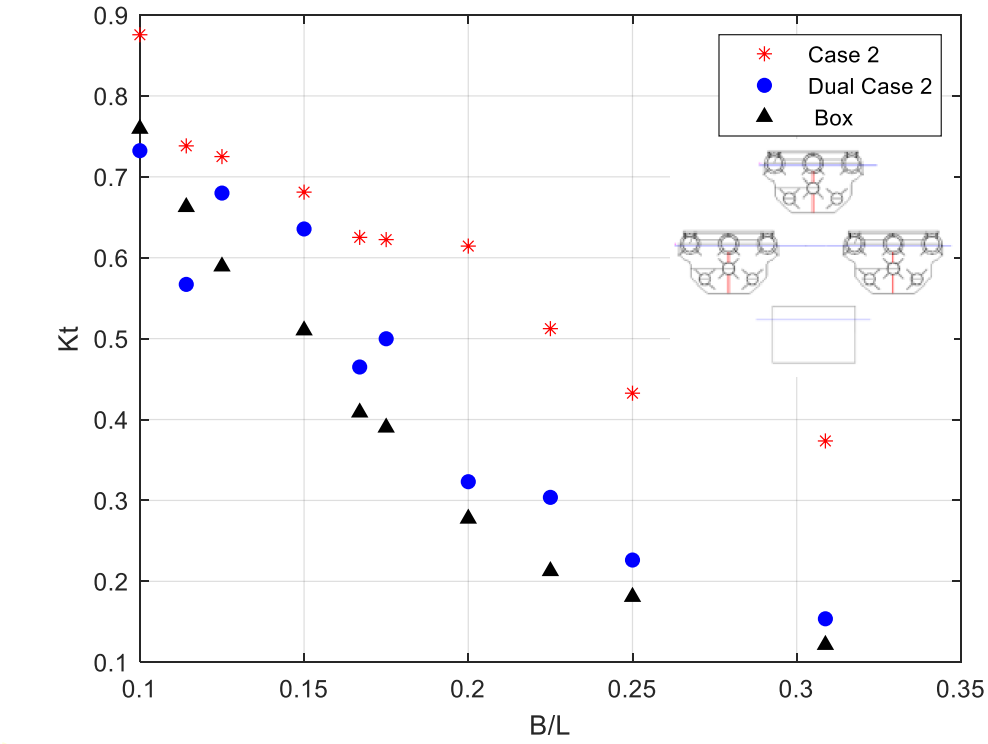

Figure 4.15: Change in the Wave Transmission Coefficient of Case 2, Dual Case 2, and Box with respect to Relative Structure Width (B/L).

Relative depth and transmission coefficient relation are given in Figure 4.16. When d/L = 0.17 for Case 2 Kt gets the highest value of 0.87 and the lowest Kt is measured as 0.12 for Box.

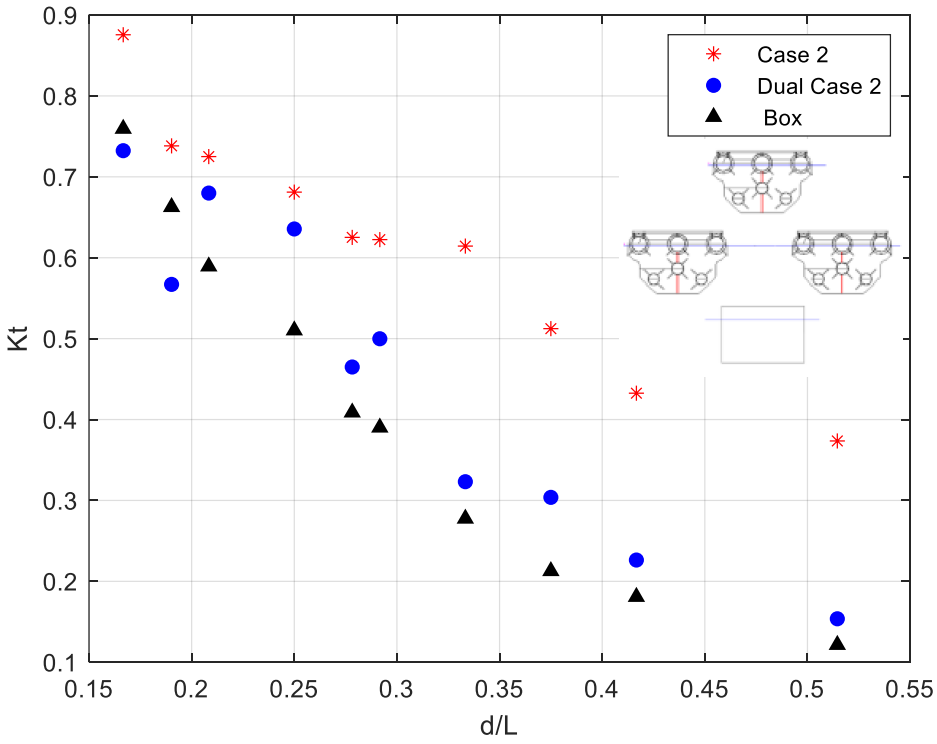

Figure 4.16: Change in the Wave Transmission Coefficient of Case 2, Dual Case 2, and Box with respect to Relative Depth (d/L).

Wave steepness and transmission coefficient relation are given in Figure 4.17. In H/L = 0.02 for Case 2, Kt gets the highest value of 0.93 and the lowest Kt is measured as 0.12 for H/L = 0.05 for Box.

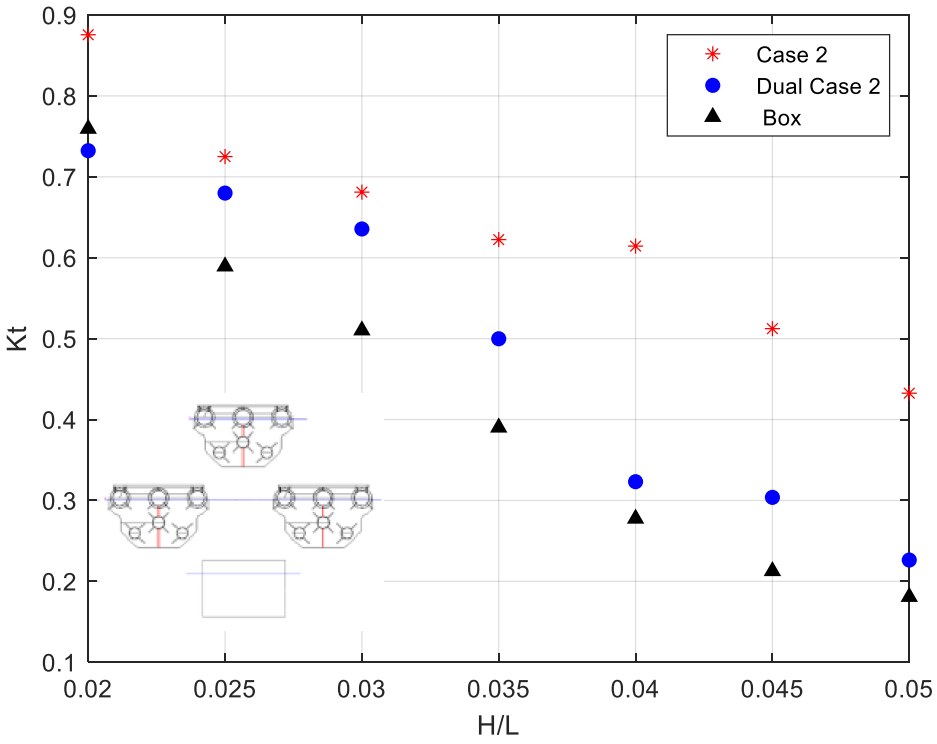

Figure 4.17: Change in the Wave Transmission Coefficient of Case 2, Dual Case 2, and Box with Wave Steepness (H/L).

4.6 Discussion of the Experimental Results

The floating platforms were tested under irregular and regular waves. Therefore, one of the focuses is comprehending the effect of wave type on wave transmission performance.

4.6.1 Irregular and Regular Waves Comparison

As can be seen from Figure 4.18 and Figure 4.19, the transmission coefficient of irregular waves is higher than regular waves. This can be explained by the fact that irregular wave series were generated by a spectrum that contains higher wave heights which results in overtopping and increasing the transmission coefficient. Results show that irregular transmitted wave energy is higher than regular waves.

According to Figure 4.18, as the B/L increases, the transmission coefficient decreases and there is a significant difference between regular and irregular waves in transmission coefficient for B/L = 0.11, 0.17, and 0.31 which corresponds to the constant wave steepness (0.042) conditions of D1, D2, and D3.

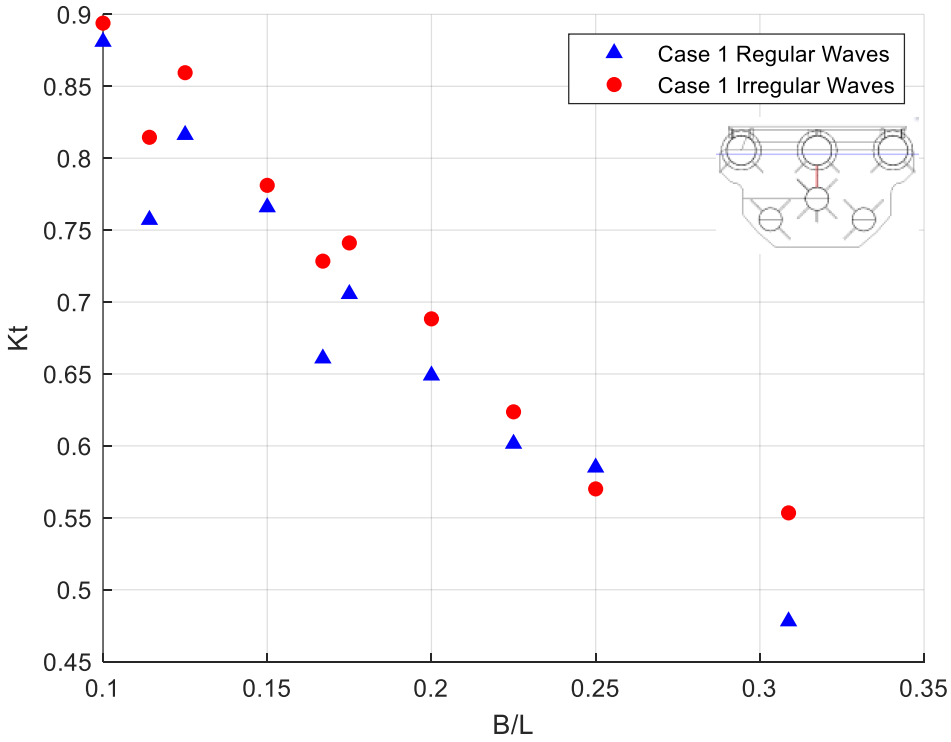

Figure 4.18: Transmission Coefficient Comparison of Regular and Irregular Waves for Case 1 with respect to Relative Structure Width (B/L).

In the wave steepness comparison, both conditions (regular and irregular) have the same pattern. When the wave steepness increases, Kt decreases. For H/L=0.05 which is the steepest wave condition, the transmission coefficient of regular waves is higher than irregular waves (Figure 4.19).

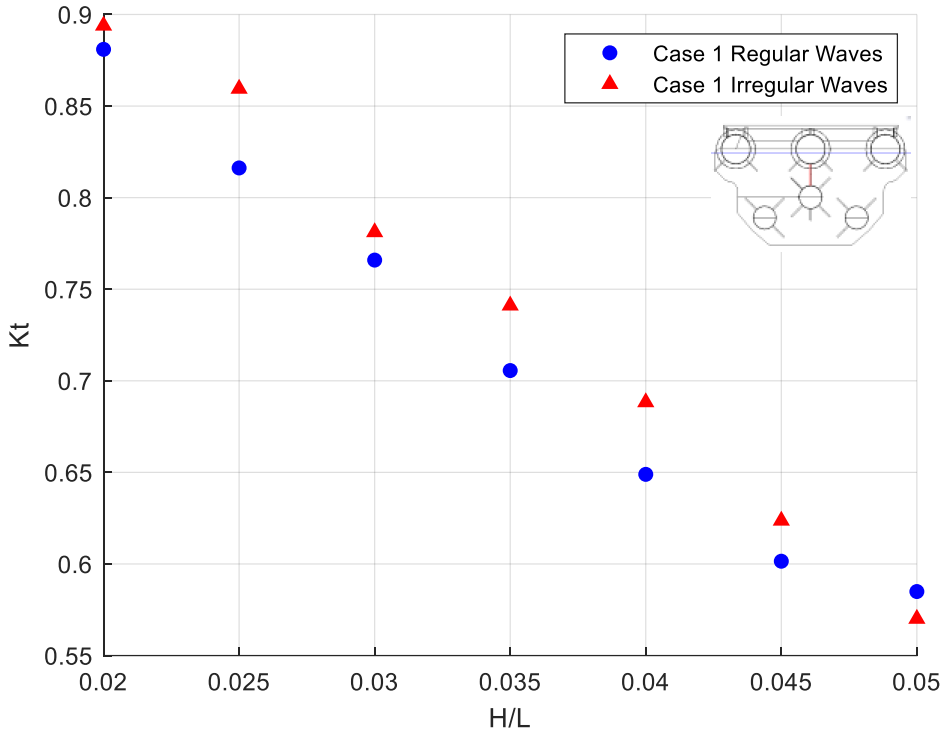

Figure 4.19: Transmission Coefficient Comparison of Regular and Irregular Waves for Case 1 with respect to Wave Steepness (H/L).

4.6.2 Investigating the Correlation between Water Depth and Wave Transmission under Regular Waves

When the water column is increased, it has higher transmission results under the same wave characteristic. For instance, Figure 4.6 shows the changes in wave transmission of Case 1 with respect to relative depth (d/L). It can be seen that the transmission coefficient of $D/d = 0.20$ (60 cm water depth) has a higher trend than $D/d =$ 0.24 and 0.30 (50 and 40 cm water depth respectively). Therefore, transmitted energy underneath the structure has a direct proportion with the water depth under the same wave properties. However, after a deep water zone, an increase in water depth is not going to cause an increase in the transmission coefficient for constant wave parameters. Also, if the water depth is kept constant and wavelength is increased, *Kt* increases. When Cases 1, 2, and 3 are compared in

terms of relative depth change (d/L), Case 1 has a wider scatter and the depth effect can be seen easily (Figure 4.6). However, when the draft is extended as in Case 2, the scatter of d/L in 40 and 50 cm water depth (D/d = 0.36 and 0.29 respectively) have a gathered pattern between d/L = 0.15 and 0.3 but whereas 60 cm water depth (D/d = 0.36) still has a separate scatters than other two water depths (Figure 4.9). Furthermore, in Case 3 this close scattering pattern shifts to the range between d/L= 0.1 and 0.2 for all water depths (Figure 4.12). This can be interpreted as when the water column is blocked with a draft increase, the effect of water depth on changing in transmission coefficient is vanishing while approaching d/L=0.1 or longer period.

4.6.3 Wave Period Limitation for a Horizontal Cylinder Floating Platform and Effectiveness of Transmission Coefficient

The most significant factor in the effectiveness of floating breakwaters is the wave period. Floating platform experiments were conducted with wave periods between 2.5 and 9 seconds for the irregular waves and a range of 2.5 and 5.3 seconds for the regular waves. In the irregular waves experiments, after 4.25 second (B/L = 0.175) in the prototype, the transmission coefficient got a value of 0.86 and considerably rose to 0.94 which are considered quite ineffective in attenuation performance. On the other hand, in this study, there were structural changes for the regular wave conditions (Cases 1, 2, and 3). Although the extension of the draft improves the transmission performance, in general, prototype wave period of 4.5 seconds (B/L = 0.125) and above significantly makes the structure inefficient in terms of attenuation. The most effective method to deal with long waves could be an increase in structure width.

4.6.4 Relative Width Effect on Attenuation Performance

Floating platform performance is strongly related to width, in this study width of the structure is kept constant. However, relative depth plots clearly show that when the relative width increases (B/L), wave transmission decreases (Figure 4.5,Figure 4.8, and Figure 4.11). Moreover, since structure width changes the floating body's inertia, the structure's natural period of oscillation changes in non-fixed structures, a detailed discussion is given in Section 6.3.2.

4.6.5 Effect of Draft Change on Wave Transmission in Structures with Constant Width and Freeboard

One of the main changes in this study is the structure's draft. Since for short waves, energy accumulates on the upper part of the water column, it is way easier to block the energy. However, when the waves have a longer period, a larger draft should be applied to block energy. Starting from Case 1 to Case 3, the draft of the structure is extended to observe its effect on transmission performance. Figure 4.20 shows the draft change in transmission coefficient. Due to the opening between horizontal cylinders in Case 1, the wave transmission coefficient has a higher trend compared to others. Moreover, in Case 2, adding a short screen improved the wave attenuation performance in the range of $B/L = 0.22$ to 0.31 or short waves. In Case 3, the scatter pattern varied dramatically from Cases 1 and 2. It shows that a big increase in draft helps a lot in wave attenuation for $B/L = 0.15$ to 0.31. However, in the long period of waves, the effect of draft change diminishes and the transmission coefficient gets similar values.

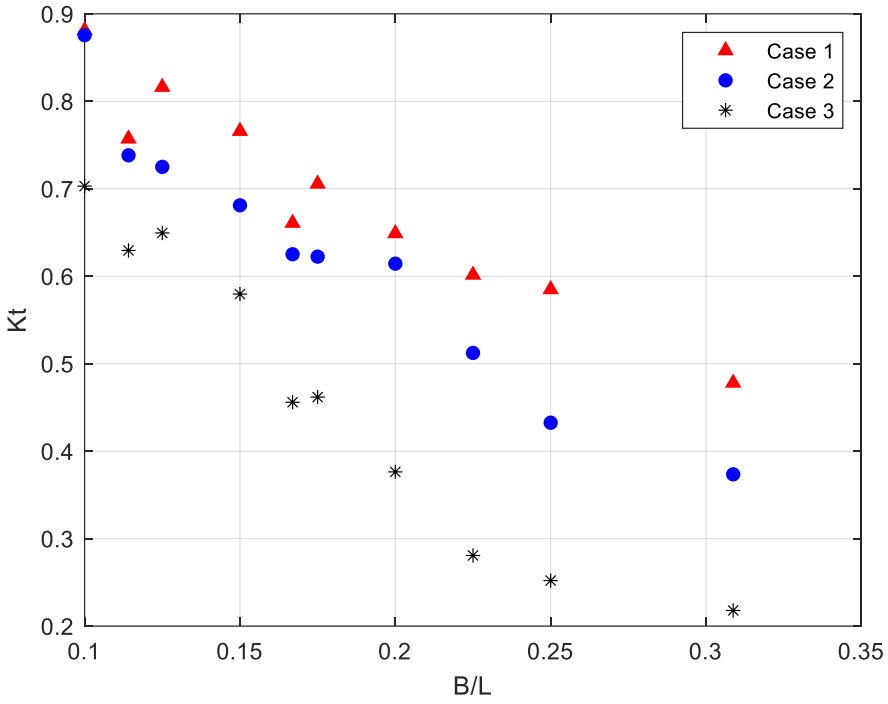

Figure 4.20: Change in the Transmission Coefficient of Cases 1, 2, and 3 in 50 cm Water Depth with respect to Relative Structure Width (B/L).

4.6.6 Wave Attenuation Performance of Horizontal Cylinder Platform in Comparison with the Box Type Platform

As Figure 4.15, Figure 4.16, and Figure 4.17 show, box transmission performance is more efficient than horizontal cylinder structure, especially in the short waves where $\frac{B}{L} > 0.2$. The reason for that difference can be correlated to bottom width geometry. Box shape has uniform geometry at the top and bottom, whereas horizontal floating platform has a trapezoidal shape, becoming narrow to the bottom. As an interpretation, the bottom width of the structure is as important as the structure draft. Moreover, structure width should be defined separately for the top and bottom parts of the structure which has a non-uniform shape.

4.6.7 Feasibility of Double Platform for Wave Attenuation Compared to Single Platform with Larger Draft

Applying a dual platform attenuates the waves significantly (Figure 4.15). However, transmission performance depends on the spacing between the two platforms. As mentioned in the literature review under the reflective box type floating breakwaters, dual box floating breakwaters are efficient in long waves when the spacing is narrow because of the continuation in width. However, reflecting short waves is achieved by large spacing since two floating boxes behave as two independent structures. In this study, spacing was kept as $(2 * B)/3$ by considering the collision possibility of two units in prototype scale and no additional spacing trials were carried out in experiments. The dual platform performed better in short waves with that 20 cm spacing.

4.6.8 Correlation of Wave Transmission Theories with Experimental Results

All transmission formulas mentioned in this study are valid for deep sea, rigid, fixed (do not move or deform significantly), and no overtopping conditions. However, there are many floating breakwaters projects which don't suit such conditions and these formulas have a large difference from each other due to that reason it is not clear to the design engineer which formula is more applicable than others (Biesheuvel, 2013). Since horizontal cylinder structure doesn't have uniform geometry, it is excluded from theories comparison. In Figure 4.21, it can be seen that all formulas are overestimating the transmission coefficient compared to Box experiments. The closest pattern belongs to the newest formula ASCE (2012).

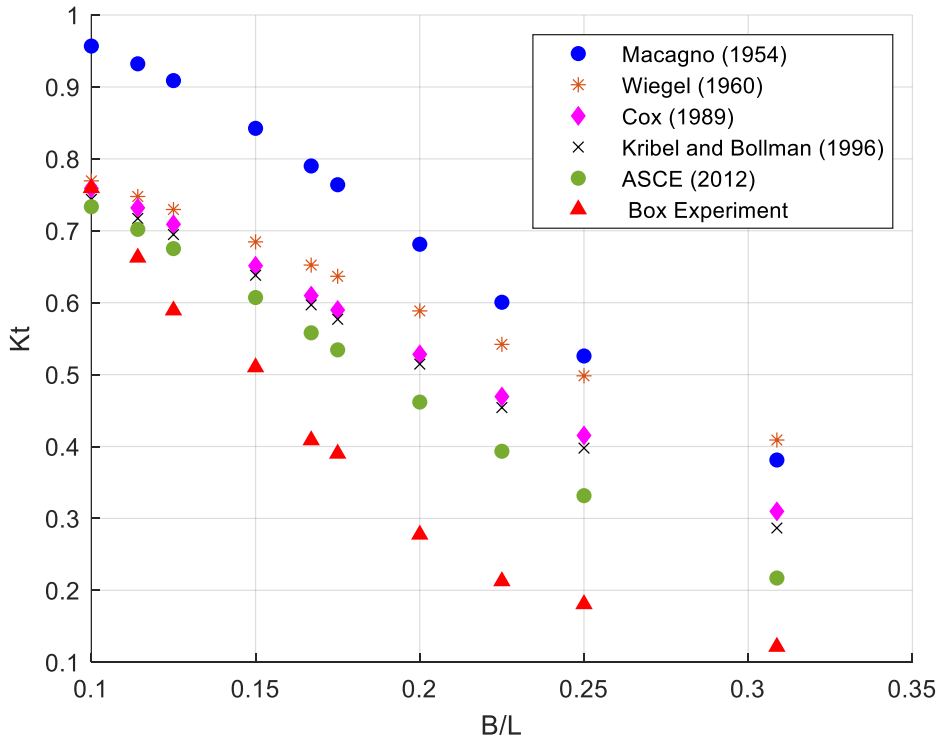

Figure 4.21: Wave Transmission Theories and Experimental Results

Since wave and floating structure interaction is a complex process, analytical formulas are neglecting many processes, such as wave dissipation, and overtopping. The proper formula should cover all wave steepness, relative width, depth, and draft effects together. Biesheuvel (2013) states that it is challenging to incorporate all relevant processes into an analytical formula also he mentioned that when comparing wave transmission theories to experimental data for fixed floating structures, it is found that nearly all theories tend to overestimate the wave transmission coefficient, particularly for shorter wave periods. Factors that can affect the accuracy of these theories include the ratio of wavelength to draft (L/D), the ratio of width to depth (B/d), and the ratio of draft to depth (D/d). For values of $L/D < 5$, the wave transmission coefficient is typically less than 30%. Although all transmission theories formulas are overestimating the results, there could be some useful recommendations for design engineers. For instance, it has been observed that when the wave transmission predicted by Macagno (1954) is less

than that predicted by Kriebel and Bollmann (1966) theory, Macagno's theory is suitable for use when the ratio of width to depth (B/d) is between 0.75 and 1 and the ratio of draft to depth (D/d) is between 0.15 and 0.4. Conversely, when the same ratios are considered, if Macagno's theory predicts higher wave transmission than Kriebel and Bollmann's theory, the latter is more suitable. For structures with large drafts (D/d > 0.4), current theories may not be adequate, and numerical or physical models should be employed instead (Biesheuvel, 2013).

When the Box structure results are checked with the recommendations for fixed floating structures given by Biesheuvel (2013), Kriebel and Bollmann (1996) should be selected theory. However, these recommendations don't take into account ASCE (2012), and also Kriebel and Bollmann (1996) still overestimate the experimental results.

4.6.9 Comparison of Transmission Coefficient in Fixed and Oscillating Floating Structures

Floating platforms are structures used to protect against water waves, and experience periodic loading due to the motion of the waves. As a result of this loading, the floating structure moves and experiences internal forces, both within itself and in its mooring system. In a three-dimensional reference frame, a floating body has six degrees of freedom, which refers to the number of ways it can move. They are surge, sway, heave, roll, pitch, and yaw.

Since the model is complex due to its non-uniform frontal face, horizontal pipes, and their positioning in the body matrix, in both experimental and numerical studies, the model was tested fixed to observe fundamental interactions which are transmission, reflection, and dissipation. In the present study, this difference could not be assessed; however, it is still possible to discuss the differences by referring to the relevant literature. According to Journée and Massie (1999), the dynamic of a floating structure is a superposition of a fixed structure under wave load plus an oscillation body at still water level. Damping force and spring force are calculated

from the oscillating body. However, wave dynamic results such as forces and moments are calculated from the fixed body under wave actions. Therefore, a fixed floating platform is a good start to examine wave load on such a complex structure. Since all degrees of freedom are restricted, it could be concluded that the fixed breakwater's transmission coefficient should be less than the oscillation one.

CHAPTER 5

NUMERICAL MODELING STUDIES

5.1 CFD Model Formulation and Description

In the scope of this study, besides the experimental studies, the open-source computational fluid dynamics (CFD) toolkit OpenFOAM release version v-1912 together with waves2Foam utility was used to assess the validity of the model in such problems, and also extend the present experimental results. For free surface water generation and absorption, the library waves2Foam which was developed by Jacobsen et al. (2012) was applied. Waves2Foam allows users to apply the relaxation zone technique which is also named passive sponge layer for the wave absorption and provides usage for various wave theories such as first-order, second-order, and fifth-order stokes theories with the cnoidal and stream function theory. In this study, stream function wave theory with main solver *waveFoam* and relaxation zone technique was applied. The details of the numerical modeling approach are presented in the forthcoming subsections.

5.1.1 CFD Mathematical Model

Reynolds-averaging methods were implemented because solving conventional forms of Navier-Stokes equations have high computational demand. Therefore, Reynolds Averaged Navier-Stokes (RANS) which includes Reynolds-averaged continuity and momentum equations given in Eq. (5.1) and Eq. (5.2), respectively, are preferred in this study, which is solved by waveFoam.

$$\frac{\partial u_i}{\partial x_i} = 0 \tag{5.1}$$

$$\frac{\partial \rho u_i}{\partial t} + u_j \frac{\partial \rho u_i}{\partial x_j} = -\frac{\partial p}{\partial x_i} + \rho g_i + \frac{\partial}{\partial x_j}(\mu_{eff} \frac{\partial u_i}{\partial x_j}) \quad (5.2)$$

Variables u_i, x_i, p, t, $g_i, \rho, \mu_{eff}, \mu$, respectively are ensemble-averaged velocity, cartesian coordinate, pressure, time and gravitational acceleration, water density, and effective dynamic viscosity which is equal to $\mu + \rho v_{turb}$, μ is the molecular dynamic viscosity and v_{turb} is the turbulent kinematic viscosity.

The volume of fluid method is adopted for free surface capturing, solving an additional advection equation. In this method fluid phases are identified by an indicator function γ. If γ value is 0, it indicates that the cell is full of gas phase and 1 indicates the fluid phase. The transition zone which is also shown in Figure 5.1 as a solid blue line is the actual free surface.

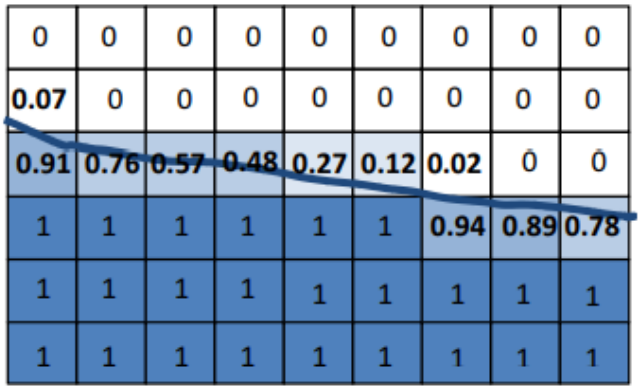

Figure 5.1: Capturing the Free Surface Interface by the Volume of Fluid Technique (adapted from Davidson et al., 2015)

Equation (5.3) which is the volume of fluid advection equation is solved by a specifically designed methodology called MULES available in the OpenFOAM environment to find the γ values.

$$\frac{\partial \gamma}{\partial t} + \frac{\partial \gamma \langle u_i \rangle}{\partial x_i} + \frac{\partial \gamma \langle 1-\gamma \rangle \langle u_i \rangle}{\partial x_i} = 0 \quad (5.3)$$

When each cell's γ values are found, the fluid density and molecular viscosity of each cell can be iterated by using Equations (5.4) and (5.5). In these equations, the

liquid phase of density and molecular viscosity is denoted as ρ_l and μ_l, gas phase of density and molecular viscosity are indicated as ρ_g and μ_g.

$$\rho = \gamma\rho_l + (1-\gamma)\rho_g \tag{5.4}$$

$$\mu = \gamma\mu_l + (1-\gamma)\mu_g \tag{5.5}$$

5.1.2 Meshing and Case Setup

Structured meshes were applied by using the blockMesh utility and cell sizes were adjusted according to each case. RefineMesh utility of OpenFOAM was used for refinement purposes and the snappyHexMesh utility of OpenFOAM was adopted for integrating the floating structure into the block (i.e. extracting the structure from the base mesh, and generating a mesh that conforms to the structure). A mesh sensitivity analysis was performed to examine the effect of varying mesh sizes on the transmission coefficient. It was determined that the most optimal results were obtained when following the recommendation of Larsen et al. (2019) to maintain a ratio of $12.5 < H/\Delta y < 15$ to accurately capture the resolution of wave height. Also, the ratio of Δx / Δy was maintained at a constant value of 2 for all cases. The case setup and layout plan were kept as same as in the experimental case. After waves are generated, they propagate toward the floating structure and transmission occurs. To analyze the wave characteristics in a good resolution, meshing was studied on a regional basis for the incident wave height H_i, transmitted wave height H_t and for the regions where the transition between the two occurs (Figure 5.2). Based on the measured transmitted wave height from physical experiments, the expected range of wave heights is examined. Then, it is determined if a second refinement is necessary to meet the meshing rules outlined above. As can be seen from (Figure 5.2) the process of refining the floating platform begins with a distance of 100 cm and a second refinement is applied 10 cm before the floating structure. Since the wave hydrodynamic actions near the water surface are more important, the transition region is ended at a distance of $Hmax$ = 7.5 cm and the

base mesh continues for another 7.5 cm in the y-axis direction before grading begins. The start of grading is adjusted to create a smooth transition in the x and y directions. After the rear wave gauge, a 0.5L distance in the x-axis transmitted meshing region ends, and a 10 cm transition region is applied. There is a 100 cm distance between the start point of the relaxation zone and the transition region, which is covered by the base mesh. This mesh continues until the end of the wave flume.

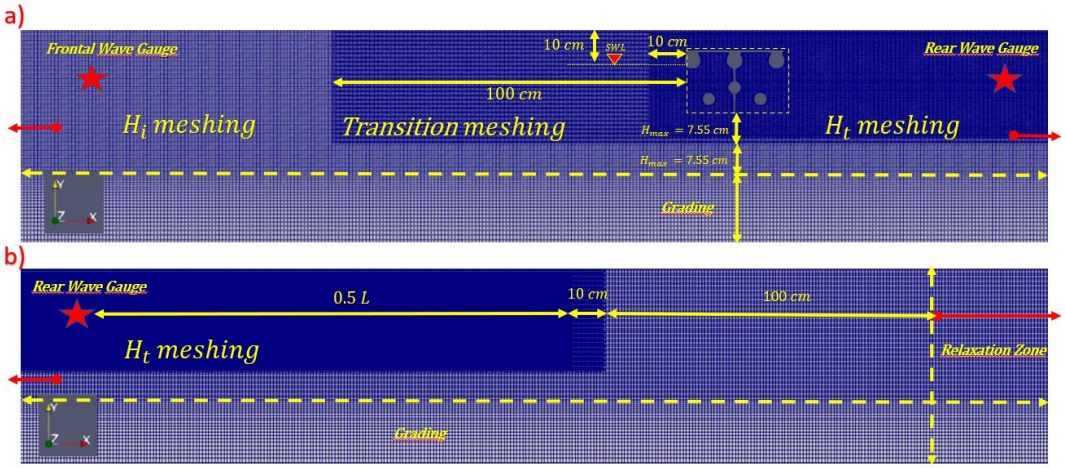

Figure 5.2: a) General Mesh Assembly between Frontal and Rear Wave Gauge b) General Mesh Assembly at the Rear Wave Gauge

5.1.3 Mesh Size

According to meshing rules mentioned in 5.1.2, mesh sizes of D2, W3, and W7 waves are given in Table 5.1. In wave W7, two rounds of refinement were performed to achieve an appropriate resolution for the transmitted wave height. However, for D2 and W3 waves, only one round of refinement was necessary to achieve a good resolution without a transition between the incident and transmitted mesh areas.

Table 5.1: Mesh Size in x and y directions

				H_i Mesh Size (cm)		Transition Mesh Size (cm)		H_t Mesh Size (cm)	
Wave Name	Wave Steepness (s_m)	H_m (cm)	$T_m(s)$	x-axis	y-axis	x-axis	y-axis	x-axis	y-axis
R50-W7	0.04	6	1	0.96	0.48	0.48	0.24	0.24	0.12
R50-D2	0.042	7.55	1.11	1	0.5	-	-	0.5	0.25
R50-W3	0.02	6	1.58	0.96	0.48	-	-	0.48	0.24

5.2 Wave Sets

Since the experimental model studies were divided into two groups, one case was selected from the group which has constant steepness (0.042) with different wave heights and periods. Therefore, the D2 case was considered the first validation case. Then, W3 and W7 cases were selected to have variety in wave steepness respectively are 0.02 and 0.04 (Table 5.2). D2, W3, and W7 wave conditions were applied for validation of the Box and Case 2 model. However, just D2 and W3 waves are applied for extended studies. All numerical models were simulated with a water depth of 50 cm.

Table 5.2: Numerical wave sets under regular waves at 50 cm water depth for validation of Box and Case 2

		Prototype		Model	
Wave Name	Wave Steepness (s_m)	H_m (m)	$T_m(s)$	H_m (cm)	$T_m(s)$
R50-W7	0.04	0.6	3.15	6	1
R50-D2	0.042	0.76	3.5	7.55	1.11
R50-W3	0.02	0.6	5	6	1.58

5.3 Numerical Cases

Box and Case 2 were validation of the numerical cases. In addition, to investigate the improvement of the wave attenuation performance of the floating platform, the structural modification was implemented to the CFD model based on Case 2

geometry. Therefore, three extended simulations denoted as Extended 1, 2, and 3 were carried out (Table 5.3). These simulations are summarized in this chapter and the results of the numerical simulations are presented in Chapter 6.

Table 5.3: Summary of numerical cases

Structure Type	Wave Name	Water Depth
Box	W3, W7, D2	50 cm
Case 2	W3, W7, D2	50 cm
Extended 1	W3, D2	50 cm
Extended 2	W3, D2	50 cm
Extended 3	W3, D2	50 cm

5.3.1 Box Case

Three wave cases were used for the numerical validation of the box structure. These were D2, W3, and W7 cases in 50 cm water depth (Table 5.2).

The rule of $12.5 < H/\Delta y < 15$ was followed for the incident and transmitted waves. For the cases when the transmitted wave height is relatively small to incident ones, the mesh size should be adjusted according to the smallest wave (transmitted) to capture its hydrodynamic properly so that W8 and W9 cases were eliminated for the numeric model. Therefore, mesh optimization was carried out to avoid a high total cell number which extremely extends the computational time.

5.3.2 Case 2

D2, W3, and W7 wave cases in 50 cm water depth were applied in Case 2 numerical simulation. Also, meshing rules in Section 5.3 were followed. The dimensions of Case 2 can be seen in Figure 5.3.

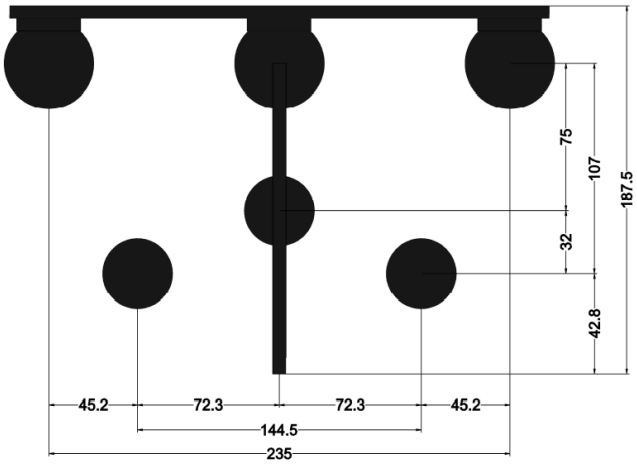

Figure 5.3: Case2 Numerical Model Cross-Section Dimensions. (All dimensions given in the figure are in millimeters.)

5.3.3 Extended 1

In Case 2, two small radius pipes were positioned on the same horizontal axis the third one is 32 mm above them and its center is in the middle of the two. However, in Extended 1, the middle pipe was modified to be on the same horizontal axis as the other two pipes. The dimensions of Case 2 can be seen in Figure 5.4.

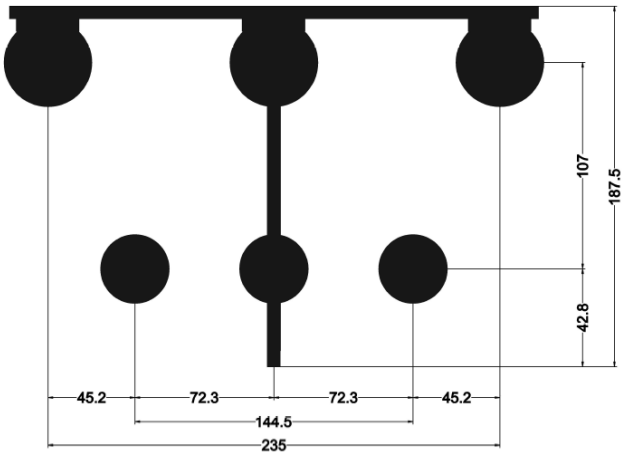

Figure 5.4: Extended 1 Numerical Model Cross-Section Dimensions. (All dimensions given in the figure are in millimeters.)

5.3.4 Extended 2

Extended 2 is the modified version of Extended 1 by stretching the exterior of two small radius pipes to the outer edge limit of a larger radius pipe. The dimensions of Case 2 can be seen in Figure 5.5.

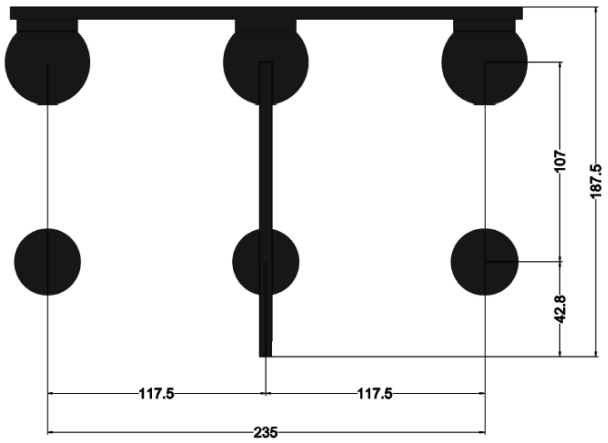

Figure 5.5: Extended 2 Numerical Model Cross-Section Dimensions. (All dimensions given in the figure are in millimeters.)

5.3.5 Extended 3

Extended 3 is the modified version of Extended 2 by pulling the middle small radius pipe up 32 mm. The dimensions of Case 2 can be seen in Figure 5.6

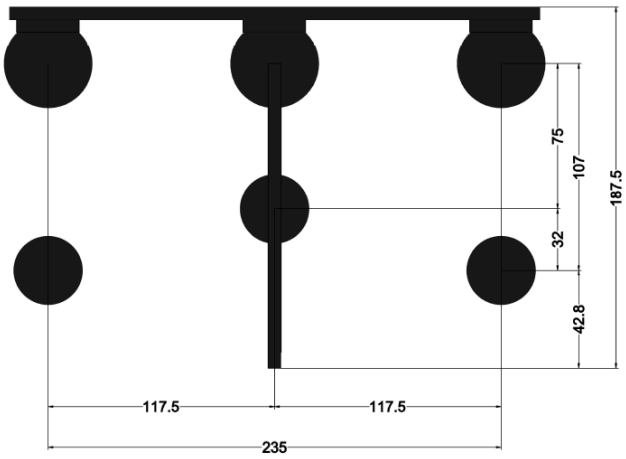

Figure 5.6: Extended 3 Numerical Model Cross-Section Dimensions. (All dimensions given in the figure are in millimeters.)

CHAPTER 6

RESULTS OF THE NUMERICAL MODELING STUDIES

6.1 Validation of the Numerical Model

Firstly, validation of the numeric model is carried out with the box structure. It is aimed to have a simple structure as a start to observe hydrodynamic similarities between the experiment and the numeric model. Then, the second part of validation is started with the short screen floating platform (Case 2).

6.1.1 Box

Three validation cases W3, W7, and D2 were simulated, and results are given in Table 6.1.

Table 6.1: Box structure experimental and numeric *Kt* results

		Prototype		Model			
Wave Name	Wave Steepness (s_m)	H_m (m)	$T_m(s)$	H_m (cm)	$T_m(s)$	*Experimental Kt*	*Numeric Kt*
R50-W7	0.04	0.6	3.15	6	1	**0.28**	**0.28**
R50-D2	0.042	0.76	3.5	7.55	1.11	**0.41**	**0.47**
R50-W3	0.02	0.6	5	6	1.58	**0.76**	**0.69**

Experimental and numerical (predicted) results are compared in Figure 6.1. It can be seen that numerical and experimental results for R50-W7, (T_m=1 s) are very similar, and there is also good agreement between the results for the other two waves R50-D2 and R50-W3.

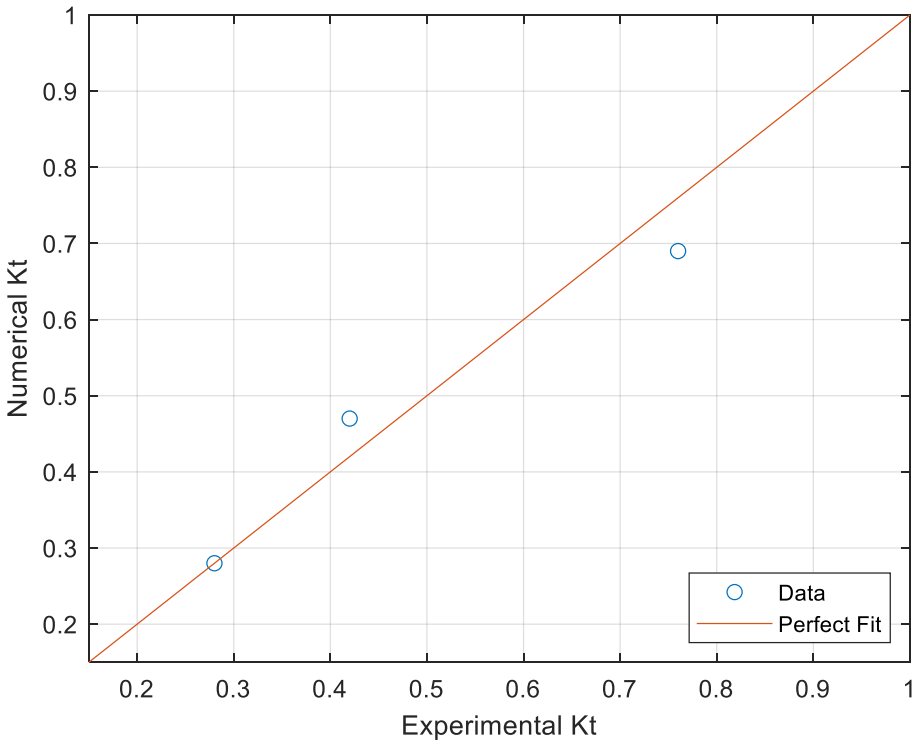

Figure 6.1: Experimental and Numerical *Kt* Values Comparison for Box

In Figure 6.2, at a ratio of B/L equal to 0.1, the data is relatively consistent. However, when the ratio of B/L is increased to 0.17, there is a wider scatter between the data. Furthermore, when the ratio of B/L is 0.2, the numerical and experimental transmission results are similar, but the ASCE (2012) formula overestimates the results.

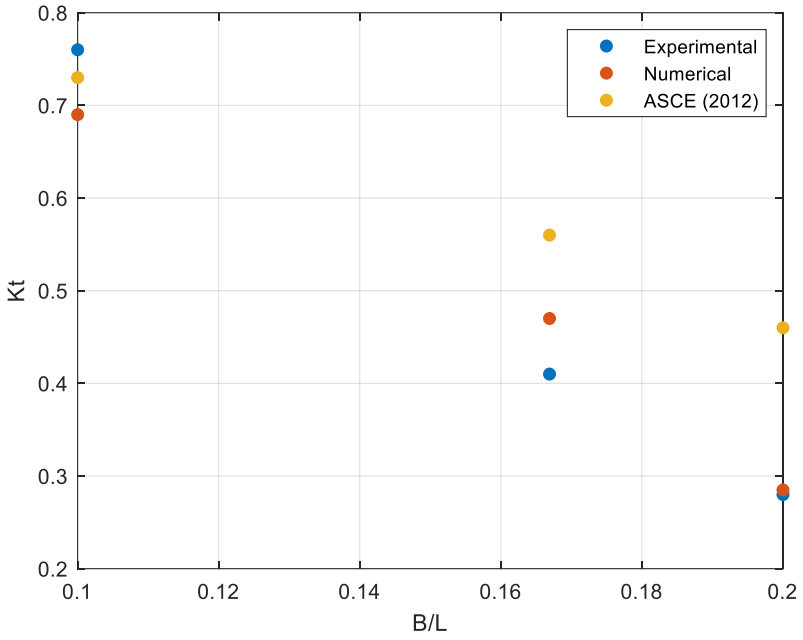

Figure 6.2: Comparison of Numerical and Experimental Validation Wave Cases with the Theoretical ASCE (2012) Results

6.1.2 Floating Platform with Short Screen (Case 2)

Similarly, to Box, three validation waves W3, W7, and D2 were modeled, and results are given in Table 6.2.

Table 6.2: Case 2 Experimental and Numeric *Kt* results

		Prototype		Model			
Wave Name	**Wave Steepness (s_m)**	**H_m (m)**	**$T_m(s)$**	**H_m (cm)**	**$T_m(s)$**	***Experimental Kt***	***Numeric Kt***
R50-W7	0.04	0.6	3.15	6	1	**0.61**	**0.57**
R50-D2	0.042	0.76	3.5	7.55	1.11	**0.63**	**0.59**
R50-W3	0.02	0.6	5	6	1.58	**0.88**	**0.92**

Experimental and numerical relation is shown in Figure 6.3. The comparison of numerical and experimental results for three cases indicates that there is overall

good agreement. However, in the case of R50-W7 and R50-D2 waves, the experimental results are slightly higher than the numerical results, whereas, in the case of R50-W3 wave, the numerical result is slightly higher than the experimental result.

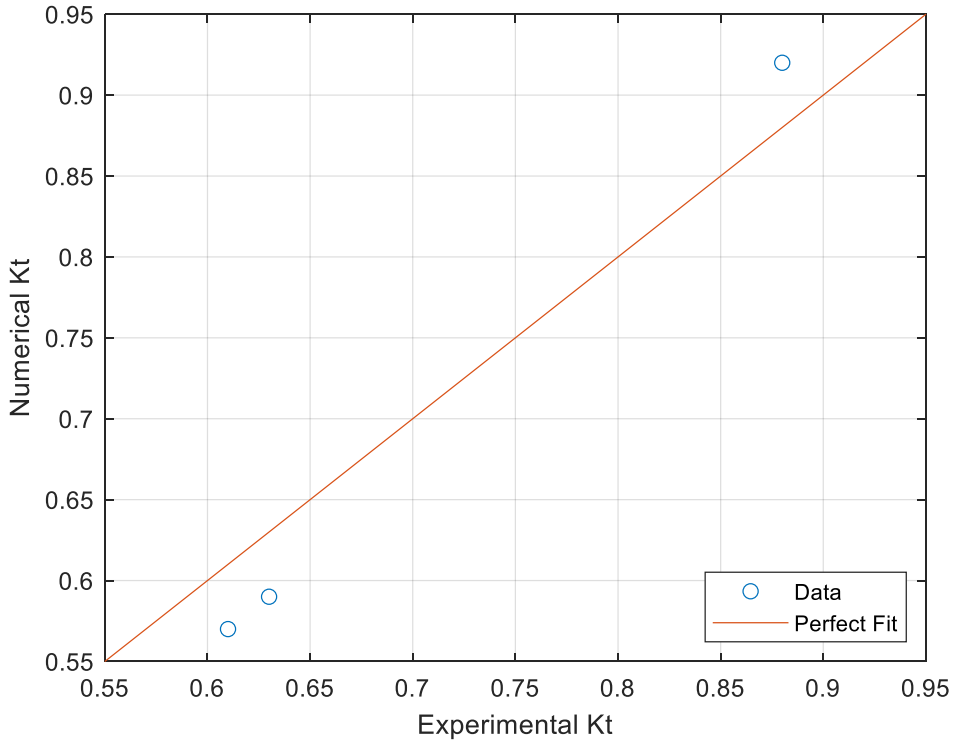

Figure 6.3: Experimental and Numerical *Kt* Values Comparison for Case 2

6.2 Extended Numerical Modelling Studies

Extended 1, 2, and 3 were numerically modelled under the same wave characteristics which are D2 ($H_m = 7.55, T_m = 1.11\ s$) and W3 ($H_m = 6, T_m = 1.58\ s$) and wave steepness of 0.042 and 0.02 respectively.

6.2.1 Transmission Results of Extended Models

Extended 1 simulated under D2, W3 regular waves in 50 cm water depth. Numerical *Kt* values are given in Table 6.3.

Table 6.3: Numerical *Kt* values for Extended 1, 2, 3 and Case 2

		Prototype		Model					
Wave Name	Wave Steepness (s_m)	H_m (m)	$T_m(s)$	H_m (cm)	$T_m(s)$	*Ext 1 Kt*	*Ext 2 Kt*	*Ext 3 Kt*	*Case 2 Kt*
R50-D2	0.042	0.76	3.5	7.55	1.11	**0.59**	**0.58**	**0.58**	**0.59**
R50-W3	0.02	0.6	5	6	1.58	**0.92**	**0.91**	**0.91**	**0.92**

6.3 Discussion of the Results

In numerical modeling, the experimental flume is replicated in the model and wave conditions are simulated at the same location as the probes in the experiments. Validation cases of Box and Case 2 showed good agreement with the experimental results (Figure 6.1 and Figure 6.3). Either in experimental or numerical models, both experimental and numerical models showed that the Box structure was more effective at dissipating wave energy due to its uniform bottom width, high energy blockage, and reflection capabilities also, it can be concluded that the numerical model also captured the overtopping wave cases coherently.

6.3.1 Impact of Horizontal Cylinder Configuration on Transmission Coefficient

In this study, three extended numerical studies were simulated which are the modification of Case 2. The transmitted energy is related to dissipated energy and reflected energy. Reflective structures attenuate the wave by friction and reflection while dissipative structures attenuate with drag forces generated by individual floating pontoons on the water surface due to wave pressure gradient. In this study

models dominantly behaved as reflective. Therefore, friction and reflection parameters play a significant role in attenuation.

To have a detailed analysis, the pipe spacing at the bottom of the structure was changed. When, Case 2, Extended 1, 2, and 3 are compared, it can be seen that Extended 2 and 3 have wider bottom pipe spacing than Case2 and Extended 1, and additionally central bottom pipe was lowered to the same horizontal axis of outer pipes in Extended 1 and 2.

Results show that changing pipe configuration doesn't have any significant effect on attenuation performance under given wave characteristics. The reason can be correlated is that the draft of the structure is the same for all numerical cases and the vertical plate was dominantly responsible for reflected energy. Moreover, the ratio between pipe spacing and wavelength was quite small to observe the spacing change effect (s/L) ratios are 0.024, 0.038, 0.04, and 0.06 for D2 and W3 wave conditions). However, if the spacing was on the order of 0.08-0.15, the wave transmission results could be affected by the spacing change.

Larger spacing pipes behave as a single body and due to vortex generation behind the pipes weak zone occurs. Therefore, larger horizontal spacing provides a larger weak zone or confined region which lowers the transmission and increases dissipated energy (Sundar et al., 2003). However, there is a relation between confinement zone and wave characteristics. As mentioned in the dual box breakwater section, the efficiency of transmission depends on the spacing between dual box structures, it is efficient in long waves when the spacing is narrow because of the continuation in width. While reflecting short waves large spacing performs better since two floating boxes behave as independent two structures.

6.3.2 Effect of Metacentric Height on Oscillating Structures

Although wave transmission results of Case 2, Extended 1, 2, and 3 are found almost the same in fixed conditions, the oscillation body case could differ in wave

transmission due to the meta-center of structure which is a function of the second moment of inertia of y-axis and center of gravity and buoyancy.

The metacentric height is a way to determine the stability of a floating object and is calculated by finding the distance between the center of gravity of a floating object and its metacenter (Figure 6.4).

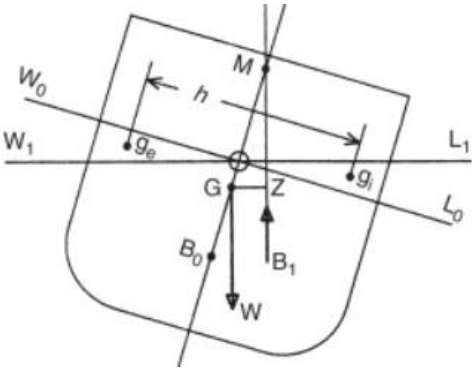

Figure 6.4: Metacentric Height of a Floating Body (adopted from Molland, 2011)

A higher metacentric height means the object is more stable and less likely to tip over. It also affects how much the object will roll, with a very high metacentric height resulting in more frequent rolling. The metacentric height is calculated using the equation given by Eq. (6.1)

$$|GM| = \frac{I_{yy}}{V} - |B_0G| \tag{6.1}$$

I_{yy} is the second moment of inertia in the y-axis, B_0 is the center of buoyancy and G is the centre of gravity, M is the metacenter and V is the submerged volume of the body. During the calculation of I_{yy} and V, the longitudinal length of 12 meters was used as the standard measurement for the manufacturer's floating platforms. Table 6.4 shows metacentric height calculation results. Since the metacentric height of all blocks is greater than zero, all models are stable.

Table 6.4: Model scale metacentric height calculation of different types of structures

Structure Type	$I_{yy}\ (mm)^4$	$\lvert B_0G \rvert$ (mm)	Sub. Volume $(mm)^3$	Model $\lvert GM \rvert$ (mm)
Box	2218804100	22.00	48388200	23.9
Case 2	407921041	46.00	5595124	26.9
Ext1	407921041	49.65	5595123	23.3
Ext2	467407988	49.65	5595123	33.9
Ext3	467407988	46.00	5595123	37.5

As shown in Table 6.4, the highest metacentric height belongs to the Extended 3 model, followed by the Extended 2 model. However, the Box, Case 2, and Extended 1 models have significantly lower metacentric heights than the other two. The lowest metacentric height belongs to the Extended 1 model due to its lowest inertia moment and highest $|B_0G|$ value. The Extended 3 model is a more suitable alternative to Case 2 as it offers higher stability and serviceability while maintaining similar performance and cost for attenuation.

CHAPTER 7

SUMMARY AND CONCLUSIONS

In this study, the transmission performance of a floating platform was examined under the influence of regular and irregular waves at different water depths and wave steepness. The transmission coefficient is measured as the draft height of the floating platform was altered. In addition, three additional numerical studies were conducted to examine wave transmission and energy dissipation of potential modifications to the selected structure. The main findings of the study are as follows:

- The transmission coefficient of irregular waves is higher than regular waves. This is likely because irregular waves have higher wave heights, which leads to more overtopping and a higher transmission coefficient. The results show that the energy transmitted by irregular waves is higher than regular waves. As the ratio of B/L increases, the transmission coefficient decreases, and there is a significant difference between regular and irregular waves for B/L values of 0.11, 0.17, and 0.31, corresponding to constant wave steepness conditions D1, D2, and D3. As the wave steepness increases, the transmission coefficient decreases for both regular and irregular waves. For the steepest wave condition (H/L = 0.05), the transmission coefficient of regular waves is higher than that of irregular waves.
- The study found that increasing the water column leads to higher transmission results under the same wave conditions. The transmission coefficient of D/d = 0.20 (60 cm water depth) was found to be higher than D/d= 0.24 and 0.30 (50 and 40 cm water depth, respectively) as observed in Figure 4.6. This suggests that the energy transmitted underneath the structure is directly proportional to the water depth under the same wave

properties. Additionally, if the water depth is kept constant and the wavelength is increased, the transmission coefficient increases. Also, when the draft is extended, the effect of water depth on changing in transmission coefficient is diminishing as the approach d/L= 0.1 or longer period.

- The wave period is the most crucial factor in determining the effectiveness of floating breakwaters. In the irregular wave experiments, the transmission coefficient reached a value of 0.86 at a wave period of 4.25 seconds (B/L = 0.175) in the prototype and rose considerably to 0.94, which is considered quite ineffective in terms of attenuation performance. Although extending the draft improves the transmission performance, in general, a wave period of 4.5 seconds (B/L = 0.125) and above significantly makes the structure inefficient in terms of attenuation.
- The effect of draft change diminishes in the long-period waves (B/L=0.1) and the transmission coefficient becomes similar for all values.
- Wave steepness (H_i/L) has an inverse proportion with the wave period or wavelength. While *sm* increases, *Kt* decreases, and more energy is reflected. As the wave period increases, wave steepness decreases and the transmission coefficient *(Kt*) increases.
- The transmitted wave energy is more effectively blocked by a box-shaped structure than by a horizontal cylinder structure which both have the same draft and width. Moreover, the bottom width of the structure is as important as the structure draft height to dissipate energy.
- The dual platform had better performance in short waves with 20 cm spacing. To further examine the influence of platform spacing on attenuation performance under different wave periods, additional tests with different platform spacing should be conducted.
- Analyzing the dynamics between waves and floating structures is complex and analytical formulas can miss important processes such as wave dissipation and overtopping. A comprehensive formula should account for all factors of wave transmission, including wave steepness, width, depth,

and draft of the structure with a wide experimental range. The study found that transmission formulas for floating breakwaters are valid for deep sea, rigid, fixed, and no overtopping conditions. All transmission formulas overestimate, but the closest formula to the experimental results is the newest formula, ASCE (2012).

- The transmission coefficient of a fixed breakwater is likely to be less than that of an oscillating breakwater because all degrees of freedom are restricted. Furthermore, metacentric height and mooring line have importance for the stability of the structure as well as for *Kt*, which is not considered in the present study as it is decided to start with a fixed version of the structure for simplicity.
- The results of the study indicate that changing the configuration of the cylinders did not significantly impact the attenuation performance. This may be since the draft of the structures was the same in all numerical cases and the vertical plate was primarily responsible for reflecting energy. Additionally, the ratio between the pipe spacing and the wavelength was too small to observe any effect on the wave transmission due to changes in spacing. However, if the spacing was closer to 0.08-0.15, the wave transmission results may have been affected by changes in spacing.
- Extended 3 has the highest metacentric height, followed by Extended 2, Case 2, Box, and Extended 1. All models are stable, as their metacentric height is above zero. It is recommended to consider Extended 3 as an alternative to Case 2 because it offers higher stability and serviceability while maintaining similar attenuation performance and cost.

In future studies, a detailed transmission formula for box-structured floating breakwaters that are fixed or anchored by piles (with only vertical movement allowed) can be developed by conducting experiments in a wide range of conditions, including shallow, intermediate, and deep water, and with various changes in geometry such as width, freeboard, and draft. A single formula may not be sufficient to cover all cases, so a piecewise equation may be suggested

for different regions. Additionally, it would be beneficial to examine the ratio between cylinder spacing and wavelength in greater detail using a large set of waves to analyze its effect on wave transmission. Additionally, the horizontal cylinder-type floating platform has been tested as fixed, but future studies should also test it as oscillating to measure the effect of six degrees of freedom on wave transmission.

REFERENCES

Akgul, M. A. (2016, June). Effect of Pipe Spacing on the Performance of a Trimaran Floating Pipe Breakwater. In *The 26th International Ocean and Polar Engineering Conference*. OnePetro.

Biesheuvel, A. C. (2013). Effectiveness of Floating Breakwaters: Wave attenuating floating structures. MSc thesis, Delft University of Technology, Delft, Netherlands

Candle, R.D. (1974). Goodyear scrap tire floating breakwater concepts. *In: Proceedings of the Floating Breakwaters Conference.* University of Rhode Island, Kingston, pp. 193–212.

Carr, J. H. (1951). Mobile breakwaters. *Coastal Engineering Proceedings*, (2), 25-25.

Cheng, X., Liu, C., Zhang, Q., He, M., & Gao, X. (2021). Numerical Study on the Hydrodynamic Characteristics of a Double-Row Floating Breakwater Composed of a Pontoon and an Airbag. *Journal of Marine Science and Engineering*, *9*(9), 983.

Chun-Yan, J., Xiang, C., Jie, C., Zhi-Ming, Y., & Atilla, I. (2015). Experimental Study of a New Type of Floating Breakwater. *Ocean Engineering*, *CV*(1998), 295–303.

Connell, K. O., & Cashman, A. (2015, November). Mathematical & CFD analysis of free floating heave-only body. In *2015 International Conference on Renewable Energy Research and Applications (ICRERA)* (pp. 467-471). IEEE.

Cox, J.C. 1989. Breakwater Attenuation Criteria and Specification for Marina Basins, In Marinas: Design and Operation". Proceedings of the International

Conference on Marinas, Southampton, UK. Computational Mechanics Publications, Southampton and Boston, pp. 139-155.

Dai, J., Wang, C. M., Utsunomiya, T., & Duan, W. (2018). Review of recent research and developments on floating breakwaters. *Ocean Engineering*, *158*(February), 132–151. https://doi.org/10.1016/j.oceaneng.2018.03.083

Davidson, D. D. (1971). *Wave Transmission and Mooring Force Tests of Floating Breakwater, Oak Harbor, Washington: Hydraulic Model Investigation* (Vol. 71, No. 3). Waterways Experiment Station.

Davidson, J., Cathelain, M., Guillemet, L., Le Huec, T., & Ringwood, J. (2015). Implementation of an openfoam numerical wave tank for wave energy experiments. In *Proceedings of the 11th European wave and tidal energy conference*. European Wave and Tidal Energy Conference 2015.

Gunbak, A. R., Ozbahceci, B. O., Kucukosmanoglu, A., & Akbas, H. L. (2014). Performance of Vertical Wall and Floating Breakwaters Combination for Datca Marina. In *From Sea to Shore–Meeting the Challenges of the Sea: (Coasts, Marine Structures and Breakwaters 2013)* (pp. 285-294). ICE Publishing.

Hales, L. Z. (1981). Floating Breakwaters: State-of-the-Art Literature Review.

Harmses, V. W., & Westerink, J. J. (1980). *Wave transmission and mooring-force characteristics of pipe-tire floating breakwaters*. University of California, Lawrence Berkeley Laboratory.

Higuera, P. (2015). Application of computational fluid dynamics to wave action on structures. Ph.D. Thesis, 1–356.

Higuera, P., Lara, J. L., & Losada, I. J. (2014). Three-dimensional interaction of waves and porous coastal structures using OpenFOAM®. Part I: Formulation and validation. *Coastal Engineering*, *83*, 243–258.

https://doi.org/10.1016/j.coastaleng.2013.08.010

Hudson, R. Y., Herrmann, F. A., Sager, R. A., Whalin, R. W., Keulegan, G. H., Chatham, C. E., and Hales, L. Z. 1979. "Coastal Hydraulic Models," Special Report No. 5, US Army Engineer Waterways Experiment Station, Vicksburg, Mississippi.

Hughes, S.A. (1993): *'Physical Models and Laboratory Techniques in Coastal Engineering', Coastal Engineering Research Center (CERC), US Army Corps of Engineers, Vicksburg, Mississippi, USA.*

Ikeno, M., Shimoda, N., & Iwata, K. (1989). A new type of breakwater utilizing air compressibility. In *Coastal Engineering 1988* (pp. 2326-2339).

Jacobsen, N. G., Fuhrman, D. R., & Fredsøe, J. (2012). A wave generation toolbox for the open-source CFD library: OpenFoam®. *International Journal for numerical methods in fluids*, *70*(9), 1073-1088.

Jones, D. B. (1978). *An Assessment of Transportable Breakwaters with Reference to the Container Off-Loading and Transfer System (COTS)*. CIVIL ENGINEERING LAB (NAVY) PORT HUENEME CALIF.

Journée, J. M. J., & Massie, W. W. (1999). Offshore Hydromechanics. Delft. *Delft University of Technology, Faculty of Mechanical Engineering and Marine Technology*.

Jung, J. H., Yoon, H. S., Chun, H. H., Lee, I., & Park, H. (2013). Numerical simulation of wave interacting with a free rolling body. *International Journal of Naval Architecture and Ocean Engineering*, *5*(3), 333-347.

Kamel, A. M., & Davidson, D. D. (1968). Hydraulic characteristics of mobile breakwaters composed of tires or spheres. TR H-68-2.

Koo, W. (2009). Nonlinear time–domain analysis of motion-restrained pneumatic

floating breakwater. *Ocean Engineering*, *36*(9-10), 723-731.

Koraim, A. S., & Rageh, O. S. (2014). Effect of under connected plates on the hydrodynamic efficiency of the floating breakwater. *China Ocean Engineering*, *28*(3), 349–362. https://doi.org/10.1007/s13344-014-0028-1

Koutandos, E., Prinos, P., & Gironella, X. (2005). Floating breakwaters under regular and irregular wave forcing: reflection and transmission characteristics. *Journal of Hydraulic Research*, *43*(2), 174-188.

Kriebel, D. L., & Bollmann, C. A. (1996). Wave transmission past vertical wave barriers. In *Coastal Engineering 1996* (pp. 2470-2483).

Larsen, B. E., Fuhrman, D. R., & Roenby, J. (2019). Performance of interFoam on the simulation of progressive waves. *Coastal Engineering Journal*, *61*(3), 380–400. https://doi.org/10.1080/21664250.2019.1609713

Lochner, R., Faber, O., & Penney, W. G. (1948). The Bombardon Floating Breakwater: The Civil Engineer in War, Vol II. London: Institute of Civil Engineers.

Loukogeorgaki, E., Yagci, O., & Sedat Kabdasli, M. (2014). 3D Experimental investigation of the structural response and the effectiveness of a moored floating breakwater with flexibly connected modules. *Coastal Engineering*, *91*, 164–180. https://doi.org/10.1016/j.coastaleng.2014.05.008.

Macagno, E. O. (1953). Fluid mechanics: experimental study of the effects of the passage of a wave beneath an obstacle. Proceedings of the Academic des Sciences.

Mansard, E. P. D., & Funke, E. R. (1980). The measurement of incident and reflected spectra using a least squares method. *Coastal Engineering 1980*, 154–172. https://doi.org/10.1061/9780872622647.008

Martinelli, L., Ruol, P., & Zanuttigh, B. (2008). Wave basin experiments on floating breakwaters with different layouts. *Applied Ocean Research*, *30*(3), 199-207.

McCartney, B. L. (1985). Floating breakwater design. *Journal of Waterway, Port, Coastal, and Ocean Engineering*, *111*(2), 304-318.

Molland, A. F. (Ed.). (2011). *The maritime engineering reference book: a guide to ship design, construction and operation*. Elsevier.

Morey, B. J. (1998). Floating breakwaters: predicting their performance (Doctoral dissertation, Memorial University of Newfoundland).

Nakamura, T., Kohno, T., & Morita, Y. (2001, June). Performance of a double-walled barrier with a front wall of inclined plate array. In *The Eleventh International Offshore and Polar Engineering Conference*. OnePetro.

Ofuya, A.O. (1968). On Floating Breakwaters. Research Report No. CE-60. Queen's University,Kingston.

Paci, A., Gaeta, M. G., Antonini, A., & Archetti, R. (2016, June). 3D-numerical analysis of wave-floating structure interaction with OpenFOAM. In *The 26th International Ocean and Polar Engineering Conference*. OnePetro.

PIANC. (1994). Review of selected standards for floating dock designs. *PIANC Report*, *93*(93).

Richey, E. P., & Sollitt, C. K. (1970). Wave attenuation by porous walled breakwater. *Journal of the Waterways, Harbors and Coastal Engineering Division*, *96*(3), 643-663.

Stitt, R. L., & Nobel, H. M. (1963). Introducing Wave-Maze Floating Breakwater. *unnumbered report, Temple City, California*.

Sundar, V., Sundaravadivelu, R., & Purushotham, S. (2003). Hydrodynamic

characteristics of moored floating pipe breakwaters in random waves. *Proceedings of the Institution of Mechanical Engineers, Part M: Journal of Engineering for the Maritime Environment*, *217*(2), 95-110.

Task Committee on Marinas 2020 of the Coasts, Oceans, Ports, and Rivers Institute of ASCE. (2012, November). Planning and design guidelines for small craft harbors. American Society of Civil Engineers.

Wiegel, R. L. (1960). Transmission of waves past a rigid vertical thin barrier. *Journal of the Waterways and harbors division*, *86*(1), 1-12.

Williams, A. N., Lee, H. S., & Huang, Z. (2000). Floating pontoon breakwaters. *Ocean Engineering*, *27*(3), 221-240.

Zhan, J. min, Chen, X. bin, Gong, Y. jun, & Hu, W. qing. (2017). Numerical investigation of the interaction between an inverse T-type fixed/floating breakwater and regular/irregular waves. *Ocean Engineering*, *137*(June 2016), 110–119. https://doi.org/10.1016/j.oceaneng.2017.03.058